Inaugural dissertation

for

obtaining the doctoral degree

of the

Combined Faculty of Mathematics, Engineering and Natural Sciences

of the

Ruprecht - Karls - University

Heidelberg

Presented by

M.Sc. Catarina da Silva Pechincha

Born in: Évora, Portugal

Oral examination: 25th January 2024

Lysosomal enzyme trafficking factor LYSET in lysosomal catabolism, nutrient generation, and pathology

Referees: Prof. Dr. Tobias Dick
Dr. Wilhelm Palm

Lysosomal enzyme trafficking factor LYSET in lysosomal catabolism, nutrient generation, and pathology

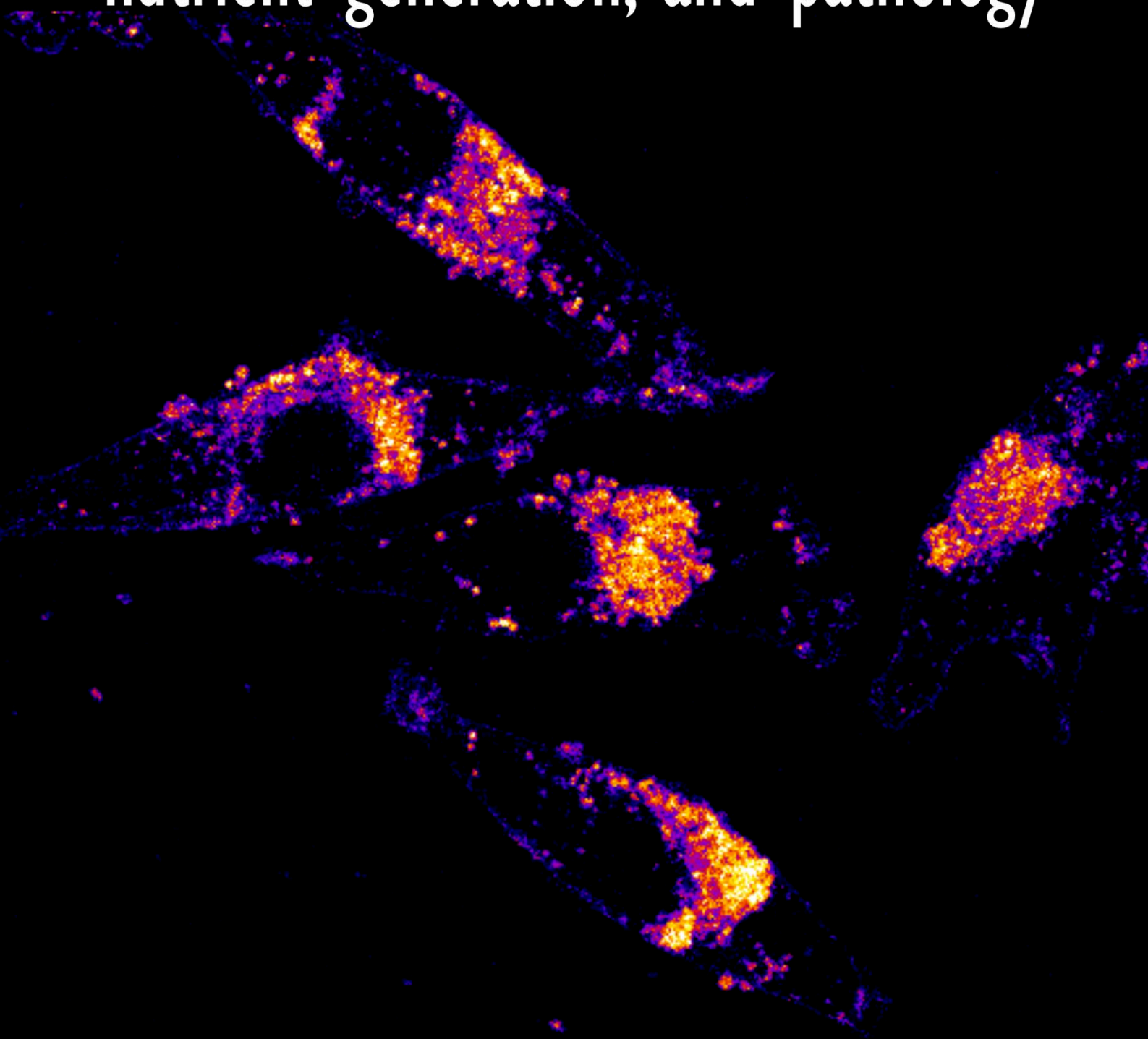

Catarina da Silva Pechincha

Table of Contents

I. Summary

Cancer cells are surrounded by a variety of nutrients, including amino acids and extracellular proteins. When in nutrient-rich conditions, cells prefer to take up free amino acids to meet their nutritional demand. However, most amino acids in the extracellular space are contained within proteins. In nutrient-poor conditions, cells can engulf extracellular proteins and degrade them in lysosomes, an organelle capable of breaking down proteins into their constituent amino acids. By generating an internal nutrient source, lysosomes play a crucial role in sustaining cellular functions during periods of starvation. This process is frequently exploited by cancer cells, enabling them to thrive in poorly vascularised, nutrient-deprived tumour environments. My PhD project aimed at identifying genes that are essential for cell proliferation when cells rely on extracellular proteins as nutrients. To this end, I developed metabolic conditions where cancer cells could either grow through the import of free amino acids or by the uptake and lysosomal degradation of extracellular proteins. By conducting genome-wide CRISPR screens in these different nutrient environments, I identified genes selectively essential when cells depend on extracellular proteins, including TMEM251, an uncharacterised transmembrane protein that we renamed to LYSosomal Enzyme Trafficking factor (LYSET). Through a comprehensive mechanistic study, I characterised LYSET as a protein responsible for anchoring GlcNAc-1-phosphotransferase (GNPT) in Golgi apparatus membranes. LYSET and GNPT mediate the tagging of degradative enzymes with the lysosomal trafficking signal, mannose-6-phosphate. LYSET-deficient cells present lysosomes lacking luminal enzymes and are incapable of degrading macromolecules from both autophagic or endocytic cargo. Cells lacking LYSET accumulate dysfunctional lysosomes, which helps explain the connection between LYSET and described hereditary metabolic disorders. In nutrient-rich conditions, LYSET-deficient cancer cells exhibited normal growth, while in starvation they exhibited an impairment in proliferation. Consistently, LYSET-deficient cells were incapable of forming tumours in mice. Thus, although LYSET is annotated as non-essential in more than a thousand CRISPR screens in DepMap, it is essential for the growth of nutrient-deprived cancer cells. In summary, LYSET is a core component of the mannose-6-phosphate (M6P) pathway, represents the mechanism for hereditary lysosomal pathologies, and grants cancer cells metabolic adaptability and resilience, representing a promising strategy to target cancer cells.

II. Zusammenfassung

Krebszellen sind von einer Vielzahl von Nährstoffen umgeben, darunter Aminosäuren und extrazelluläre Proteine. Unter nährstoffreichen Bedingungen nehmen Zellen bevorzugt freie Aminosäuren auf, um ihren Nährstoffbedarf zu decken. Die meisten Aminosäuren im extrazellulären Raum sind jedoch in Proteinen enthalten. Unter nährstoffarmen Bedingungen können Zellen extrazelluläre Proteine aufnehmen und in Lysosomen abbauen, einer Organelle, die in der Lage ist, Proteine in ihre einzelnen Aminosäuren zu zerlegen. Indem sie eine interne Nährstoffquelle schaffen, spielen Lysosomen eine entscheidende Rolle bei der Aufrechterhaltung der Zellfunktionen in Zeiten des Nährstoffmangel. Dieser Prozess wird häufig von Krebszellen ausgenutzt, die dadurch in einer schlecht durchbluteten, nährstoffarmen Tumorumgebung gedeihen können. Ziel meines Promotionsprojekts war die Identifizierung von Genen, die für die Zellproliferation unerlässlich sind, wenn Zellen auf extrazelluläre Proteine als Nährstoffe angewiesen sind. Zu diesem Zweck entwickelte ich Stoffwechselbedingungen, unter denen Krebszellen entweder durch den Import freier Aminosäuren oder durch die Aufnahme und den lysosomalen Abbau von extrazellulären Proteinen wachsen konnten. Durch genomweite CRISPR-Screens in diesen unterschiedlichen Nährstoffumgebungen identifizierte ich Gene, die selektiv wichtig sind, wenn Zellen von extrazellulären Proteinen abhängen, darunter TMEM251, ein nicht charakterisiertes Transmembranprotein, das wir in LYSosomal Enzyme Trafficking factor (LYSET) umbenannt haben. Durch eine umfassende mechanistische Studie habe ich LYSET als ein Protein charakterisiert, das für die Verankerung von GlcNAc-1-Phosphotransferase (GNPT) in Membranen des Golgi-Apparats verantwortlich ist. LYSET und GNPT vermitteln die Markierung von Abbauenzymen mit dem lysosomalen Trafficking-Signal Mannose-6-phosphat. LYSET-defiziente Zellen weisen Lysosomen auf, denen Luminalenzyme fehlen, und sind nicht in der Lage, Makromoleküle aus autophagischer oder endozytischer Ladung abzubauen. Zellen, denen LYSET fehlt, akkumulieren dysfunktionale Lysosomen, was hilft, den Zusammenhang zwischen LYSET und beschriebenen erblichen Stoffwechselstörungen zu erklären. Unter nährstoffreichen Bedingungen zeigten LYSET-defiziente Krebszellen ein normales Wachstum, während sie unter Nährstoffmangel eine Beeinträchtigung der Proliferation aufwiesen. Folgerichtig waren LYSET-defiziente Zellen in Mäusen nicht in der Lage, Tumore zu bilden. Obwohl LYSET in mehr als tausend CRISPR-Screens in DepMap als nicht essentiell eingestuft wird, ist es also für das Wachstum von Krebszellen unter

Nährstoffentzug essentiell. Zusammenfassend lässt sich sagen, dass LYSET eine Kernkomponente des Mannose-6-Phosphat (M6P)-Wegs ist, den Mechanismus für erbliche lysosomale Pathologien darstellt und Krebszellen metabolische Anpassungsfähigkeit und Widerstandsfähigkeit verleiht, was eine vielversprechende Strategie zur Bekämpfung von Krebszellen darstellt.

III. Acknowledgements

I am extremely grateful to Prof. Dr. Tobias Dick, Dr. Wilhelm Palm, Prof. Dr. Britta Brügger, and Prof. Dr. Aurelio Teleman for taking the time to be part of my PhD defense committee. I would like to extend my sincere thanks to Prof. Dr. Tobias Dick, Dr. Wilhelm Palm, Prof. Dr. Aurelio Teleman, and Prof. Dr. Sebastian Schuck for being part of my PhD journey as my Thesis Advisory Committee members.

To my supervisor, Wilhelm Palm, I feel very grateful and honoured for the trust he deposited in me to be the first PhD student in the lab. He saw bravery and strength in me, which I may have not felt when I naively applied to work with him. I wanted to have a brilliant and supportive supervisor and Wilhelm provided me with that unwavering support, invaluable guidance, and mentorship. His expertise, patience, dedication, and will to always be on the right side played a pivotal role in my personal and professional development.

To the Graduate Office, thank you for the interactions and work developed together during my time at the PhD Council and IPSCC organisation. Also, thank you to DKFZ for the funding that allowed me to develop my PhD at DKFZ, through the International PhD and CancerTRAX programs, and to the Helmholtz Association for the nomination and funding to participate in the Lindau Nobel Laureate Meeting 2023.

To the Teleman lab and Loayza-Puch lab members, many thanks for the scientific interactions and discussions that made my scientific experience in Heidelberg a lot better. Thank you to Hannes Zuber for giving me the opportunity to learn from him and his team and for the generous exchange of knowledge and reagents, which were a solid foundation for the start of my PhD project and, especially, to its end. To the Zuber lab members, thank you for the knowledge exchange over the years and for being great hosts during my visit to the IMP in Vienna. To all the co-authors of the paper resulting from this project, special thanks for being on board, even with all the difficulties and deadlines that came with it. It was a pleasure to work with you and words cannot express my gratitude.

To all the past and present members of the Palm Lab (aka “Dr. Palm and the palmitates”), I would like to express my deepest gratitude for your help and for contributing to a fun and interactive environment in the lab. Especially to Edoardo, Julia, Rafael, and Aslihan for going from colleagues to friends who listened to me and always tried to understand my frustrations with sense of humour.

During my PhD journey, I had the pleasure to get to know quite a lot of amazing people. To the “Cheese lovers”, the “PhD resistance”, the Portuguese friends and amiguinho, the PhD Council 2020, and the IPSCC organisation team, thank you for making my life more exciting

outside the lab. Our evenings in the Neckarwiese, dinners, long conversations, drinking nights, and laser tag are the memories I will take from Heidelberg.

Aos meus amigos de sempre, obrigada por me motivarem a continuar o meu caminho. Nos últimos anos, por perceberem as ausências e pelo esforço para se manterem por perto. Especialmente, à Mariana e à Filipa, por continuarmos a ser as meninas de 10 anos, que se juntavam para jogar Sims e dançar, sempre que nos reencontramos. À Catarina que ao dizer-me "quando descobrires o que nos vai fazer imortais, dás-me primeiro a mim" sabia que eu um dia ia ser cientista, quando nem eu sabia. À Joana, por ter sempre acreditado em mim e por me dar confiança ao ver e realçar sempre o meu melhor lado. Espero poder estar sempre nas suas vidas e que elas estejam na minha.

Às meninas de Bioanalíticas, por terem feito dos 3 anos de licenciatura os melhores que poderia ter vivido, que foram a base de tudo o que veio a seguir. Por juntas termos vivido a verdadeira experiência académica em Coimbra. Por serem um grande pilar na minha vida e por manterem a mesma vontade de estarmos juntar como há 10 anos, como se ainda partilhássemos o dia a dia.

Às Joanas, que se tornaram companheiras desde que nos juntaram no mesmo grupo de trabalho no início do mestrado até a esta fase final dos nossos doutoramentos, cada uma na sua cidade. Pelas partilhas das nossas inquietações e por crescerem comigo na mesma direcção, obrigada.

À minha família, por me incentivarem positivamente e por me mostrarem o vosso orgulho. Em especial aos meus pais, muito obrigada por todas as oportunidades que me deram ao longo da minha vida. Por me abrirem as portas para o Mundo ao "paitrocinarem" as viagens escolares e Erasmus que culminaram nesta aventura que foi vir para a Alemanha fazer o doutoramento. E por fim, por nos terem educado para sermos bons cidadãos. Ao meu irmão, por ter sempre apoiado as minhas decisões, por saber o que estou a pensar sem eu dizer e por ser sempre um bom campanheiro, mesmo quando estava mais "apertada". A ele e à Vânia, obrigada por me acolherem sempre e serem um exemplo a seguir. Às minhas sobrinhas, Rita, Sara e Inês, e ao meu primo Pedro, por me fazerem querer ser melhor pessoa e por cantarmos e dançarmos como uns doidos.

Ao André, por ser sempre um apoio inabalável e fundamental, por acreditar em mim e por ser um modelo de motivação e persistência. Obrigada pela compreensão e ajuda nos dias em só ia comer e dormir e tinha o jantar feito. Pelas boas conversas e por fazer de mim melhor pessoa. Pelo carinho infindável e por ser sempre o melhor abraço.

Obrigada a todos! <3

IV. Disclaimer

The work described in my Ph.D. thesis is part of the peer-reviewed published manuscript: Catarina Pechincha, Sven Groessl, Robert Kalis, Melanie de Almeida, Andrea Zanotti, Marten Wittmann, Martin Schneider, Rafael P. de Campos, Sarah Rieser, Marlene Brandstetter, Alexander Schleiffer, Karin Müller-Decker, Dominic Helm, Sabrina Jabs, David Haselbach, Marius K. Lemberg, Johannes Zuber, Wilhelm Palm. Lysosomal enzyme trafficking factor LYSET enables nutritional usage of extracellular proteins. *Science* **378**, eabn5637 (2022). DOI: 10.1126/science.abn5637

Most of the content in this thesis is described and shown in this publication. The research was originally designed and conceived by me and Wilhelm Palm with contributions from the remaining authors, as stated in chapter *4. Results*. For more details, see *V. Contributions*.

The methods sections describing proteomics and related analyses (chapter *3.2.15 LC-MS/MS analysis*) contain protocols or parts of them which were kindly provided by Dr. Dominic Helm and Martin Schneider, from the DKFZ Proteomics Core Facility. The methods section describing protein structure prediction (chapter *3.2.16 Protein structure prediction*) was kindly provided by Dr. David Haselbach. The methods section describing animal experiments (chapter *3.2.17 Mice experiments*) was kindly provided by PD Dr. Karin Müller-Decker, head of the DKFZ Tumor Models facility.

V. Contributions

Test of Cas9 induction, gene editing, and TRE3G promoter tightness evaluated by flow cytometry and immunoblotting were carried out by me and Melanie de Almeida. Transduction of the Vienna genome-wide sgRNA library was done by Melanie de Almeida.

Processing of the screen sequencing data was done by Melanie de Almeida and further analysis of the read counts was done by me.

Gibson assembly for the generation of new plasmids and site-directed mutagenesis were done by me and Marten Wittmann, as indicated. Robert Kalis generated GNPTAB mutation constructs.

Generation of iKO and bulk KO cell lines was done by me and Sven Groessl, as indicated.

Competitive proliferation assays shown in *Figure 6 B* and immunoblotting experiments in *Figure 6A* and *Figure 13A* were carried out by Sven Groessl.

In vivo experiments shown in *Figure 6D* were carried out by Karin Müller-Decker.

Mannose-6-phosphate immunoblottings of membranes prepared by me, shown in *Figure 12 A and B*, were performed by Sabrina Jabs.

Immunoblotting experiment shown in *Figure 16D* was performed by Marten Wittmann.

Samples for mass spectrometry analysis shown in *Figure 9* and *Figure 11B* were prepared by me, processed by Dominic Helm, and analysed by Martin Schneider at the DKFZ Proteomics Core Facility.

The detailed contribution of each person is mentioned in chapter *4. Results* main text and figure legends.

VI. List of abbreviations

a.u.	Arbitrary units
ATF6	Activating transcription factor 6
BFP	Blue fluorescent protein
BSA	Bovine serum albumin
cAMP	Cyclic adenosine monophosphate
CLEAR	Coordinated lysosomal expression and regulation
CREB	Camp response element–binding protein
CTSB	Cathepsin B
CTSL	Cathepsin L
DAPI	4′,6-diamidino-2-phenylindole
DMAP	DNA methyltransferase interactions
DMSO	Dimethyl sulfoxide
DQ BSA	Dequenched BSA
dsgRNA	Dual small guide RNA
EMT	Epithelial–mesenchymal transition
EndoHf	Endoglycosidase Hf
ER	Endoplasmic reticulum
ERGIC	ER-Golgi intermediate compartment
FBS	Fetal bovine serum
FC	Fold-change
GBA	Glucosylceramidase
GFP	Green fluorescent protein
GM130 (or GOLGA2)	Golgin subfamily A member 2
GNPTAB	N-acetylglucosamine-1-phosphotransferase alpha and beta
GNPTG	N-acetylglucosamine-1-phosphotransferase gamma
GOLGA1	Golgin subfamily A member 1
HEK	Human embryonic kidney
HEXA	Hexosaminidase A
iCas9	Inducible Cas9
iKO	Inducible knockout
KO	Knockout
LC3	Microtubule-associated proteins 1A/1B light chain 3
LC-MS	Liquid chromatography-mass spectrometry

LDLR	Low density lipoprotein receptor
LIMP-2	Lysosomal integral membrane protein 2
LRP1	LDLR-related protein 1
LRP2 or megalin	LDLR-related protein 2
LYSET	Lysosomal enzymes trafficking factor
M6P	Mannose-6-phosphate
MEF	Mouse embrionic fibroblast
MIT	Microphthalmia-associated transcription factor
ML	Mucolipidosis
MPR	M6P-receptors
NGS	Next generation sequencing
NSG	NOD scid gamma
PLA	Proximity ligation assay
PNGaseF	N-glycosidase F
PNS	Post-nuclear supernatant
RT-qPCR	Quantitative reverse transcription polymerase chain reaction
rtTA3	Reverse tetracycline transactivator 3
S1P	Site-1 protease
SDS	Sodium dodecyl sulfate
SEM	Standard error of mean
SFFV	Spleen focus-forming virus envelope gene
sgRNA	Small guide RNA
STAT3	Signal transducer and activator of transcription 3
TFE3	Transcription factor binding to ighm enhancer 3
TFEB	Transcription factor eb
TGN	Trans-Golgi network
TM	Transmembrane domain
TRE	Tetracycline responsive element
TRE3G	Tetracycline responsive element 3G
UCE	Uncovering enzyme α-N-acetylglucosaminidase
UDP	Uridine diphosphate
v-ATPase	Vacuolar-type ATP synthase

VII. List of tables

VIII. List of figures

1. Introduction

1.1 Lysosomes

Lysosomes are catabolically active organelles responsible for the degradation of macromolecules. Macromolecules, such as proteins, lipids, carbohydrates, and nucleic acids, are delivered to lysosomes and degraded by hydrolases (Akter *et al.*, 2020, Ballabio and Bonifacino, 2020, Yang and Wang, 2021).

Lysosomes recycle intracellular macromolecules and degrade endocytosed extracellular macromolecules. The resulting degradation products can be exported to the cytosol and used by the cell as nutrients. Due to this metabolic role, lysosomes respond to both extracellular and intracellular signals, being essential signalling hubs for energy and amino acid sensing and signal transduction (Perera and Zoncu, 2016). Furthermore, lysosomes are involved in the secretion of enzymes to the extracellular space and the maintenance of the plasma membrane (Yang and Wang, 2021). Additionally, lysosomes function as cellular storage centres. Lysosomes can store the different products of degradation and buffer the cytoplasm by storing metal ions (such as zinc, iron, copper, and calcium) avoiding their excessive release and damaging accumulation in the cytoplasm (Lawrence and Zoncu, 2019).

1.2 Lysosomal enzymes

Lysosomes are composed of hundreds of integral and peripheral membrane proteins and dozens of soluble enzymes. Lysosomal enzymes are soluble hydrolases present in the lumen of lysosomes that degrade complex macromolecules, including lipases, peptidases, nucleases, glycosidases, phosphatases, and sulfatases. Lysosomal hydrolases require an acidic pH for optimal activity. Lysosomal pH ranges from 4.5 to 5.5. This acidic pH is maintained by the lysosomal v-ATPase, which pumps protons from the cytosol to the lysosomal lumen (Akter *et al.*, 2020, Ballabio and Bonifacino, 2020, Yang and Wang, 2021, Akter *et al.*, 2023, Freeman *et al.*, 2023).

Cathepsins are the major group of lysosomal proteases and degrade a broad range of substrates. Cathepsins are most active within the acidic environment of lysosomes, however, certain cathepsins are active across a broad range of pH levels. For example, cathepsin S exhibits its peak activity at pH 6.5. Cathepsin D, which functions optimally at pH 4, has been detected with reduced kinetic rates even at pH 7.4. Furthermore, cathepsin K and H maintain

stable activity at pH 7. This suggests that cathepsins can have an important proteolytic role outside of the endolysosomal system (Yadati *et al.*, 2020). Cathepsins L, B, and D are the most abundant cathepsins in the lysosome. Within the lysosome, the optimal pH for cathepsin activity is unclear, as these studies were carried out *in vitro* using purified enzymes. Moreover, the acidic pH promotes the degradation of macromolecules by causing conformational changes in the substrates that facilitate recognition and cleavage by the enzymes (Yadati *et al.*, 2020, Akter *et al.*, 2023, Freeman *et al.*, 2023).

1.3 Lysosomal biogenesis

Lysosomal component synthesis occurs through the biosynthetic pathway, involving the endoplasmic reticulum (ER), the Golgi, the trans-Golgi network (TGN), the plasma membrane, and endosomes. Lysosomal biogenesis is increased in response to starvation and during cell growth (Yang and Wang, 2021).

1.3.1 Transcriptional regulation of lysosome biogenesis

The regulation of lysosomal biogenesis is mediated at the transcriptional level. The major regulators are MiT/TFE transcription factors. The transcription factor TFEB activates the expression of multiple lysosomal genes, including membrane and luminal proteins, such as LAMP1, v-ATPase complex proteins, and cathepsins. TFEB binds to a specific DNA sequence, the coordinated lysosomal expression and regulation (CLEAR) element, which is present in the promoters of these genes (Palmieri *et al.*, 2011). TFEB activity is controlled by its phosphorylation state, which controls the movement between the nucleus and cytoplasm. In nutrient-rich conditions, the mechanistic target of rapamycin (mTOR) is active and phosphorylates TFEB. In this inactive state, TFEB is present in the cytosol. In response to starvation, oxidative stress, or lysosomal stress, mTOR is inactive, not phosphorylating TFEB. Additionally, TFEB is dephosphorylated by the calcineurin phosphatase or protein phosphatase 2A, which leads to its translocation to the nucleus. There, TFEB binds to the promoter region of its target genes, leading to their transcription. When in the nucleus, TFEB can be rephosphorylated and exported to the cytoplasm. The coordination of the phosphatases and kinases activity allows TFEB to oscillate phosphorylation state and subcellular localisation according to cellular needs (Zhang *et al.*, 2020). Additionally, other members of the subfamily of MiT/TFE transcription factors, such as TFE3, are likewise phosphorylated by mTORC1, regulating the expression of lysosomal genes (Bajaj *et al.*, 2019, Yang and Wang, 2021). Furthermore, lysosomal reactive oxygen species and oxidative stress

activate STAT3. Activated and phosphorylated STAT3 binds to the promoter and induces expression of proteolytic hydrolases, such as cathepsins (Martínez-Fábregas *et al.*, 2018).

1.3.2 Sorting of lysosomal proteins

Proteins intended for the plasma membrane and lysosomes follow the secretory pathway. Lysosomal proteins are synthesised as precursor peptides (or pro-peptide) with an N-terminus signal peptide, responsible for their translocation to the ER. Next, these enzymes are transported in vesicles to the ER-Golgi intermediate compartment (ERGIC), pass through the Golgi, and are delivered to late endosomes via the TGN. The Golgi apparatus consists of distinct sub-compartments/cisternae: cis-, medial-, and trans-Golgi. Lysosomal proteins enter the Golgi at the cis-cisternae and ultimately exit from the trans-cisternae. During intra-Golgi transport, cargo undergoes various modifications and is sorted into vesicles emerging from the TGN. Cargo sorting into vesicles at the TGN relies on coat proteins that directly or indirectly interact with sorting signals present in the cytoplasmic domains of these cargoes. Once the clathrin-coated vesicles are formed, the vesicles are trafficked to the endolysosomal system. After cargo delivery, membrane proteins and trafficking adaptors are retrieved back to the Golgi (Gu *et al.*, 2001, Kim and Gadila, 2016, Staudt *et al.*, 2016).

Lysosomal membrane proteins reach the lysosome via vesicular trafficking due to lipid modifications and sorting signals in both N- or C-cytosolic termini (Braulke and Bonifacino, 2009, Thomas Braulke *et al.*, 2023). These sorting signals are recognised by membrane trafficking regulators and transported to the lysosome, directly or indirectly. In the direct pathway, proteins traffic in the TGN directly to late-endosomes and lysosomes. In the indirect pathway, membrane proteins go to the plasma membrane before being internalised in early endosomes and delivered to late endosomes and lysosomes. Membrane proteins can directly interact with vesicular trafficking adaptors to be sorted to the lysosome while soluble hydrolases require an additional element that mediates the interaction of the luminal proteins with the cytosolic adaptors.

1.4 The mannose-6-phosphate pathway

For lysosomal sorting, most lysosomal soluble hydrolases are modified with mannose-6-phosphate (M6P) residues that allow the recognition of these enzymes by M6P receptors (MPR). Soluble hydrolases are synthesised as precursor proteins containing a signal peptide of 20-25 residues. In the ER, the signal peptide is cleaved and the nascent protein is modified with N-linked glycans in asparagine residues (Kornfeld and Mellman, 1989, Tokhtaeva *et al.*, 2017). Once they reach the cis-Golgi, most of the lysosomal luminal enzymes are modified in the high mannose-type oligosaccharide residues with phosphate groups in a two-step enzymatic process. The first step is catalysed in the cis-Golgi by the N-acetylglucosamine (GlcNAc)-1-phosphotransferase (GNPT) complex. GNPT transfers a GlcNAc-1-phosphate from UDP-GlcNAc to a mannose residue in the modified lysosomal enzyme. The second step is catalysed in the trans-Golgi by α-N-acetylglucosaminidase, also known as the uncovering enzyme (UCE), encoded by *NAGPA*. UCE hydrolyses the GlcNAc-1-phosphodiester to expose the M6P groups (Kornfeld and Mellman, 1989, Hasanagic *et al.*, 2015). The resulting M6P residues are recognised by the MPR in the trans-Golgi network. Later, MPR release the modified lysosomal enzymes in late endosomes for lysosomal delivery (Thomas Braulke *et al.*, 2023).

1.4.1 The N-acetylglucosamine-1-phosphotransferase complex

GlcNAc-1-phosphotransferase is a heterohexameric complex of three subunits (α2β2γ2) encoded by *GNPTAB* and *GNPTG* (Bao *et al.*, 1996). *GNPTAB* encodes for the inactive GNPT α/β precursor protein which is further processed into GNPT α and GNPT β subunits. GNPT γ is a soluble protein that interacts with the GNPT α subunit in the Golgi lumen. Both GNPT α/β precursor protein and GNPT γ are synthesised in the ER and there modified with high mannose-type glycans. Upon reaching the cis-Golgi, the GNPT α/β precursor is processed into catalytically active GNPT α and GNPT β transmembrane subunits by site-1 protease (S1P). Subsequently, a small fraction of the precursor and mature forms are trafficked to the medial/trans cisternae of the Golgi and there modified into complex-type units. Then, these modified forms undergo retrograde transport back to the cis-Golgi where the GNPT complex is active (Braulke *et al.*, 2008, Encarnação *et al.*, 2011, Katrin Marschner, 2011, De Pace *et al.*, 2014, Van Meel *et al.*, 2014, Velho *et al.*, 2015).

The GNPT α/β precursor contains different domains essential for the catalytic core and UDP-GlcNAc binding site: N-terminus extension (NTE), four conserved regions (CR1–CR4) that together form a stealth domain, EF-hand domain (EF), and C-terminus extension (CTE). Additionally, in the GNPT α subunit two Notch repeats (N1 and N2), a domain associated with

DNA methyltransferase interactions (DMAP), and four spacer regions (S1-S4) have been identified. The S1 domain includes two tandem α/β roll motifs and plays a role in regulating the phosphotransferase activity by influencing the site of S1P-mediated cleavage in the precursor. The S2 domain interacts with the γ subunit. The S3 domain possibly inhibits the complex partially. The Notch repeats and DMAP domain are crucial for enzyme recognition and binding (Figure 1). GNPT γ contains an MPR homology domain and an additional DMAP domain that contributes to enzyme recognition by binding to high mannose-type glycans of lysosomal enzymes (Van Meel *et al.*, 2016, Gorelik *et al.*, 2020, Du *et al.*, 2022, Gorelik *et al.*, 2022, Li *et al.*, 2022).

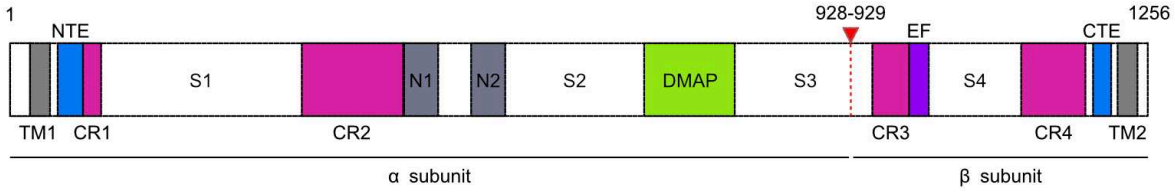

Figure 1 - Schematic representation of human GNPT α/β precursor structure.
TM = transmembrane domain; NTE = N-terminus extension; CR = conserved region; N = Notch repeats; DMAP = DNA methyltransferase interactions; red triangle signals the S1P cleavage site between residues 928 and 929; EF = EF-hand domain; CTE = C-terminus extension.

1.4.2 Site-1 protease

S1P is a membrane-bound serine protease, encoded by *MBTPS1.* S1P recognises and cleaves proteins with the consensus motif RxxL or RxLx (where R is an arginine, X is any amino acid, L is a leucine). S1P substrates include sterol regulatory element–binding proteins (SREBP) 1 and 2, activating transcription factor 6 (ATF6), members of the cAMP response element–binding protein (CREB) family, and the GNPT α/β precursor. Additionally, S1P is self-activated by autocatalytic cleavage of proS1P (Katrin Marschner, 2011, Danyukova *et al.*, 2022).

1.4.3 Mannose-6-phosphate receptors

The two MPR, 46 kDa cation-dependent MPR (CD-MPR/MPR46) and 300 kDa cation-independent MPR (CI-MPR/MPR300), are integral membrane glycoproteins that constitute the family of p-type lectins (Nancy M. Dahms, 2002). CI-MPR comprises two M6P-binding sites in the extracytoplasmatic region, while CD-MPR has only one M6P-binding site. Both receptors are present in the membrane as dimers, which facilitates the recognition of ligands with multiple M6P modifications.

MPR exhibit sorting signals in their cytoplasmic tail that allow recognition by adaptor proteins and sorting from the TGN to the endolysosomal system. The extracytoplasmatic region of the CI-MPR comprises multiple repeats with similar sequence and distribution of cysteine residues, with high similarity to a domain found in CD-MPR. These conserved regions are essential for carbohydrate recognition and ligand binding.

MPR are located in the TGN, endosomes, and plasma membrane. In the TGN, they recognise the M6P modification of newly synthesised lysosomal enzymes and get integrated into clathrin-coated vesicles for trafficking to endosomes. In the more acidic late endosome environment, the lysosomal enzymes dissociate from the MPR (Figure 2). Upon release of the lysosomal enzymes, the MPRs are recycled back to the TGN. When in the plasma membrane, MPRs can additionally reuptake enzymes that erroneously follow the secretory pathway (Jadots *et al.*, 1992, Ghosh *et al.*, 2003).

1.5 Mannose-6-phosphate independent pathways

As an alternative to M6P-dependent trafficking, various lysosomal enzymes can be trafficked to the lysosome in an M6P-independent manner (Figure 2). Patient samples and cell models showed that impairment of the M6P was not sufficient to completely abrogate the presence of intracellular lysosomal enzymes, suggesting the existence of an alternative pathway (Leroy and DeMars, 1967, Waheed *et al.*, 1982). The remaining enzymes do not bind to MPR in the TGN. These can alternatively bind two receptors in the TGN: lysosomal integral membrane protein 2 (LIMP-2) and sortilin (Stephane Lefrancois, 2003, Reczek *et al.*, 2007). These receptors deliver lysosomal enzymes to the lysosome in a similar manner as MPR, as they likewise exhibit cytoplasmic sorting motifs which allow them to be trafficked using the secretory pathways machinery.

Newly synthesised enzymes that do not bind any type of receptors in the TGN are secreted to the extracellular environment, taken up by membrane-associated proteins, and transported to lysosomes through endocytosis (Saftig and Klumperman, 2009, Hasanagic *et al.*, 2015). Several M6P-independent receptors have been described to be involved in this reuptake process, including the low-density lipoprotein receptor (LDLR), LDLR-related protein 1 (LRP1), and LRP2 (megalin) (Hiesberger *et al.*, 1998, Nielsen *et al.*, 2007, Markmann *et al.*, 2015). Hence, the sorting of enzymes via the M6P-independent pathway is very inefficient when compared to the M6P-dependent pathway.

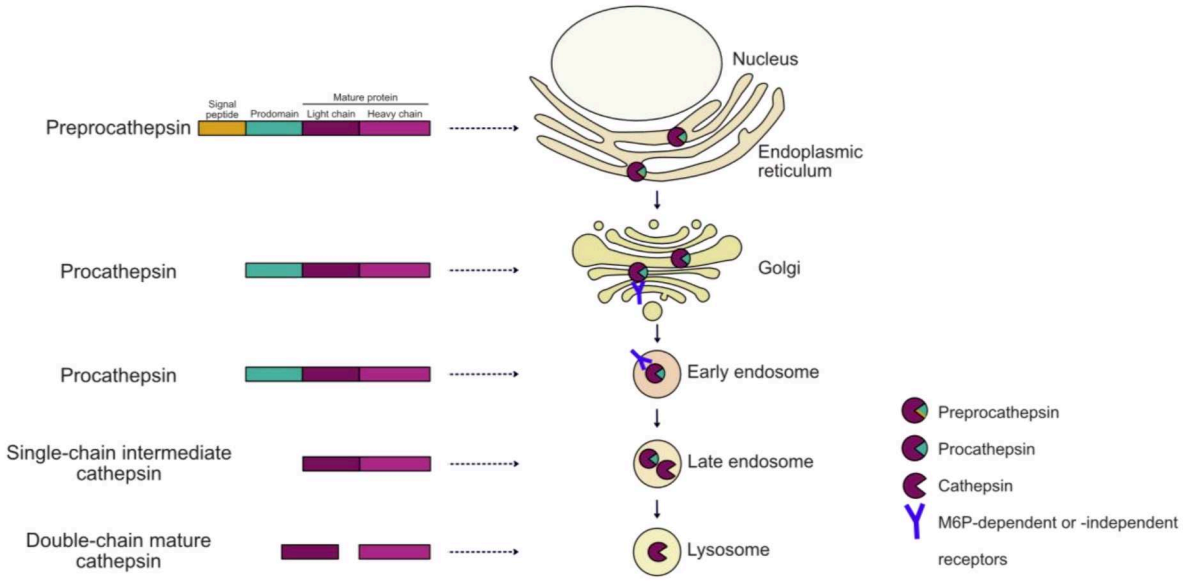

Figure 2 - Lysosomal cathepsins maturation and delivery to the lysosome.
Cathepsins are synthesised as a precursor procathepsins with an N-terminus signal peptide (preprocathepsin), which is cleaved in the endoplasmic reticulum. The resulting procathepsins, proteolytically active single-chain intermediates, pass through the Golgi and are recognised by M6P-dependent or -independent sorting receptors in the trans-Golgi network. Once in late endosomes, procathepsins are released from the receptors and get cleaved to a single-chain intermediate protein. Lastly, in lysosomes, procathepsins become active by cleavage into a two-chain mature form (an N-terminus light chain and a C-terminus heavy chain). This last processing step can be self-catalysed and/or catalysed by a different protease.

1.6 Cargo delivery to the lysosome

The lysosome serves as the central hub where both intracellular and extracellular cargo undergo degradation. Intracellular cargo reaches the lysosome through autophagy whereas extracellular cargo is internalised and subsequently transported to the lysosome via endocytosis.

1.6.1 Autophagy

Autophagy mediates the recycling of damaged organelles and aggregated or misfolded macromolecules in the lysosome, functioning as a clearance mechanism that ensures homeostasis (Klionsky *et al.*, 2021). Autophagy is initiated by the formation of autophagosomes, double-membraned vesicles that sequester intracellular cargo targeted for degradation by cargo receptors. An example of a cargo receptor is p62, or sequestosome 1 (p62/SQSTM1). p62 functions as a connecting molecule that recognises the degradation signal on the autophagic cargo and binds to LC3 on the expanding autophagosomal membrane. LC3 is an ubiquitin-like molecule that gets lipidated in the C-terminus with

phosphatidylethanolamine (PE). The lipidated form of LC3 (LC3-II) is then associated with the autophagosomal membrane. Later, the autophagosomes fuse with lysosomes, where autophagic cargo and associated receptors are degraded. In this final stage of autophagy, LC3-II is either released from the membrane or degraded in the lysosome together with the autophagic cargo. The resulting products of degradation can then be used to generate energy, provide precursor metabolites, and be used as building blocks in response to nutritional stress (Stolz *et al.*, 2014, Gómez-Virgilio *et al.*, 2022).

1.6.2 Endocytosis

Endocytosis is a process that allows cells to take up macromolecules from their environment. It represents one of the primary mechanisms through which cells interact with their surroundings, regulating nutrient uptake, cell signalling, and the removal of waste materials (Cooper, 2000). Endocytosis can be divided into phagocytosis, where cells engulf large particles, and pinocytosis, which involves the uptake of fluids and macromolecules within small vesicles.

Phagocytosis is triggered by the binding of cargo to phagocytic receptors present on the surface of phagocytic cells. This binding initiates the extension of actin-based protrusions from the cell surface, which gradually surround the particles forming a large intracellular vesicle, known as a phagosome. The phagosomes later fuse with lysosomes, where the internalised material is digested.

Receptor-mediated endocytosis, a type of pinocytosis, enables the selective uptake of specific macromolecules. Receptor-mediated endocytosis is initiated by the binding of macromolecules to specific cell surface receptors, which cluster within specialised regions of the plasma membrane known as clathrin-coated pits. These regions bud from the plasma membrane and form clathrin-coated vesicles containing the receptors and the respective ligands. Once inside the cell, the clathrin-coated vesicles fuse with early endosomes, where their content is sorted for transport to lysosomes or recycling to the plasma membrane (Palm and Thompson, 2017, Mettlen *et al.*, 2018).

Macropinocytosis is a type of pinocytosis that allows cells to non-selectively engulf macromolecules from the extracellular space. Macropinosomes are large vesicles formed by actin protrusions resulting from the ruffling of the plasma membrane (Dafna Bar-Sagi, 1986). When the membrane folds back, components of the extracellular environment surrounding the cells get internalised non-selectively. Macropinosomes can internalise large macromolecules that are usually excluded from other internalisation processes (Palm and Thompson, 2017). Once the macropinosome is inside the cell, it becomes mature and it is delivered to lysosomes in a process similar to endosome maturation. For example, once formed, macropinosome

membranes are coated with Rab5 which gets replaced by Rab7 for fusion with lysosomes (Palm, 2019, Commisso, 2022). Contrarily to other endocytic pathways, macropinocytosis is non-selective and it initiates independently of the presence of cargo but in response to growth factor signalling. Ras and PI3K downstream signalling of receptor tyrosine kinase rapidly initiate membrane ruffling via Rac1 and PAK1 kinase. Macropinocytosis is not only regulated by signalling pathways but also affects them. Amino acid pools generated by lysosomal catabolism of macropinocytosed cargo can activate mTORC1, the major regulator of growth and metabolism (Palm *et al.*, 2015).

1.7 Lysosomal storage disorders

Lysosomal storage disorders (LSDs) are rare diseases resulting from lysosomal dysfunction and impaired degradation of lysosomal substrates. Commonly, LSDs are characterised by the excessive accumulation of macromolecules in the endolysosomal system due to a deficiency in one or more hydrolases, membrane proteins, or non-enzymatic soluble lysosomal proteins (Platt *et al.*, 2012). Patients carrying LSD-driving mutations display severe growth retardation, skeletal and muscle dysplasia, and neurodegeneration (Lawrence and Zoncu, 2019).

Impaired activity of the GNPT complex due to autosomal recessive mutations results in a type of LSD named mucolipidosis II/III (ML II/III). Mutations in GNPTAB or GNPTG result in ML-II (no GNPT activity) and ML-III (reduced GNPT activity; less aggressive form). At the cellular level, impaired GNPT activity results in the loss/reduction of M6P modifications, missorting and hypersecretion of lysosomal enzymes, and accumulation of undigested lysosomal cargo (Platt *et al.*, 2012). Phenotypically, this accumulation affects particularly cartilage, bone, and connective tissues, resulting in the progressive development of skeletal and motor dysplasia, neurodegeneration, and cardiorespiratory abnormalities (Dogterom *et al.*, 2021).

More recently, mutations in *MBTPS1* were found in pediatric and young adult patients, causing an autosomal recessive skeletal disorder, spondyloepiphyseal skeletal dysplasia. Similarly to patients with ML II/III, these patients are characterised by dysmorphic facial features, short stature, variable intellectual disabilities, and clonic seizures. At the cellular level, patient-derived mutations in S1P cause a partial defect in the M6P pathway resulting in hypersecretion of lysosomal enzymes. In addition to the effect in the M6P, mutations in the S1P affect lipid biosynthesis and ER stress response. Thus, mutations in *MBTPS1* lead to a wide variety of clinical phenotypes due to the existence of multiple S1P substrates and how

the mutations affect S1P activity, stability, and substrate binding (Kondo *et al.*, 2018, Schweitzer *et al.*, 2019, Carvalho *et al.*, 2020, Thomas Braulke *et al.*, 2023).

1.8 Lysosomal function in cancer

Cancer is in part characterised by dysregulated cell growth and is often associated with alterations in cellular metabolism. One of the key hallmarks of cancer metabolism is the ability of cancer cells to adapt to the challenging nutrient-deprived microenvironments within solid tumours. To sustain their rapid proliferation and survival in these adverse conditions, cancer cells have evolved various strategies for acquiring nutrients. Alterations in lysosome biogenesis and function contribute to cancer progression, as cancer cells exploit lysosomal pathways for nutrient generation and maintenance of cell homeostasis. During nutrient scarcity, cells inactivate mTORC1 leading to an increase in autophagy and lysosomal degradation of extracellular cargo (Degenhardt *et al.*, 2006, Palm *et al.*, 2015, Ratto *et al.*, 2022).

1.8.1 Autophagy in cancer

Autophagy has an ambiguous role in tumourigenesis by both promoting and suppressing tumourigenesis. Autophagy serves as a significant homeostatic mechanism within cells, ensuring cellular integrity, maintaining redox balance, and sustaining proteostasis (Klionsky *et al.*, 2021). Given these functions, autophagy might have a protective role against cancer. Evidence suggests that loss of autophagy-related genes leads to tumour formation. Nevertheless, this effect is tissue and gene-specific, being in some cases only observable in combination with other genetic alterations (Lebovitz *et al.*, 2012). Another evidence for the role of autophagy in tumour suppression is the regulation of autophagy-related gene expression by the tumour suppressor p53 (Tasdemir *et al.*, 2008).

In established tumours, autophagy promotes tumour growth, particularly in regions where nutrients are scarce, sustaining tumour development (Degenhardt *et al.*, 2006). Preclinical studies showed that autophagy supports the growth and metabolic processes of advanced tumours, in response to oncogene signalling and/or inactivation of tumour suppressors. Thus, certain Ras-driven cancers become dependent on autophagy as these tumours rarely progress in the absence of autophagy (Debnath *et al.*, 2023). Recently, autophagy was shown to promote immune evasion by degrading MHC-I antigen, which leads to reduced T cell response and increased tumour growth (Yamamoto *et al.*, 2020).

The role of autophagy in the formation of metastasis remains controversial. Initial studies suggested that autophagy has pro-metastatic effects, by inducing cell migration,

invasion, epithelial-mesenchymal transition (EMT), resistance to detachment-induced cell death, adaptation to nutrient deprivation and hypoxia, and survival in distant tissue microenvironments. On the contrary, more recent research suggests that autophagy may limit the metastatic process by controlling the transition of metastatic cells from dormancy to an active state and metastatic recurrence (Debnath *et al.*, 2023).

In the context of cancer therapies, autophagy can sustain cancer cells' survival upon therapy-induced stress, being responsible for acquired resistance. In different tumour mouse models where autophagy was pharmacologically or genetically inhibited, tumour growth was reduced and apoptosis of cancer cells increased upon treatment (Kimmelman and White, 2017).

Controversially, autophagy does not promote cellular growth, as there is no increase in nutrient intake, but recycling of intracellular content in response to starvation, which can result in cell deterioration in the long term (Lum *et al.*, 2005, Palm and Thompson, 2017).

1.8.2 Degradation of extracellular proteins for nutrient acquisition in cancer

To overcome metabolic challenges, cancer cells accumulate genetic mutations that enhance nutrient uptake and evolve to become metabolically flexible. This enables them to adapt to fluctuating nutrient availability within the tumour microenvironment. Macropinocytosis allows cells to survive and proliferate in nutrient-poor environments by non-selectively engulfing large amounts of macromolecules from the extracellular space. These macromolecules are digested in the lysosome, a process that continuously provides the necessary building blocks to sustain survival and proliferation. Although different tumour types can exploit this external source of amino acids, most of the studies and the first evidence for the use of extracellular protein as a nutrient uptake pathway in cancer cells were observed in pancreatic cancer cells. Physiological levels of extracellular protein enable pancreatic cancer cells to continue proliferating in amino acid-deprived conditions (e.g. limited levels of leucine, glutamine, essential amino acids, etc.). Interestingly, most pancreatic cancer patients harbour oncogenic Ras mutations (Commisso *et al.*, 2013, Davidson *et al.*, 2017, Nofal *et al.*, 2017).

Macropinocytosis is controlled by intrinsic and extrinsic signalling. Intracellularly, Ras and PI3-Kinase regulate actin dynamics and macropinosome formation (Swanson, 2008, Mercer and Helenius, 2009). H-Ras and K-Ras mutations that produce a constitutively active protein potently enhance membrane ruffling (Dafna Bar-Sagi, 1986, Natalie Porat-Shliom *et al.*, 2008). Expression of constitutively active mutants of PIK3CA or deletion of PTEN was also described to enhance macropinocytosis (Amyere *et al.*, 2000, Palm *et al.*, 2017, Kim *et al.*, 2018). Extracellularly, macropinocytosis responds to growth factor signalling, such as the activation of receptor tyrosine kinase (RTK) (Swanson, 2008, Mercer and Helenius, 2009).

Cancer cells increase macropinocytosis in response to epidermal growth factor (EGF) and platelet-derived growth factor (PDGF) (K Mellström *et al.*, 1988, West *et al.*, 1989, Skorda *et al.*, 2023). Although mammalian cells express a large variety of RTKs, they signal through common downstream effectors, Ras and PI3-kinase, to induce membrane ruffling and macropinocytosis.

The conservation of macropinocytosis throughout various eukaryotes implies that this endocytic route likely developed alongside the lysosomal system as a means of obtaining nutrients (Palm and Thompson, 2017). For instance, rat carcinoma was observed to accumulate high levels of radioactively labelled albumin, indicating that tumour tissue can take up albumin from the surrounding environment (Stehle *et al.*, 1997). Similarly, in more recent studies, *in vivo* uptake of high-molecular-weight dextran was detected in pancreatic tumours from mice and human patients, providing concrete proof of macropinocytosis in cancer cells (Commisso *et al.*, 2013, Kamphorst *et al.*, 2015). Cosimo Commisso *et al.* observed that Ras-transformed cells can uptake extracellular protein via macropinocytosis and retrieve amino acids to support cell proliferation, under nutrient deficiency (Commisso *et al.*, 2013). Palm *et al.* reported that when free amino acids are depleted from the medium, mTORC1 inactivation enhances cell proliferation by increasing the lysosomal catabolism of extracellular protein. Thus, mTORC1 limits cell growth when macropinocytosis is required for proliferation. Moreover, in murine pancreatic ductal adenocarcinoma (PDAC) tumours harbouring KRAS mutation and treated with rapamycin, tumour growth was reduced in the outer regions of the tumour, characterised by a high degree of vascularisation. Conversely, within the inner poorly vascularised regions of the tumour, rapamycin treatment led to an enhancement in proliferation (Palm *et al.*, 2015). These findings underscore the significance of extracellular protein degradation through macropinocytosis in supporting the nutritional needs of cancer cells within the complex tumour microenvironment.

While much attention has been focused on albumin, it is important to recognise that the extracellular matrix and cellular debris, which constitutes a significant portion of extracellular biomass in tissues, represents another potential nutrient source. Indeed, cancer cells can utilise other alternative external sources of nutrients, such as vesicular bodies, cell debris, or collagen (Krajcovic *et al.*, 2013, Davidson *et al.*, 2017, Olivares *et al.*, 2017, Jayashankar and Edinger, 2020).

2. Aim of the thesis

Cancer cells are surrounded by a variety of nutrients, including amino acids and extracellular proteins. When in nutrient-rich conditions, cells preferentially take up free amino acids to meet their nutritional demand. However, most of the amino acids in the extracellular space are contained within proteins. Cells can engulf extracellular proteins and degrade them into their constituent amino acids in lysosomes. This process is frequently exploited by cancer cells, enabling them to thrive in poorly vascularised tumours. However, the ability of cells to utilise extracellular proteins as a nutrient source remains incompletely elucidated. In my PhD project, I aimed at better understanding the mechanisms that mediate cell proliferation when cells depend on amino acid acquisition from extracellular protein. To this end, I conducted pooled genome-wide CRISPR screens that selected proliferating pancreatic cancer cells in different metabolic conditions, where cancer cells grow either by the import of free amino acids or by the uptake and lysosomal degradation of extracellular proteins. One particularly striking hit was the uncharacterised gene TMEM251/LYSET. I then focused on the mechanistic characterisation of LYSET function. First, I assessed the impact of LYSET on the metabolic adaptation of cells growing by generating amino acids through lysosomal albumin catabolism and in tumour growth in mice. Next, I characterised LYSET as a component of the mannose-6-phosphate pathway for lysosomal enzyme sorting and its role in lysosomal biogenesis. Finally, I characterised the role of LYSET in hereditary LSDs. Thus, my PhD project revealed the role of LYSET in lysosomal catabolism, nutrient generation, and pathologies.

3. Materials and methods

3.1 Materials

3.1.1 Cell lines

Table 1 - List of cell lines

Cell line name	Source
MIA PaCa-2	ATCC CRL-1420
AsPC-1	ATCC CRL-1682
HAP1	(Jan E. Carette *et al.*, 2009)
Hs766t	ATCC HTB-134
MCF-7	ATCC HTB-22
Panc1	ATCC CRL-1469
Panc03.27	ATCC CRL-2549
PaTu 8988T	DSMZ ACC 162
SKMEL-30	DSMZ ACC151
HEK 293T	ATCC CRL-3216
SV40 large T-immortalised MEFs	(Palm *et al.*, 2015)

3.1.2 Cell culture reagents

Table 2 - List of cell culture reagents

Cell culture reagent	Company	Catalogue number/ reference
DMEM/F-12	Gibco	11320033
DMEM	Gibco	41965039
FBS	Gibco	10270106
Glutamine	Gibco	25030081
Puromycin	Santa Cruz Biotechnology	sc-108071A
Blasticidin	Santa Cruz Biotechnology	sc-495389
Geneticin (G418)	GIBCO/Invitrogen	10131035
Hygromycin	GIBCO/Invitrogen	10687010
Doxycycline	Sigma Aldrich	J67043
Amino acid-free, glucose-free DMEM/F-12	US Biological	D9807-11
Glucose	Sigma Aldrich	G7021
Sodium bicarbonate	Sigma Aldrich	S5761
Probumin® Bovine Serum Albumin Media Grade	Sigma Aldrich	810683

3.1.3 Primary antibodies

Table 3 - List of primary antibodies for immunoblot and immunofluorescence

Antibody	Company	Catalogue number/ reference
TMEM251/LYSET	Atlas antibodies	HPA048559
GM130	BD Biosciences	610822
APC anti-CD46	Biolegend	352405
Golgin-97/GOLGA1	Cell Signaling	13192
SQSTM1/p62	Cell Signaling	39749
Myc-tag 9B11	Cell Signaling	2276
Flag-tag	Genscript	A00187-200
GAPDH	Origene	TA802519
Calreticulin	Cell Signaling	12238S
Cathepsin B	R&D Systems	AF953
Cathepsin L	R&D Systems	AF952
Glucosylceramidase	R&D Systems	MAB7410
Hexosaminidase A	R&D Systems	AF6237
Mouse cathepsin B	R&D Systems	AF965-SP
ATF-6α	Santa Cruz Biotechnology	sc-22799
B-actin	Sigma Aldrich	A5441
M6P-scfv	Kind gift from Thomas Braulke	(Muller-Loennies *et al.*, 2010)
GNPTAB α-subunit	Kind gift from Thomas Braulke	(De Pace *et al.*, 2014)
Lc3	Kind gift from Tullia Lindsten	(Cheong *et al.*, 2014)

3.1.4 Secondary antibodies

Table 4 - List of secondary antibodies for immunoblot and immunofluorescence

Antibody	Company	Catalogue number/ reference
Alexa Fluor 488 anti-rabbit	Life Technologies	A11034
Alexa Fluor 647 anti-mouse	Life Technologies	A21236
HRP anti-goat	Life Technologies	31402
HRP anti-sheep	Life Technologies	A16047
HRP anti-mouse	Cytiva	NA931
HRP anti-rabbit	Cytiva	NA934

3.1.5 Fluorescent probes

Table 5 - List of fluorescent probes used for confocal microscopy and flow cytometry

Fluorescent Probe	Company	Catalogue number/ reference
Alexa Fluor 647 BSA	Life Technologies	A34785
Oregon Green 488 10 kDa dextran	Life Technologies	D7170
Alexa Fluor 568 10 kDa dextran	Life Technologies	D22912
DQ Green BSA	Life Technologies	D12050
Hoechst 33342	Life Technologies	H1399
Lysotracker Red	Life Technologies	L7528

3.1.6 Chemicals, inhibitors, and solutions

Table 6 - List of chemicals, inhibitors, and solutions

Inhibitor name	Company	Catalogue number/ reference
Bafilomycin A1	Cayman Chemical	AZD8055
MG132	Cayman Chemical	13697
Thapsigargin	Tocris	1138
Benzamidine	Sigma Aldrich	12072
E64	Serva	21100
AEBSF	Serva	12745
Aprotinin	Serva	13718
Leupeptin	Serva	51867
Pepstatin	Serva	52682
Halt Protease Inhibitor Mix	Thermo Fisher Scientific	78429
Halt protease and phosphatase inhibitor cocktail	Thermo Fisher Scientific	78444
Sodium orthovanadate	MP Biomedicals	159664
Sodium fluoride	Alfa Aesar	A13019
Sodium pyrophosphate	Alfa Aesar	A17546
Sodium glycerophosphate	Alfa Aesar	A16269
ProLong™ Gold Antifade Mountant with DNA Stain DAPI	Life Technologies	P36935
Polyethylenimine (PEI, MW 25000)	Polysciences	24314
Polybrene	Tocris	7711
Proteinase K	NEB	P8107S
Skim milk powder	Gerbu Biotechnik	1602
Mass Spec Grade water	Thermo Fisher Scientific	51140
Tris Base	Sigma Aldrich	648310
DNAse-free RNAse	Sigma Aldrich	11119915001
UltraPure™ SDS Solution 10%	Thermo Fisher Scientific	15553027
Phenol	Th. Geyer	10673955
2-propanol	Serva	39559
TEMED	Carl Roth	2367

APS	Thermo Fisher Scientific	17874
SDS	Serva	20765
Triton X-100	Sigma Aldrich	93443
Agarose	Sigma Aldrich	A9539
Acrylamide	Carl Roth	A121.1
NuPAGE™ LDS Sample Buffer (4X)	Thermo Fisher Scientific	NP0007
DTT	Thermo Fisher Scientific	R0861
β-mercaptoethanol	Sigma Aldrich	M3148
NH4Cl	Th. Geyer	12579
Fatty acid-free BSA	EMD Millipore	126579
BSA for blocking solutions	Serva	11930
Receptor-grade BSA Fraction V	Serva	11924
Clarity Max Western ECL substrates	Bio-Rad	1705062
SuperSignal West Atto	Thermo Fisher Scientific	A38554
Amersham ECL Prime	Cytiva	RPN2232
Trizol	Invitrogen	15596026
Chloroform	Carl Roth	7331
Isopropanol	Serva	39559
Ethanol	Th. Geyer	11832330
EDTA	Sigma Aldrich	E9884
Oligo-dT	Life Technologies	18418012
dNTP mix 10 MM	Life Technologies	R0194
SYBR green master mix	Life Technologies	4309155
Normal goat serum	Life Technologies	10000C
Paraformaldehyde	Sigma Aldrich	P6148
Sucrose	Sigma Aldrich	S0389
Tris-HCl	Thermo Fisher Scientific	A18494
Sodium chloride	Fisher Scientific	10735921
HEPES	Life Technologies	15630080
Magnesium chloride	VWR	SIALM2670
Calcium chloride	Sigma Aldrich	C3306
Magnesium acetate	Sigma Aldrich	M5661

Potassium chloride	Carl Roth	6781.1
Glycerol	VWR	E520
PMSF	Carl Roth	6367.2

3.1.7 Backbone vectors

Table 7 - List of plasmids and backbone vectors used for cloning

Vectors	Source
psPAX2	Addgene 12260
pCMV-VSV-G	Addgene 8454
Gag-Pol	Addgene 14887
pRRL-SFFV-rtTA3-IRES-EcoR-PGK-PuroR	(de Almeida *et al.*, 2021)
pRRL-SFFV-rtTA3-IRES-EcoR-PGK-HygroR	(de Almeida *et al.*, 2021)
pLentiv2-TRE3G-Cas9-P2A-BFP	(de Almeida *et al.*, 2021)
pLentiv2-TRE3G-Cas9-P2A-GFP	(de Almeida *et al.*, 2021)
pLenti-hU6-sgRNA-iT-EF1as-Thy1.1-P2A-NeoR	(de Almeida *et al.*, 2021)
pLenti-hU6-sgRNA-iT-EF1α-mCherry-P2A-NeoR	(de Almeida *et al.*, 2021)
Dual-hU6-sgRNA-mU6-sgRNA-EF1α-mCherry-P2A-PuroR	(de Almeida *et al.*, 2021)
Dual-hU6-sgRNA-mU6-sgRNA -Ef1a-Thy1.1-P2A-NeoR	(de Almeida *et al.*, 2021)
pSpCas9(BB)-2A-GFP (PX458)	Addgene 48138
pLenti-Cas9-BlastR	Addgene 52962
pLenti-Cas9-EGFP-PuroR	Addgene 86145
pLenti-CRISPR v2-PuroR	Addgene 52961
pBabe-PuroR	Addgene 1764
pRRL-pUbC-tagRFP-T-Hygro	A kind gift from Florian Schmidt
pLV-EF1a-IRES-NeoR	Addgene 85139
pLV-Ef1a-IRES-Hygro	Addgene 85134
pLV-Ef1a-IRES-Blast	Addgene 85133
pcDNA3.1-GNPTAB-myc	A kind gift from Thomas Braulke

3.1.8 Generated plasmids

Table 8 - List of plasmids generated in this study

Generated plasmids	Backbone vector
PX458 + respective sgRNA	PX458
pLenti-hU6-sgRNA-iT-EF1as-Thy1.1-P2A-NeoR + respective sgRNA	pLenti-hU6-sgRNA-iT-EF1as-Thy1.1-P2A-NeoR
pLenti-hU6-sgRNA-iT-EF1α-mCherry-P2A-NeoR + respective sgRNA	pLenti-hU6-sgRNA-iT-EF1α-mCherry-P2A-NeoR
Dual-hU6-sgRNA-mU6-sgRNA-EF1α-mCherry-P2A-PuroR + respective sgRNA	Dual-hU6-sgRNA-mU6-sgRNA-EF1α-mCherry-P2A-PuroR
Dual-hU6-sgRNA-mU6-sgRNA -Ef1a-Thy1.1-P2A-NeoR + respective sgRNA	Dual-hU6-sgRNA-mU6-sgRNA -Ef1a-Thy1.1-P2A-NeoR
pLenti-CRISPR v2-PuroR + respective sgRNA	pLenti-CRISPR v2-PuroR
pBabe LYSET_iso1-PuroR	pBabe-PuroR
pBabe LYSET_iso2-PuroR	pBabe-PuroR
pRRL-pUb-LYSET_iso2-HygroR	pRRL-pUbC-tagRFP-T-Hygro
pRRL-pUb-LYSET^{R45W}-HygroR	pRRL-pUbC-tagRFP-T-Hygro
pRRL-pUb-LYSET^{Y72X}-HygroR	pRRL-pUbC-tagRFP-T-Hygro
pLV-EF1a-C-Flag-IRES- BlastR	pLV-EF1a-IRES-BlastR
pLV-EF1a-GNPTAB-Flag- BlastR	pLV-Ef1a-IRES-BlastR
pLV-EF1a-GNPTAB-myc-BlastR	pLV-EF1a-IRES-BlastR
pLV-EF1a-GNPTAB-myc-NeoR	pLV-Ef1a-IRES-NeoR
pRRL-pUb-GNPTAB-myc-HygroR	pRRL-pUbC-tagRFP-T-Hygro
pRRL-pUb-GNPTAB^{K4Q}-myc-HygroR	pRRL-pUbC-tagRFP-T-Hygro
pRRL-pUb-GNPTAB^{S15Y}-myc-HygroR	pRRL-pUbC-tagRFP-T-Hygro
pRRL-pUb-GNPTAB_Q36L,E39L-myc-HygroR	pRRL-pUbC-tagRFP-T-Hygro

3.1.9 sgRNA sequences

Table 9 - List of sgRNA sequences

Gene	Specie	Name	sgRNA sequence 1	sgRNA sequence 2
AAVS1	human	AAVS1_sgRNA1	GCTGTGCCCCGATGCACAC	
CD46	human	CD46_sgRNA1	GGAGTACAGCAGCAACACCA	
TSC2	human	TSC2_sgRNA1	GCACCAGAAGGAATTCCG	
TSC2	human	TSC2_sgRNA2	GAGACACATCACCTACTTGG	
LYSET	human	LYSET_sgRNA1	GGATGGGATGGATTGGAGT	
LYSET	human	LYSET_sgRNA2	GAATGATGAACTTCCGTCAG	
ATF4	human	ATF4_sgRNA1	GGGGAAGAGGTTGTAAGA	
ATF4	human	ATF4_sgRNA2	GGTCATCTATACCCAACA	
SLC7A5	human	SLC7A5_sgRNA1	GGAACATCACGCTGCTCAA	
SLC7A5	human	SLC7A5_sgRNA2	GTGAACTGCTACAGCGTGA	
TGFBRAP1	human	TGFBRAP1_sgRNA1	GTCGTTGGTGCCCACGTAG	
TGFBRAP1	human	TGFBRAP1_sgRNA2	GGGTGCAGATCGTCAAGG	
VPS18	human	VPS18_sgRNA1	GGCAAATGAGCCCAACCACG	
VPS18	human	VPS18_sgRNA2	GCGAGTCTGGGAGTACCCAG	
GNPTAB	human	GNPTAB_sgRNA1	GATTGACGTTGTTTACACCT	
GNPTAB	human	GNPTAB_sgRNA2	GACAGAGAAATCCGAACAC	
LYSET	human	LYSET_dsgRNA1	GGATGGGATGGATTGGAGT	GAGCTGATCCCAAAACAG
LYSET	human	LYSET_dsgRNA2	GAATGATGAACTTCCGTCAG	GAGCTGATCCCAAAACAGT
GNPTAB	human	GNPTAB_dsgRNA1	GATTGACGTTGTTTACACCT	GGAGGAGCAGAAAGCAATG
GNPTAB	human	GNPTAB_dsgRNA2	GACAGAGAAATCCGAACAC	GACAATCCGGTCAATCATGTG
Chr1.1	human	Chr1.1_dsgRNA1	GACAATGAACATAAGCACAT	GTTTGGCCTGAAATCCCACC
Chr1.3	human	Chr1.3_dsgRNA1	GAGCAGCAAACACTTGAAGT	GACAATGAACATAAGCACAT
Lyset	mouse	Lyset_dsgRNA1	GAATGATGAACTTCCGTCAG	GAGCGGATCCCAAAACAGT
Lyset	mouse	Lyset_dsgRNA2	GAGCGGATCCCAAAACAGT	GAAATCAATGAGACTTACAAC
Gnptab	mouse	Gnptab_dsgRNA1	GTGAGGTTAAAATAGATCG	GGAGTGAAATATTTACCC

Gnptab	mouse	Gnptab_dsgRNA2	GAAACAAAAGGCAACCTGG	GATACACCTGATAATGCACA G
Chr1.1	mouse	Chr1.1_dsgRNA1	GACAATGAACATAAGCACAT	GTTTGGCCTGAAATCCCACC
Chr1.3	mouse	Chr1.3_dsgRNA1	GAGCAGCAAACACTTGAAGT	GACAATGAACATAAGCACAT

3.1.10 Commercial kits

Table 10 - List of commercial kits

Kits	Company	Catalogue number/ reference
Pierce BCA Protein Assay Kit	Thermo Fisher Scientific	23227
Bio-Rad Protein Assay Dye Reagent	Bio-Rad	5000006
Precision Plus Protein Dual Color Standards	BioRad	1610374EDU
DNA 1Kb ladder	NEB	N3200L
DNA 100bp ladder	NEB	N3231L
HiFi DNA Assembly Master Mix	NEB	E2621X
QIAprep Spin Miniprep Kit	QIAGEN	27106
QIAquick PCR Purification Kit	QIAGEN	28106
QIAquick Gel Extraction Kit	QIAGEN	28706X4
NEBuilder® HiFi DNA Assembly Cloning Kit	NEB	E2621L
Q5 Site-Directed Mutagenesis Kit	NEB	E0554S
Pierce Protein Concentrator PES with 10 kDa molecular weight cut-off	Thermo Fisher Scientific	88527
Duolink In Situ Red Starter Kit Mouse/Rabbit	Sigma Aldrich	DUO92101
AmpliTaq Gold™	Thermo Fisher Scientific	43-118-20
MycoAlert Mycoplasma Detection	Lonza	LT07

3.1.11 Enzymes

Table 11 - List of commercial enzymes

Enzymes	Company	Catalogue number/ reference
SuperScript III Reverse Transcriptase	Invitrogen	18080093
T7 DNA Ligase	NEB	M0318
T4 Polynucleotide Kinase	NEB	M0201
FastDigest Esp3I	NEB	FD0454
FastDigest BpiI	Thermo Fisher Scientific	FD1014
EcoRI-HF	NEB	R3101
BamHI	NEB	R3136
Q5® High-Fidelity DNA Polymerase	NEB	M0491L
Endo H	NEB	P0702
PNGase F	NEB	P0710

3.1.12 Buffers

Table 12 - List of buffers and respective recipes

Buffer	Recipe
PBS 10X (1 L)	80 g NaCl
	14.4 g Na2HPO4
	2.4 g KH2PO4
	2 g KCl
	pH to 7.4
	miliQ H2O up to 1 L
	Autoclave at 121°C.
SDS-PAGE Running & Transfer Buffer 10x (1 L)	30.3 g Tris base
	144 g Glycine
	miliQ H2O up to 1 L
SDS-PAGE Running Buffer	1x SDS-PAGE Running & Transfer Buffer
	0.1 % SDS
Transfer Buffer	1x SDS-PAGE Running & Transfer Buffer
	0.02 % SDS
	10-20 % methanol
TBST	20 mM Tris base
	150 mM NaCl
	0.1 % Tween-20
	pH to 7.5
Western Blot Stripping Buffer	200 mM Glycine
	0.1 % SDS
	pH 2.2
Ponceau S Staining Solution	0.2 % Ponceau S
	5 % Glacial Acetic Acid
Standard protein lysis buffer	50 mM HEPES pH 7.4
	40 mM NaCl
	2 mM EDTA
	1 mM Na orthovanadate

	50 mM NaF
	10 mM Na pyrophosphate
	10 mM Na glycerophosphate
	1% Triton X-100
Homogenisation buffer	10 mM HEPES (pH 7.4)
	250 mM sucrose
	1 mM MgCl2
	1 mM CaCl2
	1.5 mM MgAc
	1 mM DTT
	1x protease inhibitors
RIPA buffer	150 mM NaCl
	1% Igepal CA-30
	0.5% Na deoxycholate
	0.1% SDS
	50 mM Tris-HCl pH 7.4
	1x protease inhibitors
Nuclei separation lysis buffer	10 mM HEPES pH 7.4
	0.1% Triton X-100
	10 mM KCl
	1.5 mM MgCl2
	340 mM sucrose
	10% glycerol
	1 mM DTT
	1 mM PMSF
Nuclei lysis buffer	50 mM Tris-HCl pH 7.4
	1% Triton X-100
	0.1% SDS
	400 mM NaCl
	1 mM EDTA
Laemmli Sample Buffer (4x)	250 mM Tris pH 6,8
	50 % Glycerol

	5 % SDS (20 %)
	0.05 % Bromophenol Blue
	10 % beta-Mercaptoethanol
BSA solution for Antibodies	5 % BSA
	0.2125 % NaCl
	0.025 % NaAzide
Genomic DNA extraction lysis buffer	10 mM Tris-HCl
	150 mM NaCl
	10 mM EDTA
	0.1% SDS
Tris/Borate/EDTA (TBE) Buffer	89 mM Tris base
	89 mM Boric acid
	2 mM Na_2EDTA pH 8
4 % paraformaldehyde (100ml)	4 g Paraformaldehyde
	20 ml miliQ H2O
	80 µl 1N NaOH
	Dissolve at 65 ^oC
	10 ml 10x PBS
	70 ml miliQ H2O
	pH 7.2-7.3
Immunofluorescence blocking solution	0.5 % BSA
	4 % normal goat serum
	in PBS
Flow cytometry buffer	5 % FBS in PBS

3.1.13 Acrylamide gels recipe

Table 13 - Acrylamide gel recipes for SDS-PAGE

Resolving Gel %	Solutions	Volume for 5 mL
7.5 %	H_2O	2.45 mL
	1,5 M Tris pH 8,8	1.25 mL
	30% Rotiphorese	1.25 mL
	10% SDS	50 µL
	10% APS	50 µL
	TEMED	5 µL
10 %	H_2O	1.979 mL
	1,5 M Tris pH 8,8	1.237 mL
	30% Rotiphorese	1.633 mL
	10% SDS	50 µL
	10% APS	50 µL
	TEMED	5 µL
12 %	H_2O	1.732 mL
	1,5 M Tris pH 8,8	1.237 mL
	30% Rotiphorese	1.93 mL
	10% SDS	50 µL
	10% APS	50 µL
	TEMED	5 µL
15 %	H_2O	1.237 mL
	1,5 M Tris pH 8,8	1.237 mL
	30% Rotiphorese	2.425 mL
	10% SDS	50 µL
	10% APS	50 µL
	TEMED	5 µL

Stacking Gel %	Solutions	5 mL
5 %	H_2O	3.424 mL
	1,5 M Tris pH 6,8	634 µL
	30% Rotiphorese	836 µL
	10% SDS	50.352 µL
	10% APS	50 µL
	TEMED	5 µL

3.1.14 Instruments

Table 14 - List of instruments

Instrument	Company
ChemiDoc Imaging system	Bio-Rad
Leica TCS SP5 confocal microscope	Leica
CASY Cell Counter and Analyzer	OMNI Life Sciences
Guava easyCyte flow cytometer	Merck
Lightcycler 480	Roche
Infinite 200 Pro plate reader	Tecan
Synergy H1 plate reader	BioTek
LAS 4000 Gel Imager	Fuji
LSR Fortessa Cell Analyzer	Becton Dickinson (BD) Biosciences
FACSAria III cell sorter	Becton Dickinson (BD) Biosciences
DigestPro MSi robotic system	INTAVIS Bioanalytical Instruments AG
Ultimate 3000 UPLC system	Thermo Fisher Scientific
Orbitrap Exploris 480 mass spectrometer	Thermo Fisher Scientific
Multi-Mode Plate Reader Synergy H1	BioTek
HiSeq 2500 platform	Illumina

3.1.15 Software and tools

Table 15 - List of software and tools

Software	Source
NEBbuilder Assembly Tool	nebuilder.neb.com
online oligo design tool	www.pcr-tagging.com
Image Lab (version 3.0.1.14)	BioRad
ImageJ / FIJI (version 1.52e)	(Schindelin *et al.*, 2012)
MaxQuant (version 1.6.14.0)	(Tyanova *et al.*, 2016)
GraphPad Prism (version 9.0.0)	Prism
Leica LAS AF software (v2.6.3.8173)	Leica
FACSDiva software (version 8.0, FACSAria I)	Becton Dickinson (BD) Biosciences
FlowJo™ Software (version v10.6)	BD Life Sciences
R-package limma	(Ritchie *et al.*, 2015)
UCSF ChimeraX	https://www.cgl.ucsf.edu/chimerax/

3.1.16 Miscellaneous

Table 16 – List of miscellaneous materials

Other	Provider
PVDF membranes	Biorad 1620184
Nitrocellulose membranes	Biorad 1620112
KIMBLE Dounce tissue grinder	Sigma Aldrich
8-well chambered coverslips	IBIDI 80826
16-well chamber slides	Thermo Fisher Scientific 178599
Acclaim PepMap300 C18, 5 µm, 300 Å wide pore	Thermo Fisher Scientific 11362223
NanoEase MZ Peptide analytical column	Waters 186008794
PhaseLock Gel – LIGHT	QuantaBio 733-2477
AMPure XP Bead-Based Reagent	Beckman Coulter A63881
DexoMAG C	Liquids Research
LS MACS column	Miltenyi Biotec 130-042-401

3.2 Methods

3.2.1 Cell culture

All cell lines (Table 1) were maintained at 37 °C and 5 % CO_2 and routinely tested for mycoplasma contamination (MycoAlert Mycoplasma Detection). Human cell lines were authenticated by Single Nucleotide Polymorphism typing by Multiplexion. Cells were cultured in DMEM/F-12 supplemented with 10 % FBS and 2 mM glutamine. HEK 293T were cultured for viral production in DMEM supplemented with 10 % FBS and 2 mM glutamine.

3.2.1.1 Starvation cell culture medium

Experiments with amino acid-deficient and protein-rich cell culture media were performed using amino acid-free and glucose-free DMEM/F-12. Glucose and sodium bicarbonate were re-added to standard DMEM/F-12 concentrations and media pH was adjusted to 7.3 with HCl. For the amino acid-rich medium, all amino acids were re-added to standard DMEM/F-12 concentrations (Table 17). The leucine-poor medium was prepared with 10 % FBS and 5 µM leucine, protein-rich media with supplementation of 4 % probumin, and media were replenished every second day.

Table 17 - List of amino acids and concentration of each in standard DMEM/F-12

Amino acid	Concentration in DMEM/F-12	Provider	Catalogue number/ reference
Alanine	50 M	Sigma Aldrich	A0325000
Arginine:HCl	699 M	Sigma Aldrich	A1271000
Asparagine:H2O	50 M	Sigma Aldrich	Y0000305
Aspartate	50 M	Sigma Aldrich	A9256
Cysteine:HCl:H2O	100 M	Sigma Aldrich	C3290000
Cystine:2HCl	100 M	Sigma Aldrich	C3300000
Glutamate	50 M	Sigma Aldrich	G8415
Glutamine	2.5 mM	Gibco	25030
Glycine	250 M	Sigma Aldrich	G5417
Histidine:HCl:H2O	150 M	Sigma Aldrich	H0755000
Isoleucine	416 M	Sigma Aldrich	I0460000
Leucine	450 M	Sigma Aldrich	L0375000
Lysine:HCl	499 M	Sigma Aldrich	L0900000

Methionine	116 µM	Sigma Aldrich	M0960000
Phenylalanine	215 µM	Sigma Aldrich	P1150000
Proline	150 µM	Sigma Aldrich	P3350000
Serine	250 µM	Sigma Aldrich	S0450000
Threonine	449 µM	Sigma Aldrich	T8441
Tryptophan	44 µM	Sigma Aldrich	T2610000
Tyrosine:2Na:H2O	248 µM	Sigma Aldrich	T1145
Valine	452 µM	Sigma Aldrich	V0030000
Glucose	17.5 mM	Sigma Aldrich	G7021
Bicarbonate	2.4 g/L	Sigma Aldrich	S5761

3.2.2 Lentivirus and retrovirus production and transduction

For lentiviral production, HEK 293T cells were co-transfected with the expression lentiviral plasmid, psPAX2 and pCMV-VSV-G. For retroviral production, HEK 293T cells were co-transfected with the expression retroviral plasmid, Gag-Pol and pCMV-VSV-G. DNA was transfected into HEK293T using polyethylenimine (PEI, MW 25000) and the cell culture medium changed after 6 h and 24 h. Two days after transfection, supernatants containing the viral particles were filtered through a 0.45 µm PES filter. Target cells were transduced at 10 – 50 % transduction efficiency by the addition of viral supernatant and 10 µg/ml polybrene.

3.2.3 Generation of iCas9 cells

Cell lines expressing a doxycycline-inducible Cas9 cassette were generated essentially as described previously (Michlits *et al.*, 2020). MIA PaCa-2 and MEFs were sequentially transduced with pRRL-SFFV-rtTA3-IRES-EcoR-PGK-PuroR or pRRL-SFFV-rtTA3-IRES-EcoR-PGK-HygroR and pLentiv2-TRE3G-Cas9-P2A-BFP, selected with 50-100 µg/ml hygromycin B and/or 1-2 µg/mL puromycin either by Melanie de Almeida or me. Upon selection, cells were sorted in single cells into 96-well plates using a FACSAria III by Melanie de Almeida or me. iCas9-BFP or iCas9-GFP expression was induced with 0.15 – 1 µg/ml doxycycline and Cas9 induction, gene editing, and TRE3G promoter tightness evaluated by flow cytometry and immunoblotting.

3.2.4 Proliferation-based CRISPR screen

The genome-wide CRISPR screens were performed using a MIA PaCa-2 iCas9 clone upon transduction with the Vienna sgRNA library encoded in pLenti-hU6-sgRNA-iT-EF1as-Thy1.1-P2A-NeoR, as described previously (Michlits *et al.*, 2020, de Almeida *et al.*, 2021). The percentage of MIA PaCa-2 cells transduced with the sgRNA library was determined after 4 days of transduction by immunostaining and flow cytometry analysis of Thy1 expression. Upon selection of cells with 0.5 mg/mL geneticin, Cas9 expression was induced with 0.15 µg/ml doxycycline for three days before the start of the screen. At the onset of the screen (day 0), cells were plated in the different nutrient conditions and cultured in 0.1 µg/ml doxycycline. On day 2 of the screens, cells were switched to doxycycline-free media and cultured for a total of approximately 14 population doublings or for an equivalent time in the leucine-deficient medium, where cells barely proliferated. Cell culture medium was replenished at periodic intervals: in amino acid-rich (AA-rich) ± 4 % albumin conditions, cells were replated every 3 days with an additional media change after 1.5 days; in leucine-poor (Leu-poor) ± 4% albumin media, cells were replated every 4 days, with an additional media change after 2 days. On day 0, an initial cell population was harvested in two replicates. After selection in the different metabolic conditions, cells corresponding to > 600-fold library representation were harvested at the following time points: AA-rich days 12 and 18, AA-rich + 4 % albumin days 15 and 21, Leu-poor day 23, and Leu-poor + 4 % albumin days 24 and 32. Cellular pellets were stored at −80 °C until the processing of all samples in parallel.

3.2.5 Preparation of next-generation sequencing libraries

Upon collection of CRISPR screen samples, the genomic DNA of all samples was isolated and next-generation sequencing (NGS) libraries were prepared. For that, cells were lysed in 10 mM Tris-HCl, 150 mM NaCl, 10 mM EDTA, 0.1% SDS, and proteinase K for 24-48 h at 55 °C shaking at 1200rpm, digested with DNAse-free RNAse for 1-2 h at 37 °C shaking at 1200rpm, and DNA extracted by two rounds of phenol extraction and 2-propanol precipitation using Phase-Lock-Gel Light tubes followed by two washes with 70 % EtOH. Isolated genomic DNA was subjected to ten freeze-thaw cycles to enhance polymerase chain reaction (PCR) efficacy. The Vienna library sgRNA cassettes were amplified by nested PCR. Barcoded NGS libraries of the different samples were generated using a two-step PCR protocol. In the first PCR, 1 µg of genomic DNA was amplified in 50 µL reactions using 0.2 µl of AmpliTaq Gold. For each sample, the resulting PCR products were pooled and purified using AMPure XP magnetic PCR purification beads. In the second PCR, standard Illumina adapters were introduced using 10 ng of DNA and 0.2 µl of AmpliTaq Gold. The resulting

libraries were pooled and sequenced on a HiSeq 2500 platform. Primers used for library amplification are listed in Table 18.

Table 18 - List of primers for screen populations library preparation

Primer ID	Sequence (5' to 3')
First PCR	
F1	GCATACGAGATAGCTAGCCACC
R1	CTCTTTCCCTACACGACGCTCTTCCGATCTNNNNNNXXXXTTCCAGCATAGCTCTTAAAC
Second PCR	
F2	CAAGCAGAAGACGGCATACGAGATAGCTAGCCACC
R2	AATGATACGGCGACCACCGAGATCTACACTCTTTCCCTACACGACGCT

In primer sequences, NNNNNN denotes random nucleotides, XXXX denotes sample-specific barcodes.

3.2.6 Analysis of pooled CRISPR screens

Raw sequencing reads were quantified by Melanie de Almeida using the *crispr-process-nf* Nextflow workflow available at https://github.com/ZuberLab/crispr-process-nf. Briefly, all guides in the sgRNA library were padded with Cs to equal length before creating an index for bowtie2 (v2.3.0). Random hexamer nucleotides were trimmed using fastx_trimmer from the fastx-toolkit (v0.0.14) (http://hannonlab.cshl.edu/fastx_toolkit/) before demultiplexing via 4mer sample barcodes with fastx_barcode_splitter (--mismatches 1 --bol). Next, barcodes and 20mer spacer were trimmed using fastx_trimmer and reads were aligned with bowtie2 (-L 18 --score-min 'C,0,-1' -N 0 --seed 42) and quantified with featureCounts (v1.6.1) by Melanie de Almeida (de Almeida *et al.*, 2021). Before the calculation of gene enrichment and depletion using MAGeCK (v0.5.9) (Wei Li *et al.*, 2014), count tables were filtered to exclude sgRNAs with less than 50 counts in day 0 replicates. Read counts were median normalised and average $\log_2$ fold change (Log_2 FC), p value, and FDR calculated. Depletion or enrichment of sgRNAs was calculated for each screen condition and time point by comparison to day 0. If two samples were collected at different time points for the same condition, the two timepoints were merged into one dataset, representing for each gene the time point with the maximal effect (more significant p value). For comparison of the two media conditions where leucine was either provided in its monomeric form (AA-rich) or contained in proteins (Leu-deficient + 4% albumin), changes in sgRNA abundance were calculated by comparison of the endpoints.

3.2.7 Generation of knockout cells

MIA PaCa-2, PaTu 8988T, and HEK293T clonal LYSET and GNPTAB knockout cells were generated by transfection of pSpCas9(BB)-2A-GFP harbouring LYSET sgRNA 1, LYSET sgRNA 2 or GNPTAB sgRNA 1. For clonal growth, single MIA PaCa-2 and PaTu 8988T GFP-positive cells were sorted via FACS into 96-well plates using a FACSAria III cell. HEK293T GFP-positive cells were sorted in bulk. Knockout specificity in single cell-derived clones was confirmed by lentiviral re-expression of LYSET or GNPTAB cDNA.

For the generation of inducible knockout (iKO) cells, iCas9 lines were transduced with Dual-hU6-sgRNA-mU6-sgRNA-EF1α-mCherry-P2A-PuroR harbouring dual sgRNAs (dsgRNA) targetting human or mouse LYSET and GNPTAB or with pLenti-hU6-sgRNA-iT-EF1α-mCherry-P2A-NeoR (de Almeida *et al.*, 2021) harbouring sgRNAs against indicated screen hits. Upon selection of sgRNA-positive cells with 0.5 mg/mL geneticin, 1-2 µg/mL puromycin, or by sorting of mCherry-expressing cells, Cas9 expression was induced with 0.2-0.3 µg/ml doxycycline for 4 days.

Constitutive bulk LYSET knockouts in SKMEL-30 and HAP1 cells were generated by sequential transduction of pLenti-Cas9-BlastR or pLenti-Cas9-EGFP-PuroR and Dual-hU6-sgRNA-mU6-sgRNA-EF1α-mCherry-P2A-PuroR harbouring dsgRNA 1 against human LYSET. Cas9-positive and dsgRNA-positive cells were selected with 1-2 µg/mL blasticidin and 1-2 µg/mL puromycin. Constitutive bulk LYSET knockouts in other human cell lines (AsPC-1, Hs766t, MCF7, Panc1, Panc 3.27, and PaTu8988T) were generated by transduction of LYSET sgRNAs in pLenti-CRISPR v2-PuroR.

For CRISPR-Cas9 editing experiments, controls were sgRNAs targetting non-coding chromosome regions (AAVS1, Chr1.1 or Chr1.3). sgRNA sequences are listed in Table 9.

3.2.8 Generation of LYSET and GNPTAB expression constructs

LYSET isoform 1 (NM_001098621.4) and isoform 2 (NM_015676.3) were amplified from a MIA PaCa-2 cDNA library. If not otherwise indicated, experiments were performed using LYSET isoform 2, which is the evolutionarily conserved isoform that is predominantly expressed in most cell types analysed. LYSET isoforms 1 and 2 were cloned into pBabe-PuroR using restriction enzyme cloning. LYSET isoform 2 was additionally cloned into pRRL-pUbC-tagRFP-T-Hygro and mutated to LYSET^{R45W} and LYSET^{Y72X} by site-directed mutagenesis (Q5 Site-Directed Mutagenesis Kit).

GNPTAB cDNA was amplified from pcDNA3.1-GNPTAB-myc and subcloned into pLV-EF1a-C-Flag-IRES-NeoR. GNPTAB-myc was mutated to GNPTAB^{K4Q}, GNPTAB^{S15Y} and GNPTAB^{Q36L,E39L} by site-directed mutagenesis and re-cloned into pLV-EF1a-IRES- BlastR or

pRRL-pUbC-tagRFP-T-Hygro. When not otherwise indicated, cloning was performed using the HiFi DNA Assembly Master Mix. Primers for cDNA amplification and re-cloning were designed using the NEBuilder Assembly Tool and are listed in Table 19.

Table 19 - List of primers used for cDNA cloning

Primer name	Sequence (5' to 3')
BamHI-TMEM251/LYSET_iso1_fw	AGTCggatccTCTGAAATGCCAAAG
BamHI-TMEM251/LYSET_iso2_fw	AGTCggatccTGGAGAATGATGAACTTC
TMEM251/LYSET-EcoRI_rev	AGTCgaattcTTACGTGTCAATCAGTTG
pUb-TMEM251/LYSET_iso2_fw	ttggctttttgttagacggATGATGAACTTCCGTCAG
TMEM251/LYSET-pRRL_rev	tcgacggccagtgaattatgTTACGTGTCAATCAGTTG
EF1a-GNPTAB_fw	tccatttcaggtgtcgtgagATGCTGTTCAAGCTCCTG
GNPTAB-pLV_rev	catcgtcatccttgtaatctactctgattcgattggg
GNPTAB-myc-pLV_rev	tagagcggccgccctcgaggctacagatcctcttctgag
pUbC-GNPTAB-Fw	ttggctttttgttagacggATGCTGTTCAAGCTCCTG
GNPTAB-myc-pRRL-Rev	tcgacggccagtgaattatgctacagatcctcttctgag

3.2.9 Cell proliferation assays

For competitive proliferation assays, gene editing was induced with doxycycline for 3 days. At the onset of the experiment, sgRNA-mCherry-positive iCas9 cells were co-cultured with non-sgRNA-expressing control cells in 24 well-plates in the different media conditions and passaged as indicated. The percentage of sgRNA-mCherry+ cells was quantified using a Guava easyCyte flow cytometer at the onset of the experiment, when passaged, and at the end of the experiment.

3.2.10 Immunoblotting

Cells were rinsed with ice-cold PBS, lysed in ice-cold lysis buffer (50 mM HEPES pH 7.4, 40 mM NaCl, 2 mM EDTA, 1 mM Na orthovanadate, 50 mM NaF, 10 mM Na pyrophosphate, 10 mM Na glycerophosphate, 1% Triton X-100, 1x Halt protease and phosphatase inhibitor cocktails) for 15 min on ice. Samples were centrifuged at 14,000 g for 5 min at 4 °C and supernatant with solubilised proteins collected. For analysis of GNPTAB glycosylation, 20 µg of protein per sample was treated with Endo H or PNGase F for 3 h at 37 °C, according to the manufacturer's protocol. Samples were denatured in Laemmli buffer supplemented with β-mercaptoethanol for 15 min at 65 °C.

To analyse secreted proteins, cells were plated in 6 well-plates and the next day standard cell culture medium was replaced with 1 ml OptiMEM. After 24 h the resulting supernatants were cleared by centrifugation at 1,000 g for 5 min to remove possible cells followed by 18,000 g for 20 min to clear cell debris. Protein concentrations were determined with the Pierce BCA Protein Assay and equal protein amounts analysed.

To detect GNPTAB-myc, cells were plated in 10 cm dishes and organelle-enriched fractions were prepared the day after. To this end, cells were rinsed with ice-cold PBS, resuspended in 10 mM HEPES (pH 7.4), 250 mM sucrose, 1 mM MgCl2, 1 mM CaCl2, 1.5 mM MgAc, 1 mM DTT, protease inhibitors, and homogenised by 15 strokes with a KIMBLE Dounce tissue grinder with a large clearance pestle. Post-nuclear supernatants (PNS) were generated by centrifugation at 800 g for 5 min, and organelles pelleted by centrifugation at 18,000 g for 30 min. Pellets were resuspended in ice-cold lysis buffer. Where indicated, lysosomal protease inhibitors were 20 µM leupeptin, 20 µM pepstatin, 20 µM E64, and 20 µM AEBSF. Samples were denatured in Laemmli buffer supplemented with β-mercaptoethanol for 15 min at 65 °C.

For analysis of the endogenous GNPT α-subunit, PNS were prepared as above and organelle-enriched fractions were obtained by centrifugation at 100,000 g for 60 min. Pellets were resuspended in ice-cold lysis buffer and further centrifuged at 14,000 g for 20 min to remove insolubilised proteins. Samples were denatured in Laemmli buffer + β-mercaptoethanol for 15 min at 65 °C and analysed by separation on standard Tris-glycine-SDS protocols. Where indicated, samples were deglycosylated for 4 h with PNGase F before denaturation. Lysosomal protease inhibitors were 100 µM leupeptin, 100 µM pepstatin, and 14 µM E64.

For analysis of ATF6 cleavage and nuclear import**,** cells were rinsed with ice-cold PBS, lysed in ice-cold lysis buffer (10 mM HEPES pH 7.4, 0.1% Triton X-100, 10 mM KCl, 1.5 mM MgCl2, 340 mM sucrose, 10% glycerol, 1 mM DTT, 1 mM PMSF) for 15 min and nuclei pelleted by centrifugation at 2,000 g for 4 min. PNS were collected and nuclei were resuspended in ice-cold nuclei lysis buffer (50 mM Tris-HCl pH 7.4, 1% Triton X-100, 0.1% SDS, 400 mM NaCl, 1 mM EDTA).

To detect cellular M6P-modified proteins, organelle fractions were prepared as above. M6P modification of newly synthesised lysosomal proteins was analysed in supernatants upon induced secretion with NH4Cl. To this end, cells were cultured in 10 cm dishes with 6 mL OptiMEM supplemented with 10 mM NH_4Cl for 24 h; supernatants were centrifuged at 1,000 g for 5 min, subsequently at 18,000 g for 20 min, and concentrated 10-fold using a Pierce Protein Concentrator PES with 10 kDa molecular weight cut-off. Sample preparation and Tris-glycine-SDS running and transfer protocols were done by me. Membranes were blocked using 3 % receptor-grade BSA in TBST for at least 1 h at room temperature by Sabrina Jabs. Membranes

were incubated overnight at 4 °C with 5 µg/ml M6P-scFv in blocking solution, followed by five washes with TBST, incubation with myc antibody for 1 h at room temperature, and another five washes with TBST by Sabrina Jabs.

Unless otherwise indicated, samples were denatured in Laemmli buffer supplemented with β-mercaptoethanol for 5 min at 95 °C and run in SDS gel electrophoresis and immunobloted following standard Tris-glycine-SDS protocols. Immunoblots were developed with ECL substrates Clarity Max Western, SuperSignal West Atto, or Amersham ECL Prime on a ChemiDoc Imaging system. When samples were analysed using multiple antibodies on different membranes, sample preparation, electrophoresis, and immunoblotting were performed in parallel under identical conditions. LC3 was analysed on PVDF membranes, other proteins were analysed on nitrocellulose membranes.

3.2.11 Fluorescence confocal microscopy

For immunostainings, cells were seeded on coverslips. After 16-24 h, cells were rinsed with ice-cold PBS, fixed for 15 min with 4 % paraformaldehyde in PBS at room temperature, and permeabilised for 5 min with 0.05 % Triton X-100 in PBS. After rinsing with PBS, cells were blocked for 30 min with 4 % normal goat serum in 0.5 % BSA in PBS, incubated with primary antibodies (1:400 dilution) for 1.5 h in blocking solution, washed two times with blocking solution, and incubated with Alexa Fluor-conjugated secondary antibodies (1:1000) in blocking solution for 1 h. Coverslips were rinsed once with PBS, incubated for 5 min with 10 µg/ml Hoechst 33342 in PBS, washed two times with PBS, and mounted on microscope slides with Prolong Antifade. TMEM251/LYSET and Flag-tag antibodies were cleared up by pre-incubation of the antibody solution in LYSET KO and Flag-tag-non expressing cells, respectively, to remove unspecific staining.

For live imaging, cells were seeded on 8-well chambered coverslips 16-24 h before the experiment onset. For DQ BSA fluorescence dequenching, the medium was supplemented for 6 h with 0.1 mg/ml DQ BSA and 1 h with 0.5 µg/ml Hoechst before imaging. For Lysotracker Red, the medium was supplemented for 1 h with 50 nM Lysotracker Red and 0.5 µg/ml Hoechst before imaging. Live imaging experiments were performed in a humidified chamber at 37 °C and 5 % CO_2.

For albumin uptake experiments, cells were seeded on 8-well-chambered coverslips. Cells were incubated for 15 min with 0.1 mg/ml Alexa Fluor 647 BSA. Subsequently, cells were washed three times with ice-cold PBS on ice, fixed for 15 min with 4% paraformaldehyde in PBS at room temperature, stained with 10 µg/ml Hoechst in PBS for 5 min, washed for 5 min with PBS, and imaged immediately.

For endosomal cargo trafficking experiments, cells were incubated for 4 h with 0.1 mg/ml 10 kDa dextran Oregon Green, followed by a 20 h chase in fresh media, for lysosomal labelling. Upon lysosomal labelling with the first dextran, cells were incubated for 30 min with 0.1 mg/ml 10 kDa dextran Alexa Fluor 568, washed three times with ice-cold PBS on ice, fixed for 15 min with 4% paraformaldehyde in PBS at room temperature, stained for 5 min with 10 µg/ml Hoechst in PBS, washed for 5 min with PBS, and imaged immediately.

For proximity ligation assays (PLA), cells were plated in 16-well chamber slides. Cells were rinsed with ice-cold PBS, fixed for 10 min with 4 % paraformaldehyde in PBS at room temperature, and permeabilised for 5 min with 0.1 % Tween-20 in PBS. The assays were performed with the Duolink In Situ Red Starter Kit Mouse/Rabbit, according to the manufacturer's protocol. All the primary antibodies used in the PLA were diluted 1:1200 in the provided Antibody Diluent.

All microscopy experiments were imaged with a Leica TCS SP5 confocal microscope using a 40x or 63x, 1.40 oil objectives. Fluorescence signal per cell was quantified using the particle analyser function of Fiji (Schindelin *et al.*, 2012), as indicated, where the integrated signal density of each fluorescent probe was normalised to cell number in the randomly chosen fields of view acquired across the whole sample.

3.2.12 Flow cytometry

DQ BSA dequenching and Lysotracker accumulation in acidic organelles were quantified by flow cytometry. Cells were seeded on 24 well-plates 16-24 h before the experiment onset. Prior to harvesting, cells were cultured for 6 h in the presence of 50 µg/ml DQ BSA and/or 1 h in the presence of 25 nM Lysotracker Red. Living cells were collected by trypsinisation and resuspended in flow cytometry buffer (5 % FBS in PBS) for further analysis on an LSR Fortessa Cell Analyzer.

3.2.13 RT qPCR

For quantitative reverse transcription PCR (RT-qPCR), cells were seeded in triplicates on 6 well-plates 16-24 h before RNA extraction. RNA was extracted with Trizol followed by one round of chloroform extraction, isopropanol precipitation overnight at -20 °C, two washes with 70-80 % ethanol, and RNA elution with water by incubation at 55 °C shaking 400 rpm for 10 min. cDNA was prepared from 1 µg RNA using random hexamers and SuperScript III Reverse Transcriptase according to the manufacturer's protocol. RT-qPCR was performed using SYBR green master mix. Relative gene expression was calculated using the delta-delta Ct method ($2^{-\Delta\Delta Ct}$ method) using ACTB as an internal control. qPCR reactions were performed

with a Lightcycler 480. For qPCR primers, see Table 20. Each primer pair was tested and only primer pairs with efficiency equal to 2 ± 0.2 were used.

Table 20 – List of RT-qPCR primers

Gene	Species	Forward Sequence (5' to 3')	Reverse Sequence (5' to 3')
ACTB	human	CCAACCGCGAGAAGATGA	CCAGAGGCGTACAGGGATAG
CTSB	human	AGAGTTATGTTTACCGAGGACCT	GATGCAGATCCGGTCAGAGA
CTSL	human	CGTGACGCCAGTGAAGAATCA	CGCTCAGTGAGACAAGTTTCC
GNPTAB	human	GGGCTCTACGTGTGCTTCTTG	ATTGATCTCGGCTCCATTCCA
GNPTG	human	GGTGAACAACCCGTTCTTGC	CTTGCCCGAGAGTCGGAAG
HEXA	human	ACGTCCTTTACCCGAACAACT	CGAAAAGCAGGTCACGATAGC

3.2.14 Sample preparation for proteomics

For analysis of lysosomal protein content, I prepared lysosomal-enriched fractions using a magnetic enrichment protocol. Cells were plated in 15 cm dishes (2 plates per condition) and later incubated with 10 % ferromagnetic nanoparticles (DexoMAG C, Liquids Research), 10 mM HEPES in DMEM/F-12 for 14 h for loading of lysosomes, followed by a 6 h chase in fresh medium. Cells were rinsed twice with ice-cold PBS, scraped out of the plate with 5 mL homogenisation buffer (10 mM HEPES pH 7.4, 250 mM sucrose, 1 mM MgCl2, 1 mM CaCl2, 1.5 mM MgAc, 1 mM DTT, protease inhibitors), and pelleted by centrifugation at 150 g for 5 min. Cells were resuspended in 1.5 mL homogenisation buffer and homogenised by 15 strokes with a KIMBLE Dounce tissue grinder with a large clearance pestle. Homogenate was centrifuged at 200 g for 10 min to obtain the PNS fraction. LS MACS columns were equilibrated with 1 ml 0.5% BSA in PBS and PNS loaded on them. The column was washed three times with 1 ml wash buffer (0.1 mM sucrose in PBS in the presence of protease inhibitors) and lysosomal-enriched fractions eluted with 400 µl elution buffer (0.5 mM sucrose in PBS in the presence of protease inhibitors) after detaching the column from the magnet. Protein concentrations of the PNS and lysosomal-enriched fractions were determined by Bradford assay and equal protein amounts were subjected to further analysis.

For analysis of secreted proteins, MIA PaCa-2 cells were cultured in 6 wp with OptiMEM. After 24 h, the medium was collected and centrifuged at 1,000 g for 5 min followed by 18,000 g for 20 min. Protein concentrations were determined by BCA assay, equal protein amounts precipitated with chloroform-methanol and subjected to further analysis.

3.2.15 LC-MS/MS analysis

Protein digestion was performed via tryptic in-gel digestion. To this end, proteins were run for 0.5 cm into an SDS gel. After Coomassie staining, the total sample was cut out and digested with trypsin as described previously (Shevchenko *et al.*, 2006), adapted to a DigestPro MSi robotic system. Analysis was carried out on an Ultimate 3000 UPLC system connected to an Orbitrap Exploris 480 mass spectrometer. Analysis times and methods were chosen according to expected sample complexity or dynamic range as follows: MIA PaCa-2 secretome 90 min; MIA PaCa-2 lysosomal fraction 120 min; MIA PaCa-2 PNS 150 min total LC-MS/MS analysis time. Before the analytical separation, peptides were online desalted on a trapping cartridge (Acclaim PepMap300 C18, 5 µm, 300 Å pore) for 3 min using 30 µl/min flow of 0.05 % Trifluoroacetic acid in water. The analytical multistep gradient was carried out on a nanoEase MZ Peptide analytical column (300 Å, 1.7 µm, 75 µm x 200 mm) using solvent A (0.1 % formic acid in water) and solvent B (0.1 % formic acid in acetonitrile). The concentration of solvent B was linearly ramped up from 2 % to 30 % according to the total analysis procedure (72 min, 102 min, or 132 min), followed by a quick ramp up to 78 % B. After 2 min, the concentration of solvent B was lowered back to 2 % and a 10 min equilibration step was appended. Eluting peptides were analysed in the mass spectrometer using data-dependent acquisition (DDA) mode. A full scan at 60k resolution (90 min method) or 120k resolution (120 min, 150 min methods), (380-1400 m/z, 300 % AGC target, 45 ms maxIT) was followed by 1.5 s (90 min) or 2 s (120 min, 150 min method) of MS/MS scans. Peptide features were isolated with a window of 1.4 m/z and fragmented using 26 % NCE. Fragment spectra were recorded at 15k resolution (100 % AGC target, 22 ms (150 min) or 54 ms (90 min, 120 min)). Unassigned and singly charged eluting features were excluded from fragmentation and dynamic exclusion was set to 35 s.

3.2.15.1 Proteomics data analysis

Data analysis was carried out by Dominic Helm with MaxQuant (version 1.6.14.0) (Tyanova *et al.*, 2016) using an organism-specific database extracted from UniProt with default settings (from 27.02.2020 containing 74,830 entries). Identification FDR cutoffs were 0.01 on the peptide level and 0.01 on the protein level. Match between runs (MBR) option was enabled to transfer peptide identifications across RAW files based on accurate retention time and m/z. For LFQ analysis, fractions were set in a way that MBR was only performed within each condition. LFQ quantification was based on the MaxLFQ algorithm (Cox *et al.*, 2014); a minimum of 2 quantified peptides per protein was required for protein quantification. MIA PaCa-2 PNS and lysosomal fractions from the same MS experiment were analysed in individual parameter groups with separate LFQ normalisation. The re-quantify option was

enabled to stabilise very large or small ratios (Cox *et al.*, 2009). Advanced ratio estimation was turned off to avoid interference with ratio inversion due to label swap.

3.2.15.2 Proteomics statistical analysis

Proteomic statistical analysis and description of the procedure was done by Martin Schneider. The SILAC ratios with swapped labels were inverted, and the LFQ values ratio log2 transformed. Adapted from the Perseus recommendations (S. Tyanova and J. Cox, 2018), protein groups with non-zero LFQ intensity in 70% of the samples of at least one of the conditions were used for statistics. LFQ values were normalised via variance stabilisation normalisation (W. Huber *et al.*, 2002). Missing LFQ values being absent in one condition were imputed with random values drawn from a downshifted (2.2 SD) and narrowed (0.3 SD) intensity distribution of the individual samples. For missing LFQ values with complete absence in one condition, the R package missForest was used for imputation (S. Tyanova and J. Cox, 2018). The statistical analysis for LFQ values was performed with the R-package limma (Ritchie *et al.*, 2015). *P* values were adjusted with the Benjamini–Hochberg method for multiple testing. The reference proteome 'Human Golgi Apparatus' from UniProt was used to generate sub-proteomes.

3.2.16 Protein structure prediction

Structures of human and Drosophila GNPTAB were predicted five times using a local version of ColabFold by David Haselbach, at IMP in Vienna (Mirdita *et al.*, 2022). The models with the best pLDDT scores were used. The transmembrane helices were visualised and the surface hydrophobicity and charge were calculated in UCSF ChimeraX (E. F. Pettersen *et al.*, 2021). To obtain a model of the transmembrane domain of the complex between human LYSET and GNPTAB, the analysis was restricted to the membrane region. Several different sequence variants were predicted five times each. Restricting the analysis to the membrane region yielded high pLDDT and PAE scores, indicating reliable models.

3.2.17 Mice experiments

MIA PaCa-2 cells were lentivirally transduced with pLenti-CRISPR V2-PuroR encoding LYSET sgRNA 1, LYSET sgRNA 2 or AAVS1 sgRNA 1, selected with puromycin, and used for subcutaneous transplantations into 7-week-old female randomised NOD scid gamma (NSG) mice recruited from the Center for Preclinical Research at the DKFZ, Heidelberg, under isoflurane inhalation anesthesia. $4x10^6$ MIA PaCa-2 cells were suspended in 100 µl PBS and injected subcutaneously into the right flank of mice. Tumour volume was regularly measured

with a caliper and calculated as *Volume = (Length x Width^2)/2*. Necropsies were taken when a pre-defined humane endpoint was reached or once the tumour diameter reached 1.3 cm. Mice were maintained at 22 ± 2 °C, relative humidity of 55 ± 10 %, and a photoperiod of 12 h light : 12 h dark with food and water given *ad libitum*. Animal experiments were performed under the approved guidelines of the responsible national authority, the local Governmental Committee for Animal Experimentation (RP Karlsruhe, Germany, license G20/21).

3.2.18 Statistical analysis

LC-MS/MS proteomics datasets were analysed as described above. In other experiments, *P* values were calculated using a two-tailed unpaired t-test with Welch correction.

4. Results

4.1 Genome-wide CRISPR screens to identify genes involved in extracellular protein-dependent cell proliferation

To identify genes and cellular processes required for extracellular protein-dependent proliferation, I conducted pooled genome-wide CRISPR-Cas9 screens, in collaboration with the Zuber Lab at IMP in Vienna. Cell proliferation was sustained by the uptake of monomeric amino acids or by internalisation and lysosomal catabolism of extracellular protein.

4.1.1 Selection of screening conditions

Prior to the screens, it was crucial to select a mammalian cell line able to proliferate using extracellular protein as an amino acid source and to optimise the media conditions in which the cells would depend on free amino acids or extracellular protein to support proliferation.

To select a mammalian cell line suitable for the screen, I sought a human cancer cell line with low ploidy to facilitate CRISPR editing, and able to proliferate using extracellular protein as an amino acid source. Upon extensive tests with different cell lines, I chose MIA PaCa-2, a cell line derived from human pancreatic adenocarcinoma (Figure 3A). MIA PaCa-2 expresses the oncogenic $KRas^{G12D}$ mutation and is commonly used in the field because it displays high levels of internalisation and degradation of extracellular proteins (Commisso *et al.*, 2013, Nofal *et al.*, 2017, Waters and Der, 2018). To control the timing of gene editing, a single-cell clone of MIA PaCa-2 harbouring an inducible tight Cas9 expression system was engineered (MIA PaCa-2 iCas9). For this, Melanie de Almeida, a PhD student from the Zuber Lab at IMP in Vienna, lentivirally transduced MIA PaCa-2 cells with the transactivator rtTA3 followed by selection with antibiotics (Figure 3B). Next, Melanie transduced the inducible Cas9-BFP expression cassette, sorted BFP-expressing single cells, and selected a clone that did not exhibit basal Cas9 activity and that rapidly responded to doxycycline treatment for expression of Cas9 and gene editing (de Almeida *et al.*, 2021). To confirm the tightness and editing efficiency of the MIA PaCa-2 iCas9 clone, I transduced it with an sgRNA against a non-essential surface protein, CD46 sgRNA 1, and tested the knockout efficiency upon 3 days of doxycycline treatment. By flow cytometry analysis of immunostained CD46, I could observe that CD46 protein is lost from the surface of the cell only upon doxycycline treatment and at high efficiency after 3 days of treatment (Figure 3C).

The use of a clonal cell line with inducible Cas9 expression under the control of a tight tetracycline responsive element (TRE) promoter is a great advantage for the execution of a whole-genome CRISPR screen (Michlits *et al.*, 2020). This system allows a more efficient and controlled gene editing on the screening populations and selection for both sgRNA enrichment and depletion to systematically discover genes that can regulate proliferation dependent on amino acids acquisition through endolysosomal albumin proteolysis.

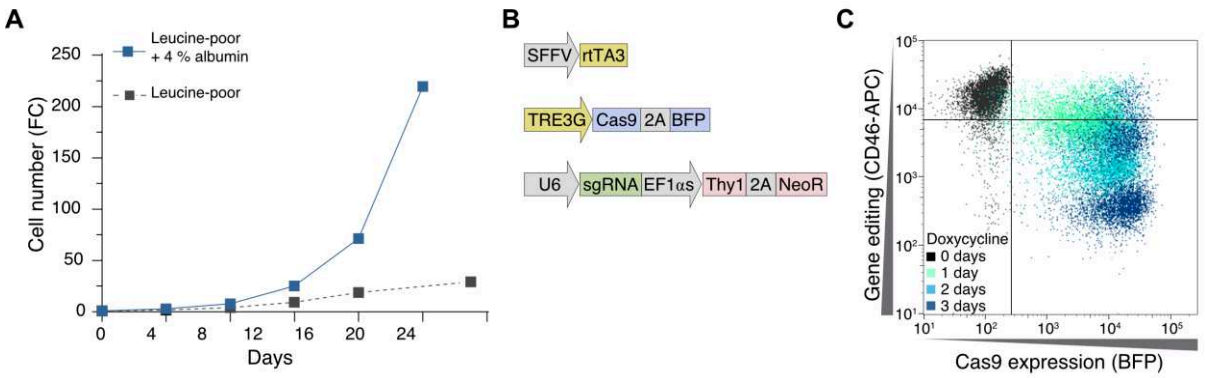

Figure 3 - Establishment of inducible Cas9 (iCas9) MIA PaCa-2 cells proliferating using albumin.
(A) Proliferation of MIA PaCa-2 iCas9 cells in leucine-poor ± 4% albumin medium. Cells were split and counted every 4 days and media was replenished every 2 days. Data are shown as cumulative fold-change to day 0. (B) Schematic representation of the iCas9 plasmid system engineered in MIA PaCa-2 cells. rtTA3 is constitutively expressed under the SFFV promoter. Cas9 and BFP are downstream of the tetracycline-responsive element (TRE3G) and separated by the self-cleaving peptide P2A. (C) Flow cytometry analysis of Cas9/BFP expression and the surface protein CD46 in MIA PaCa-2 iCas9 cells upon transduction with CD46 sgRNA, antibiotic selection, and 100 ng/ml doxycycline treatment for the indicated periods. CD46 was stained with anti-CD46-APC antibody before analysis.

Next, I tested different medium formulations to optimise the screening metabolic conditions. To reach the final screen conditions, I tested the following parameters: cell culture media formulation, type of commercial cell culture-approved albumin, albumin concentration, lot of fetal bovine serum (FBS), and amino acid deprivation method (Table 21, data not shown).

To enforce the uptake of monomeric amino acids or the internalisation and lysosomal catabolism of extracellular protein, the essential amino acid leucine was kept in the medium in its monomeric form or depleted to 5 µM and provided in the form of extracellular protein. Albumin was chosen as the extracellular source of protein because it is the predominant protein in mammalian plasma, constituting the major pool of extracellular amino acids (Palm, 2019).

Table 21 – Tested cell culture media parameters and their importance.

Media parameters	Importance of testing
Culture media (DMEM, DMEM/F-12, RPMI)	The concentration of the constituents of the cell culture media are different (including amino acids concentrations)
Cell culture-approved BSA	Different manufacturers' BSA produce different effects on cells when supplemented in the media, due to the possible presence of contaminants, pH alteration of the media, etc.
BSA concentration	Selection of the best albumin-dependent proliferation conditions without inducing cellular stress at long-term
FBS	Slightly different compositions, even from the same supplier, are enough to induce cell stress and different responses to BSA supplementation (variability between different lots)
AA deprivation method – leucine levels	Different cell lines have different amino acid demands to sustain survival and low concentration has a big influence on the selective albumin-dependent proliferation

4.1.2 Screen setup and execution

Before the start of the screens, Melanie de Almeida had transduced the MIA PaCa-2 iCas9 cells with the Vienna genome-wide sgRNA library encoded in pLenti-hU6-sgRNA-iT-EF1as-Thy1.1-P2A-NeoR (Figure 4A), selected them with neomycin and tested the percentage of MIA PaCa-2 cells transduced with the sgRNA library after 4 days of transduction by immunostaining and flow cytometry analysis of Thy1 expression (data not shown). To prepare the cells for the screens, I expanded the MIA PaCa-2 iCas9 cells and cultured them with doxycycline to induce Cas9 expression and knockout generation. After 3 days of 0.3 µg/ml doxycycline incubation, I collected a day 0 representation of the library (> 600-fold) and plated the cells in the different metabolic conditions either rich or deficient in leucine and/or albumin in the presence of 0.1 µg/ml doxycycline (Figure 4A and B). On day 2 of the screen, cells were switched to a doxycycline-free medium until approximately 14 population doublings. In the leucine-deficient medium, where cells barely proliferated, cells were kept for an equivalent period. Cell culture medium was replenished periodically: in amino acid-rich (AA-rich) ± 4 % albumin conditions, cells were counted and replated every 3 days with an additional media change after 1.5 days; in leucine-poor (Leu-poor) ± 4% albumin media, cells were counted and replated every 4 days, with an additional media change after 2 days (Figure 4B).

After selection in the different metabolic conditions, cells corresponding to > 600-fold library representation were harvested at the following time points: AA-rich days 12 and 18; AA-rich + 4 % albumin days 15 and 21; Leu-poor day 23; Leu-poor + 4 % albumin days 24 and 32. Of note, the collection of the samples was planned to allow for the comparison of the different conditions at both a similar time and similar population doublings (Figure 4B).

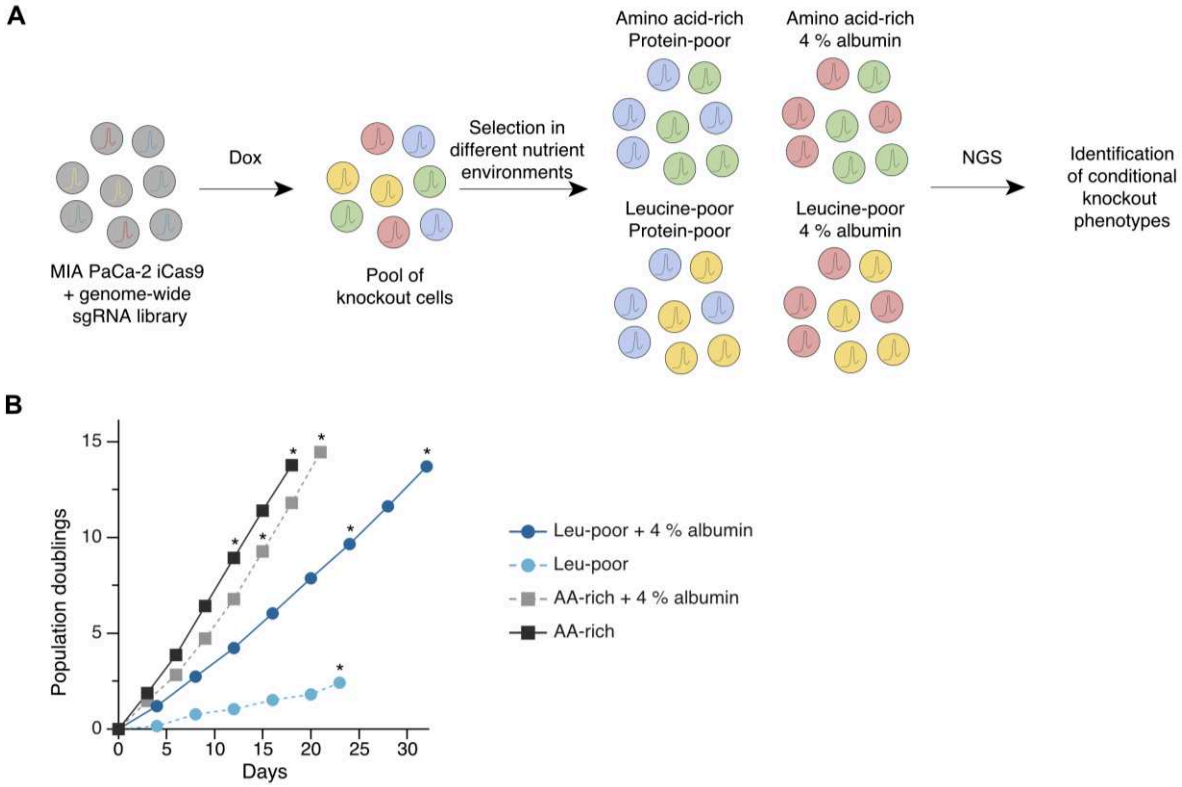

Figure 4 - CRISPR screen to identify components required for cell proliferation supported by extracellular proteins as nutrients.

(A) Experimental design of the CRISPR screen procedure. (B) Proliferation of screen populations in the different nutrient environments. Data are shown as population doublings. * denotes the harvesting time points of > 600-fold library representation for the different populations.

4.1.3 Screen hits

To identify genes specifically essential or detrimental in individual screen conditions, I quantified changes in sgRNA representation in the different metabolic conditions using MAGeCK. By comparing the representation of the sgRNAs of each target gene in the different populations relative to day 0, I identified multiple genes whose depletion is well tolerated in amino acid-rich medium and either essential or detrimental in leucine-poor ± albumin. Amongst the pathways essential when cells depend on albumin to proliferate, I found endolysosomal trafficking regulators, amino acid transporters, and amino acid sensors. In contrast, I identified growth factors signalling, heparan sulfate synthesis, and sodium-coupled chloride cotransporter-related genes as being unfavourable for albumin-dependent proliferation (Figure 5A).

To validate several of these genes, I performed competitive proliferation assays in conditions where the cells import free amino acids or uptake and degrade extracellular proteins. I cloned two independent sgRNAs targetting each gene into pLenti-hU6-sgRNA-iT-EF1α-mCherry-P2A-NeoR and transduced them into MIA PaCa-2 iCas9 cells (Table 9). As a control, cells were transduced with the same plasmid encoding AAVS1 sgRNA 1, a sequence targetting a non-codifying region of the human genome. Upon selection of the cells with neomycin, untransduced cells and cells expressing the sgRNAs were cultured for 3 days in the presence of 200 ng/mL doxycycline to induce Cas9-BFP expression and hence the editing of the genome in the targeted sequences (iKO). At the onset of the competition proliferation assay, untransduced MIA PaCa-2 iCas9 and MIA PaCa-2 iCas9 cells expressing the pLenti-hU6-sgRNA-iT-EF1α-mCherry-P2A-NeoR cassette were plated in co-culture and the percentage of mCherry-positive cells ($mCherry^+$) assessed on day 0 and every 4 days for 12 days (Figure 5B).

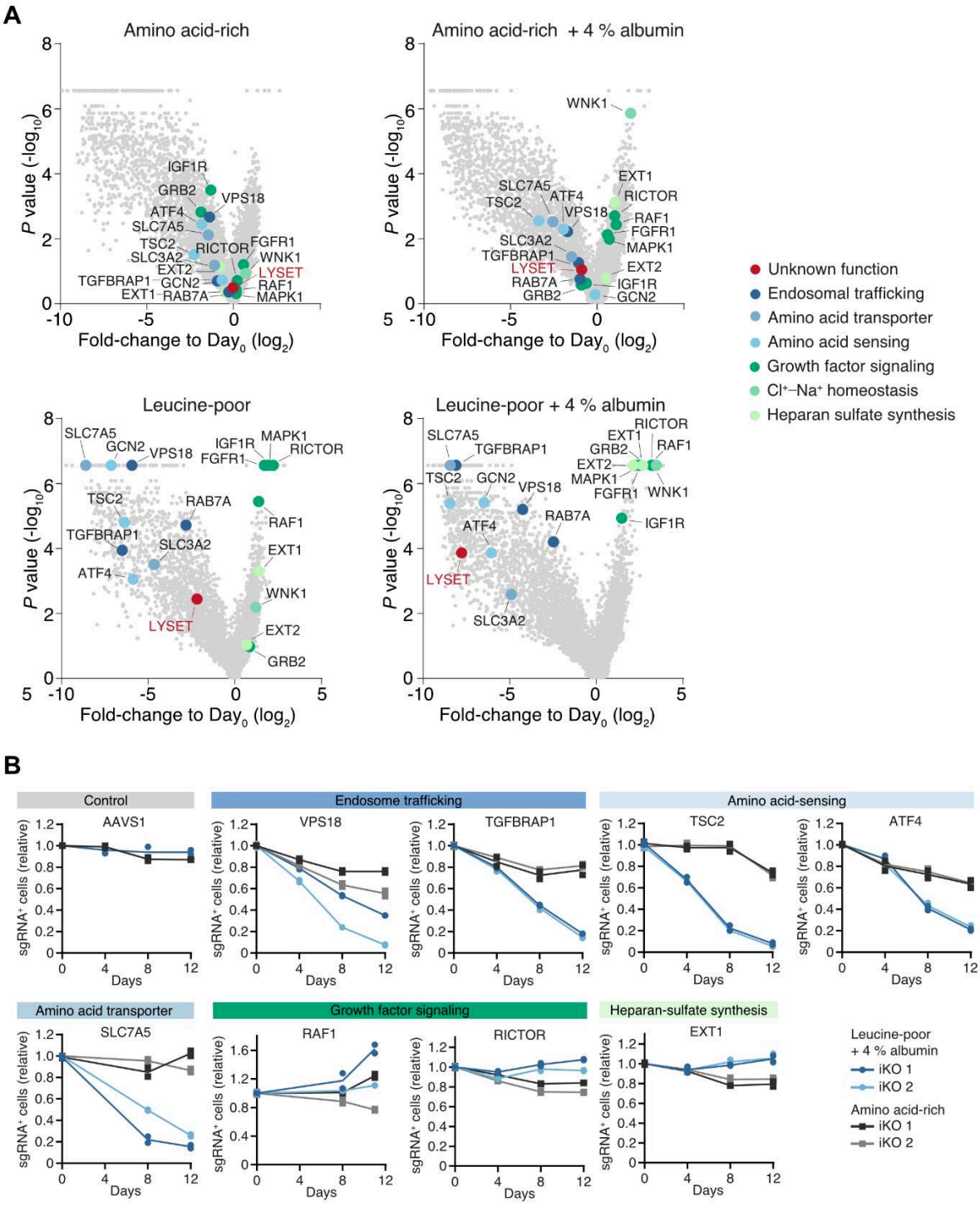

Figure 5 - Screen hits selection and validation.

(A) Gene-level enrichment or depletion of sgRNAs in the different nutrient conditions in the proliferation-based CRISPR screen compared to the starting population (Day 0). Selected hits are highlighted across screening conditions. (B) Competitive proliferation assays of MIA PaCa-2 iKO cells expressing sgRNAs targetting indicated genes (sgRNA+) against non-sgRNA-expressing controls, in leucine-poor + 4% albumin medium and amino acid-rich medium. Data are represented as means and individual replicates. N = 2.

4.2 TMEM251/LYSET

One prominent and uncharacterised hit selectively essential for extracellular protein-dependent proliferation was the protein TMEM251 (Figure 5A), which hereafter is referred to as LYSosomal Enzyme Trafficking Factor (LYSET). LYSET is a small protein predicted to contain two transmembrane domains, N- and C- termini facing the cytosol, and no predicted/identifiable domains or post-translation modifications. Interestingly, data from DepMap on other shRNA and CRISPR screens widely identified LYSET (TMEM251) as a non-essential gene (https://depmap.org).

For further validation and characterisation of LYSET, I depleted LYSET from different cell types using three methods: (1) inducible knockout (iKO), where sgRNAs targetting LYSET were delivered in bulk to iCas9-expressing cells and the knockouts were induced by treatment with doxycycline; (2) bulk constitutive LYSET knockout (bulk KO) via lentiviral transduction of cells with pLenti-CRISPR v2-PuroR encoding LYSET sgRNAs followed by selection with puromycin; (3) single cell-derived LYSET knockout clones (clonal KO) generated via transient transfection of cells with pSpCas9(BB)-2A-GFP harbouring LYSET sgRNAs followed by single cells sorting of GFP-positive cells.

4.2.1 LYSET is required when cells feed on extracellular proteins *in vitro* and *in vivo*

To validate LYSET as selectively essential when cells feed on extracellular protein, I performed competitive proliferation assays in amino acid-rich and leucine-poor medium supplemented with albumin. As above, I plated MIA PaCa-2 LYSET iKO cells together with MIA PaCa-2 untransduced cells and assessed the percentage of mCherry$^+$ cells on day 0 and every 4 days (data not shown). Later, Sven Groessl, a PhD student in our lab, cloned LYSET dual-sgRNAs into Dual-hU6-sgRNA-mU6-sgRNA-EF1α-mCherry-P2A-PuroR, transduced them into MIA PaCa-2 iCas9, and repeated the competitive proliferation assay in all four screen conditions (Figure 6A). In amino acid-rich conditions, LYSET iKO cells did not show a growth disadvantage when competing with control untransduced cells. In contrast, in leucine-poor medium ± 4 % albumin, LYSET iKO cells were outcompeted, confirming the pooled CRISPR screens results (Figure 6B).

To assess the importance of LYSET in the growth of tumour cells *in vivo*, MIA PaCa-2 cells were subcutaneously transplanted into the right flank of NSG mice and tumour growth followed over time. For this, I prepared bulk LYSET KO MIAPaCa-2 cells (Figure 6C). Upon selection and expansion of the cells, I suspended 4x10^6 cells in PBS for transplantation. Karin Müller-Decker, head of the DKFZ Tumor Models facility, subcutaneously transplanted these

cells into the right flank of NSG mice and followed tumour formation and growth over time. Using this subcutaneous model, LYSET-depleted cells showed impairment in their ability to form tumours (Figure 6D). Collectively, these data showed that LYSET is required for extracellular protein-dependent growth of cancer cells *in vitro* and for tumour growth *in vivo*.

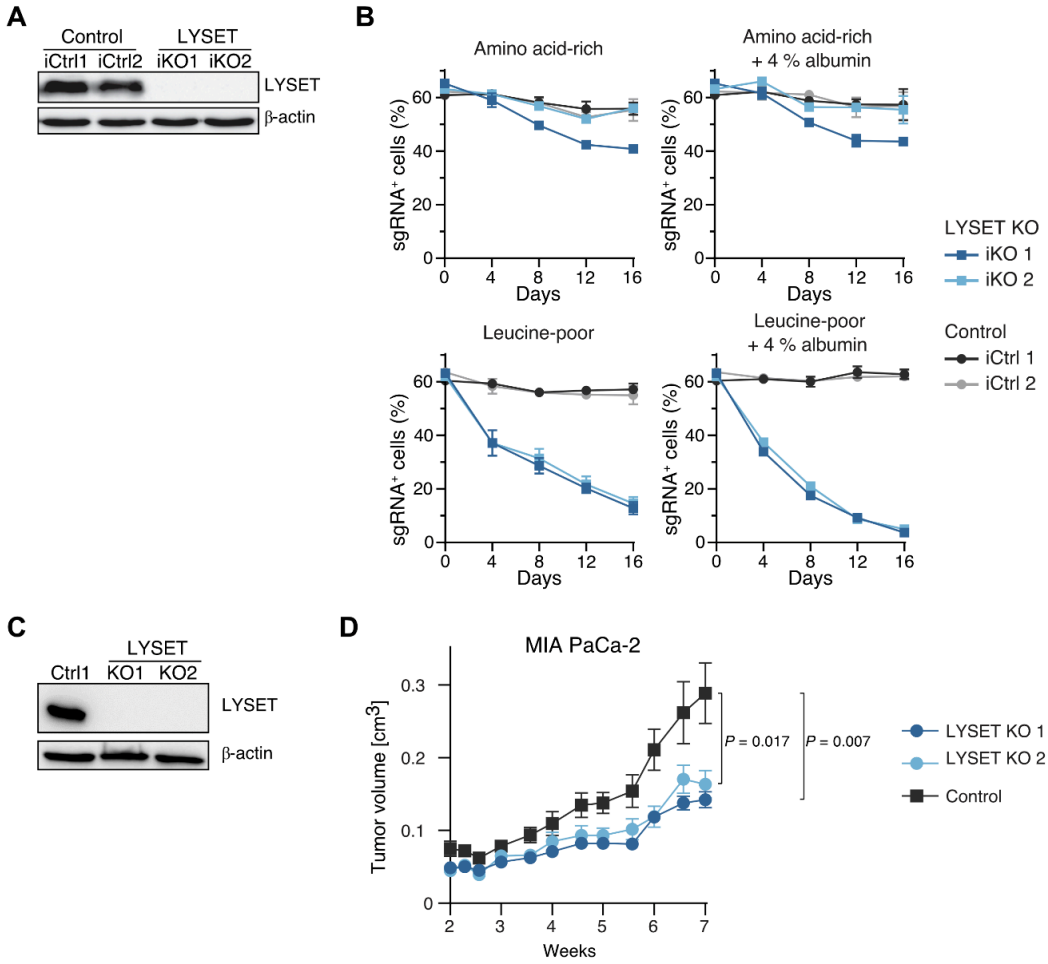

Figure 6 - LYSET is required when cells feed on extracellular proteins *in vitro* and *in vivo*.
(A) Immunoblot of MIA PaCa-2 iCas9 cells transduced with control or LYSET dsgRNA after induction of Cas9 with 200 ng/mL doxycycline for 3 days. (B) Competitive proliferation assays of MIA PaCa-2 LYSET iKO cells against non-sgRNA-expressing controls in the different screening conditions (amino acid-rich, amino acid-rich + 4% albumin, leucine-deficient, leucine-deficient + 4% albumin). Data are represented as means ± SD. N = 3. Experiment performed by Sven Groessl. (C) Immunoblot of bulk LYSET KO populations upon lentiviral transduction and antibiotic selection of MIA PaCa-2 cells. (D) Tumour growth upon subcutaneous injection of bulk MIA PaCa-2 LYSET KO cells in NSG mice. Data are represented as means ± SEM. N = 10 mice per condition. Data produced jointly with Karin Müller-Decker.

4.2.2 LYSET is required for lysosomal degradation of endocytic and autophagic cargoes

To determine the cellular process in what LYSET is required for the nutritional use of extracellular proteins, I examined its possible function in endocytosis, delivery of endocytic vesicles to the lysosome, and lysosomal catabolism of extracellular protein. For this, I generated MIA PaCa-2, PaTu8988t, AsPC-1, and MCF-7 bulk LYSET KO cells and MIA PaCa-2 clonal LYSET KO.

To test the uptake of extracellular protein, bulk MIA PaCa-2 LYSET KO and control cells were incubated with fluorescently labelled albumin for 4 h. Subsequently, cells were washed, fixed with formaldehyde, and imaged by confocal microscopy. The amount of fluorescently labelled albumin taken up by the cell was analysed using the particle analyser function of Fiji. Image analysis presented no reduction in the ability of LYSET-depleted cells to uptake extracellular protein (Figure 7A). To test the delivery of endocytic cargo to the lysosome, bulk MIA PaCa-2 LYSET KO cells were subsequently incubated with two dextrans. Cells were incubated with an Oregon Green labelled dextran for 4 h, chased in fresh media for 20 h for lysosomal labelling, pulsed with Alexa Fluor 568 labelled dextran for 30 min, washed, fixed with formaldehyde, and imaged by confocal microscopy. My results showed no reduction in the co-localisation of the Alexa Fluor 568 dextran in vesicles pre-labelled with the Oregon Green dextran, suggesting that endosomal cargo delivery was not overly altered in LYSET-depleted cells (Figure 7B). Thus, LYSET is dispensable for the uptake and delivery of extracellular cargo to the lysosome.

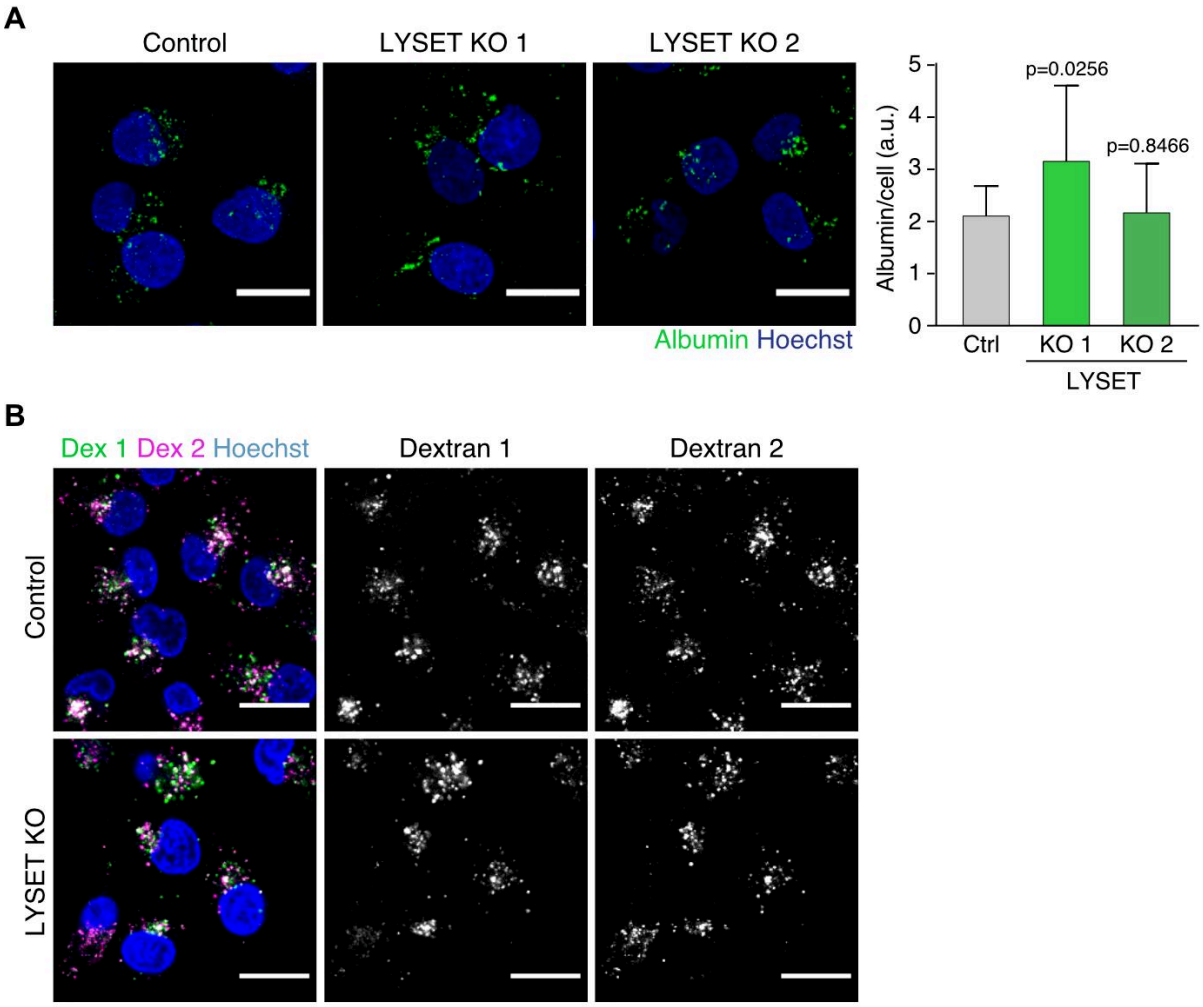

Figure 7 - LYSET is dispensable for uptake and delivery of extracellular macromolecules to the lysosome. (A) Confocal microscopy detection of intracellular fluorescently labelled albumin in bulk MIA PaCa-2 LYSET KO cells after 15 min of uptake. Scale bars = 20 µm. Quantification of albumin uptake/cell is represented as mean ± SD. N = 12 randomly chosen fields of view with ≥ 8 cells each. (B) Trafficking of endocytic cargo to lysosomes in bulk MIA PaCa-2 LYSET KO cells. Cells were pulsed with dextran 1 (Oregon Green) for 4 h and chased in fresh media for 20 h to label lysosomes. Cells were then pulsed with dextran 2 (Alexa Fluor 568) for 30 min, and co-localisation of the two dextrans was analysed by microscopy. Scale bars = 20 µm.

To test the lysosomal catabolism of extracellular protein, cells were incubated with a fluorescently labeled albumin probe that becomes dequenched and fluorescent upon degradation (DQ BSA). Both analyses of DQ BSA fluorescence intensity by live confocal imaging and flow cytometry in MIA PaCa-2 clonal LYSET KO showed that lysosomal catabolism of DQ BSA was strongly reduced in LYSET-deficient cells (Figure 8A to D). Thus, LYSET is required for the lysosomal degradation of albumin.

As the lysosome is the organelle where endocytosis and autophagy converge (Palm and Thompson, 2017, Lawrence and Zoncu, 2019), I assessed the levels of the autophagy-related proteins, p62 and LC3-II, in LYSET-depleted cells. To this end, MIA PaCa-2, PaTu-8988t, AsPC-1, and MCF-7 bulk LYSET KO cells were collected for immunoblotting upon treatment with bafilomycin A1 or DMSO (Control). Bafilomycin A1 is a pharmacological v-ATPase inhibitor and consequently a lysosomal catabolism inhibitor, commonly used to block autophagic cargo degradation in the lysosome. Upon autophagy blockage, there is an increase in the levels of p62 and LC3-II, two proteins present in the autophagosome and hence degraded through autophagy. Loss of LYSET led to an increase in p62 and LC3-II levels to a similar extent as bafilomycin A1 treatment of control cells in most cell lines (Figure 8E). This data suggested that the lysosomal ability to degrade autophagic cargo is impaired in LYSET-deficient cells. Thus, LYSET is required for lysosomal catabolism of both endocytic and autophagic cargoes.

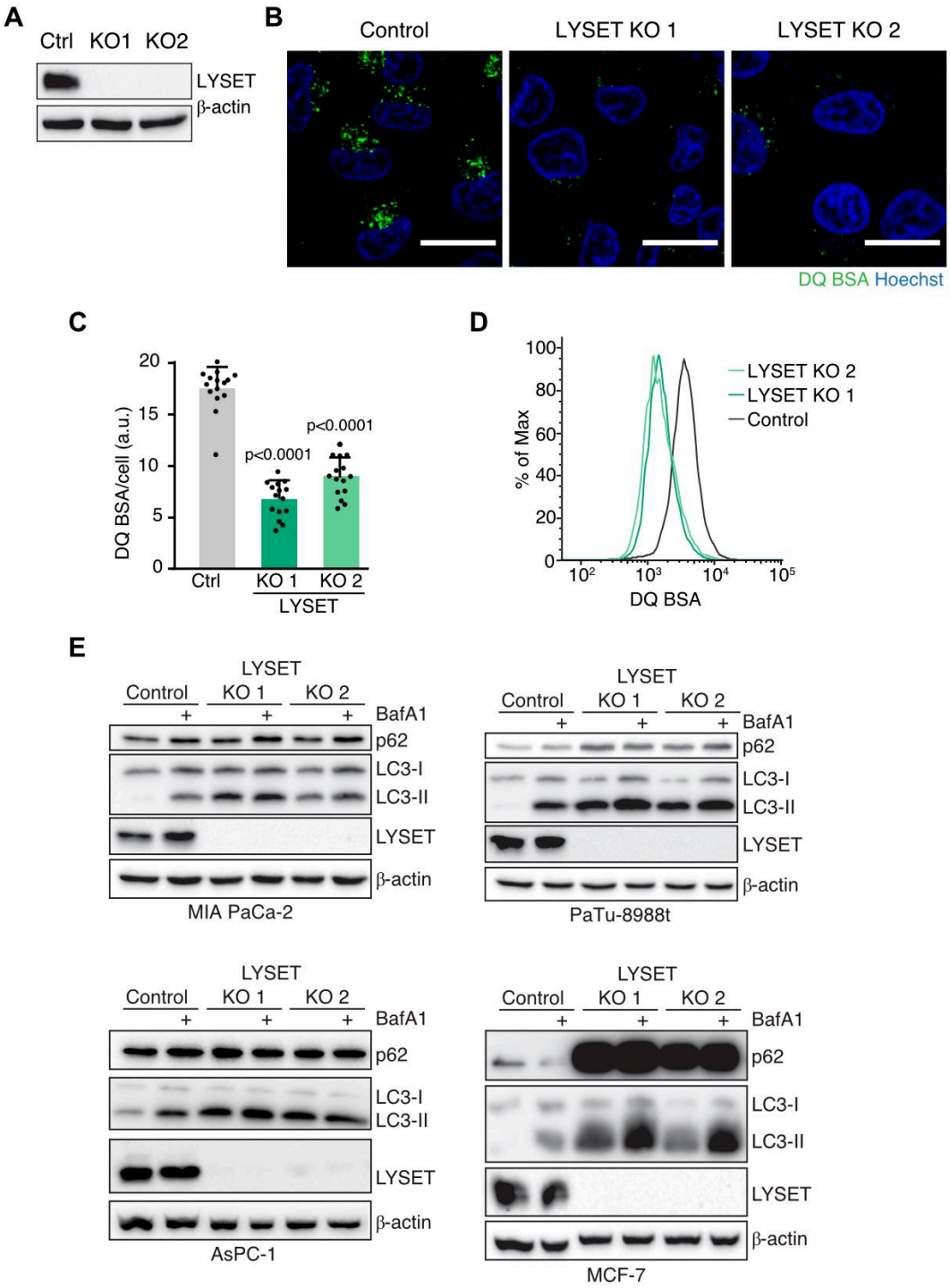

Figure 8 - LYSET is required for lysosomal degradation of endocytic and autophagic cargoes.
(A) Immunoblot of MIA PaCa-2 clonal LYSET KO. (B) Confocal microscopy detection of lysosomal DQ BSA degradation in MIA PaCa-2 clonal LYSET KO cells. Scale bars = 20 mm. (C) Quantification of confocal images represented in (B). Data are represented as means ± SD. N = 15 randomly chosen fields of view with ≥10 cells. P values were calculated by unpaired two-sided t-test with Welch correction. a.u., arbitrary units. (D) Flow cytometry analysis of lysosomal DQ BSA degradation in MIA PaCa-2 clonal LYSET KO cells. (E) Immunoblot of autophagosomal proteins (p62 and LC3) in the indicated control and bulk LYSET KO cell lines ± 100 nM bafilomycin A1 for 3 h.

4.3 LYSET is part of the machinery for lysosomal enzyme trafficking

4.3.1 LYSET is required for the sorting of lysosomal enzymes

To understand why LYSET is required for lysosomal function, changes in the proteome of clonal LYSET KO MIA PaCa-2 cells were determined by liquid chromatography-mass spectrometry and label-free quantification (LC-MS) analysis. To this end, I prepared protein lysates from PNS control and LYSET-depleted cells and submitted them to the DKFZ Proteomics Core Facility. Further processing and measurement were conducted by Dominic Helm and data analysis by Martin Schneider. Amongst the proteins whose levels increased in LYSET-depleted cells, were autophagy-related proteins, which confirmed my previous observation for p62 and LC3 (Figure 8E, Figure 9A). Most of the proteins depleted in LYSET-deficient cells were lysosomal luminal enzymes (Figure 9A). Lysosomal membrane proteins were unaltered (Figure 9B).

To better understand the loss of lysosomal enzymes and determine the composition of lysosomes in LYSET-depleted cells, I prepared lysosomal-enriched fractions for LC-MS analysis. MIA PaCa-2 cells were incubated with ferromagnetic nanoparticles (DexoMAG C) for 14 h followed by a 6 h chase in fresh medium, for loading of lysosomes. Cells were collected and homogenised with a tissue grinder. Nuclei were removed from the homogenate by centrifugation to obtain a PNS. Next, the PNS was loaded in a magnetic column, from where DexoMAG C-containing vesicles were then eluted. The resulting lysosomal-enriched eluate was submitted to the DKFZ Proteomics Core Facility for further processing, measurement, and data analysis. Most of the 49 identified lysosomal luminal enzymes were strongly depleted in lysosomes from clonal LYSET KO MIA PaCa-2 cells (Figure 9C). Lysosomal membrane proteins were not altered (Figure 9D). This suggested that LYSET is specifically required for the luminal composition of the lysosome, but not for broad lysosomal biogenesis.

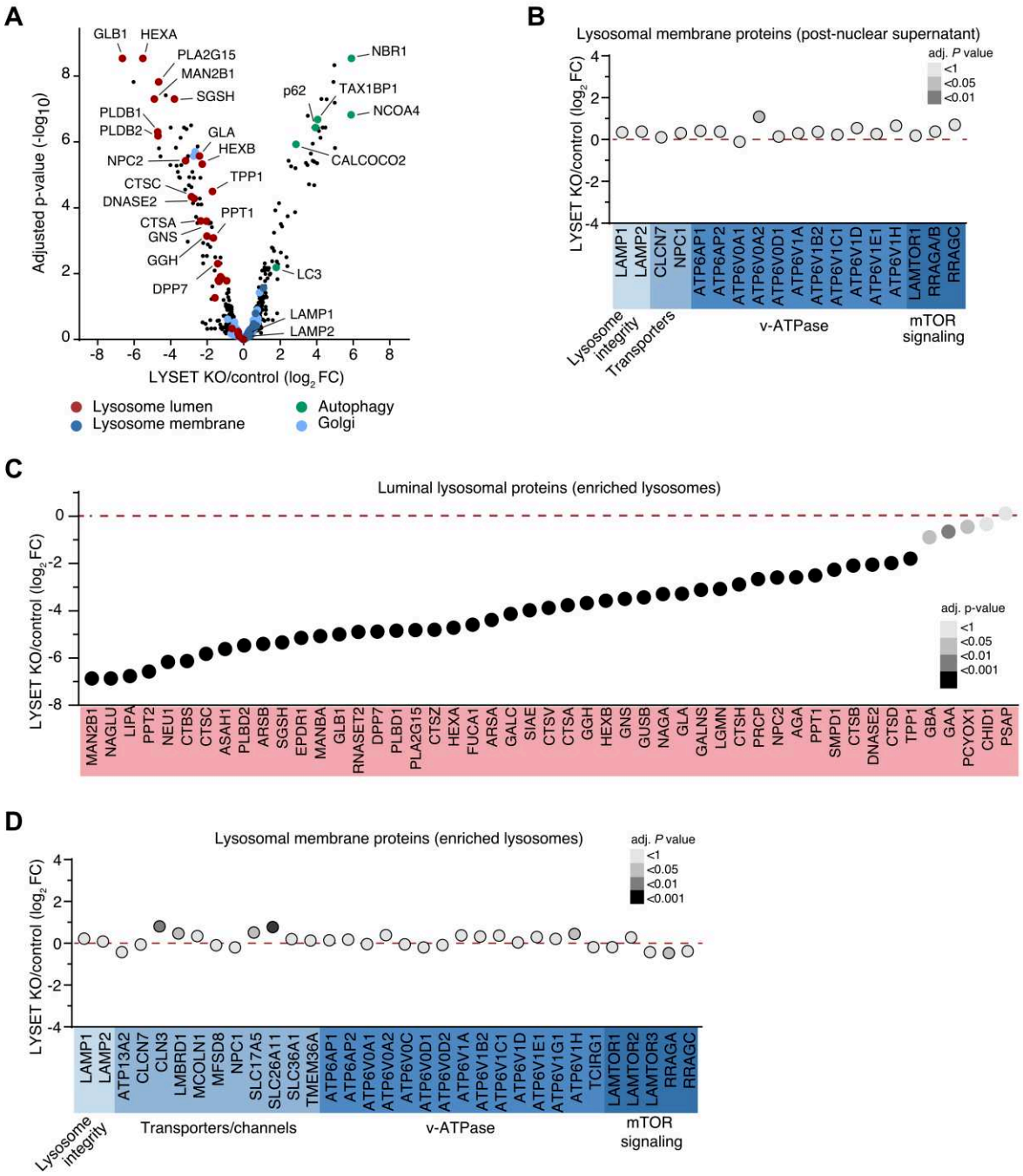

Figure 9 - LYSET is required for the luminal composition of the lysosome, but not for generic lysosomal biogenesis.

(A) Liquid chromatography-mass spectrometry and label-free quantification analysis of post-nuclear supernatants from MIA PaCa-2 clonal LYSET KO cells. Data are presented as Log_2 fold change (Log_2 FC) of proteins detected in MIA PaCa-2 clonal LYSET KO compared with control cells. N = 5 biologically independent experiments. (B) Changes in lysosomal membrane proteins of post-nuclear supernatants from MIA PaCa-2 clonal LYSET KO compared with control cells. Subset from data in (A). (C and D) Changes in lysosomal luminal proteins (C) and membrane proteins (D) analysed by liquid chromatography-mass spectrometry and label-free quantification of lysosomal-enriched fractions from MIA PaCa-2 clonal LYSET KO cells. Data are presented as Log_2 fold change (Log_2 FC) of proteins detected in MIA PaCa-2 clonal LYSET KO compared with control cells. N = 5 biologically independent experiments. Data were produced jointly with Dominic Helm and data analysed by Martin Schneider.

To assess why lysosomal luminal enzymes were mostly absent from the lysosome of LYSET-deficient cells, I determined the mRNA and protein levels of three lysosomal hydrolases (cathepsin B, cathepsin L, and hexosaminidase A). All three chosen proteins are synthesised as immature pro-enzymes, processed during vesicle trafficking, and activated when reaching the mature form in the lysosome. mRNA from MIA PaCa-2 clonal control and clonal LYSET KO cells was extracted with Trizol, reversely transcribed to cDNA, and subsequently quantified by RT-qPCR. LYSET-deficient cells did not show reduced mRNA levels for any of the three analysed proteins (Figure 10A). To assess lysosomal enzyme protein levels, I immunoblotted cathepsin B, cathepsin L, and hexosaminidase A in cell lysates from a panel of pancreatic cancer cell lines with bulk LYSET KO. Protein levels of the immature forms of the three proteins were not decreased. On the contrary, the mature forms were strongly decreased in a variety of LYSET-deficient cell lines (Figure 10B). This is consistent with the lysosomal-enriched fraction proteomic results (Figure 9C).

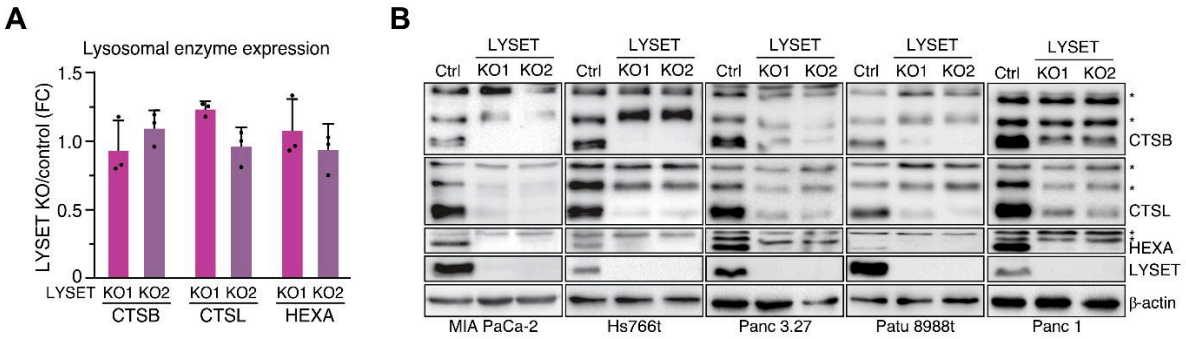

Figure 10 - Lysosomal enzymes are not delivered to the lysosome of LYSET-deficient cells.
(A) RT-qPCR analysis of the lysosomal enzymes cathepsin B (CTSB), cathepsin L (CTSL), and hexosaminidase A (HEXA) mRNA levels in MIA PaCa-2 clonal LYSET KO cells. Data are represented as means ± SD. *N* = 3. (B) Immunoblot of the lysosomal enzymes CTSB, CTSL, and HEXA in indicated bulk LYSET KO cell lines upon 7 days of transduction and antibiotic selection. * denotes immature enzymes.

To understand the fate of lysosomal luminal enzymes that do not reach the lysosome in LYSET-depleted cells, I analysed secreted proteins by immunoblotting and LC-MS (together with the DKFZ Proteomics Core Facility). Clonal LYSET KO MIA PaCa-2 cells were cultured for 24 h in OptiMEM. After this period, the medium was collected, cleared by centrifugation, and analysed. The immature forms of both cathepsin B and L were significantly increased in the secreted fraction of LYSET-depleted cells when analysed by immunoblotting (Figure 11A). In the LYSET-depleted secretome LC-MS analysis, luminal lysosomal enzymes were consistently increased (Figure 11B). Thus, LYSET ablation leads to an aberrant secretion of luminal lysosomal enzymes. These data suggest that LYSET is required for the correct trafficking of lysosomal enzymes to the lysosome.

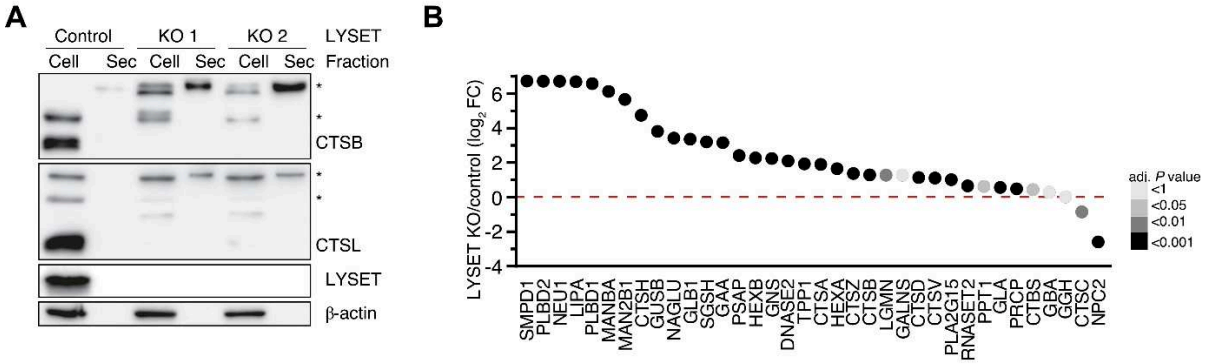

Figure 11 - Luminal lysosomal enzymes are secreted in LYSET-depleted cells.
(A) Immunoblot for cathepsin B and L (CTSB and CTSL) in cellular or secreted fractions from MIA PaCa-2 control and clonal LYSET KO cells. * denotes immature enzymes. (B) Liquid chromatography-mass spectrometry and label-free quantification analysis of luminal lysosomal proteins in secreted fractions of clonal MIA PaCa-2 LYSET KO cells. Data are presented as Log_2 fold change (Log_2 FC) of proteins detected in clonal MIA PaCa-2 LYSET KO compared with control cells. N = 5 biologically independent experiments. Data were produced jointly with Dominic Helm and data analysed by Martin Schneider.

4.3.2 LYSET is a core component of the mannose-6-phosphate pathway for lysosomal enzyme trafficking

Most soluble lysosomal enzymes are modified with a M6P residue by GNPTAB in the Golgi, for correct sorting to the endolysosomal system. To detect M6P modifications, I prepared protein lysates from MIA PaCa-2 clonal LYSET and GNPTAB KO cells and analysed them by SDS gel electrophoresis followed by a transfer to nitrocellulose membranes. Further blocking and immunoblotting were done by Sabrina Jabs, Junior Group Leader in the Christian-Albrechts-Universität zu Kiel, using a single-chain antibody fragment that detects M6P residues (Muller-Loennies *et al.*, 2010). LYSET-depleted cellular lysates revealed a substantial decrease in M6P-modified proteins (Figure 12A). Interestingly, LYSET depletion phenotype was comparable to the M6P loss observed in the GNPTAB-depleted cells. To determine M6P levels in newly synthesised lysosomal enzymes, I induced their secretion with ammonium chloride, collected the medium in which the cells were cultured, and prepared them for immunoblotting, as before. M6P residues were barely detected in secreted enzymes from LYSET- and GNPTAB-depleted cells (Figure 12B). I determined the protein levels of the acid glucosylceramidase (GBA), which does not require M6P modifications to be trafficked to the lysosome. By immunoblotting, I observed that GBA protein levels are not changed in LYSET-deficient cells, consistent with the proteomics data (Figure 9C and Figure 12C). Thus, data

suggested that LYSET is required for the lysosomal trafficking of enzymes depending on the M6P pathway.

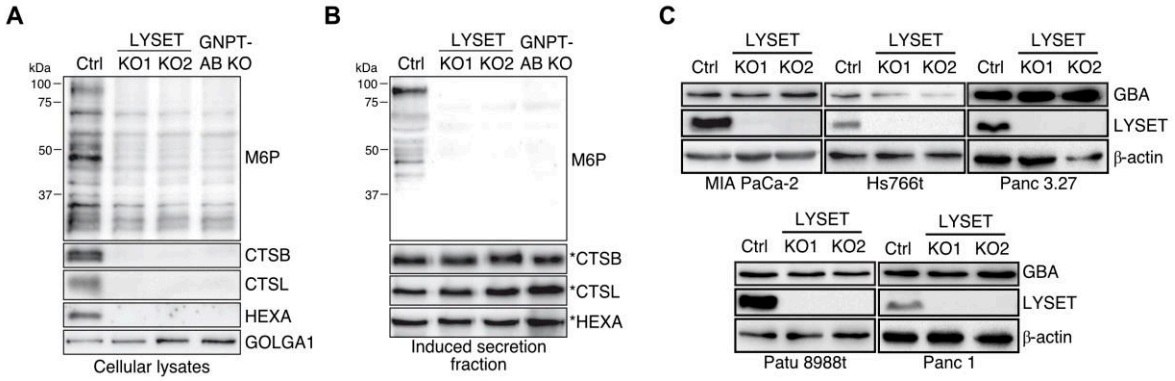

Figure 12 - LYSET is required for the trafficking of luminal lysosomal enzymes that depend on the mannose-6-phosphate pathway.

(A and B) Immunoblot of mannose-6-phosphate (M6P) modification in organelle-enriched fractions (A) and newly synthesised proteins detected in the secreted fraction upon treatment with NH4Cl to induce protein secretion (B) of clonal LYSET and GNPTAB KO MIA PaCa-2 cells. * denotes immature enzymes. Data produced jointly with Sabrina Jabs. (C) Immunoblot of glucosylceramidase beta 1 (GBA) in the indicated control and bulk LYSET KO cell lines. LYSET and β-actin data are as in Figure 10B.

To more widely understand the functional and phenotypic similarities between LYSET and GNPTAB knockout, I genetically ablated either protein in MIA PaCa-2 cells and MEFs and performed a comparative analysis. MEF iCas9 cells were generated by me and subsequent LYSET iKO induction with 300 µg/ml doxycycline for 3 days was done by Sven Groessl. By immunoblotting, I observed that LYSET and GNPTAB iKO caused a strong reduction in mature lysosomal enzymes present in cellular lysates (Figure 13A and B). Furthermore, depletion of either LYSET or GNPTAB led to hypersecretion of immature cathepsin L (Figure 13C). This suggested a comparable defect in the sorting of lysosomal enzymes. Additionally, both LYSET and GNPTAB depletion led to the accumulation of the autophagic cargo proteins p62 and LC3-II (Figure 13A and B). By flow cytometry and live cell imaging analysis of DQ BSA, I observed a reduction in lysosomal albumin degradation when either protein was depleted in MEFs (Figure 13D and E). In summary, LYSET depletion resembles GNPTAB depletion phenotypically, suggesting that LYSET is an important component of the M6P pathway.

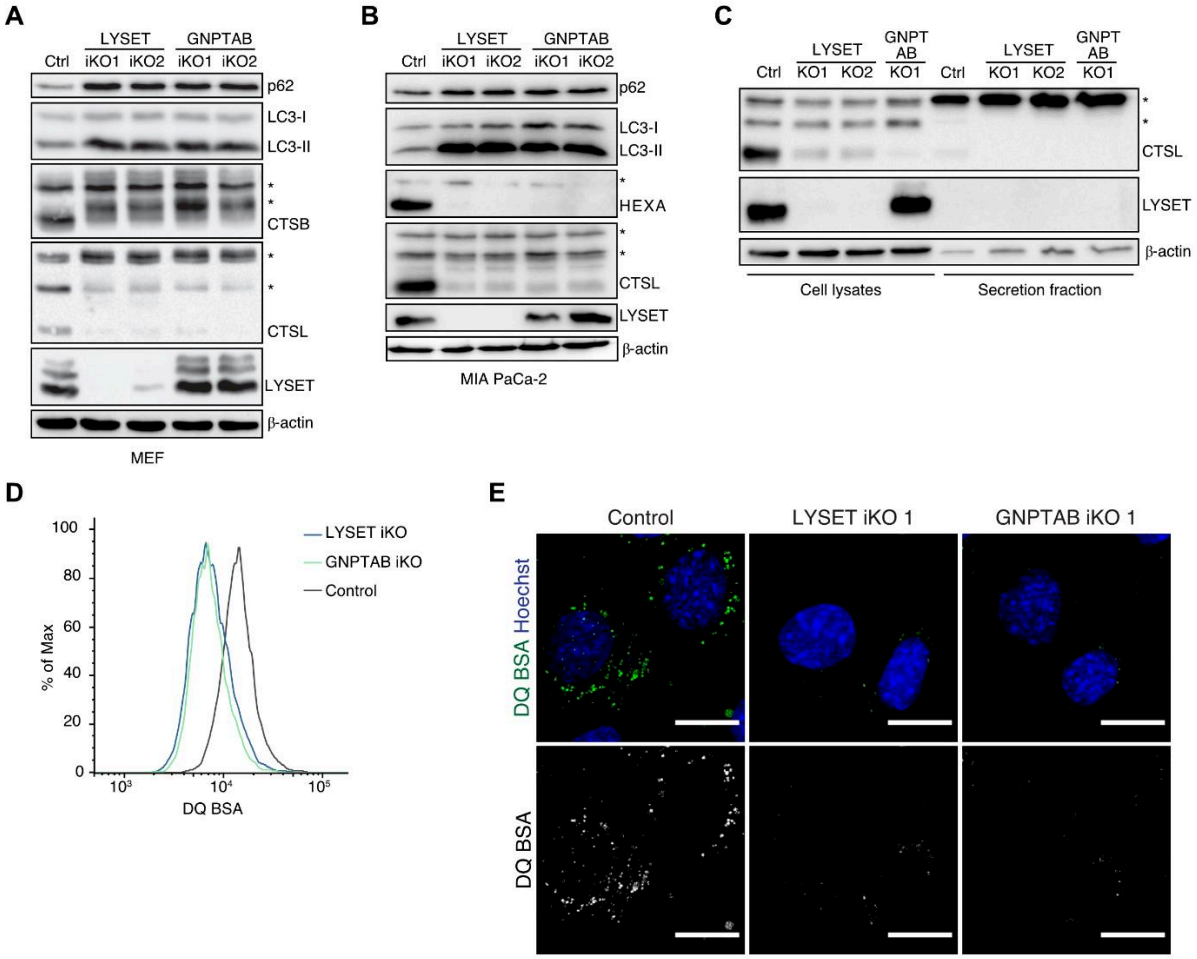

Figure 13 - LYSET and GNPTAB knockout show similar lysosomal phenotypes.
(A) Immunoblot of p62 and LC3 and luminal lysosomal enzymes (CTSL and CTSB) from Lyset iKO and Gnptab iKO MEFs, upon 7 days of knockout induction (3 days in 300 ng/mL doxycycline followed by 4 days without doxycycline). * denotes immature enzymes. Experiment performed by Sven Groessl. (B) Immunoblot of p62 and LC3 and luminal lysosomal enzymes (CTSL and HEXA) from MIA PaCa-2 LYSET iKO and GNPTAB iKO cells, upon 7 days of knockout induction (3 days in 200 ng/mL doxycycline followed by 4 days without doxycycline). * denotes immature enzymes. (C) Immunoblot of CTSL in cellular lysates and secreted fraction from endogenously depleted LYSET or GNPTAB MIA PaCa-2 cells. * denotes immature enzymes. (D) Flow cytometry analysis of DQ BSA degradation in iCas9 MIA PaCa-2 cells transduced with LYSET dsgRNA 1, GNPTAB dsgRNA 1, or Chr dsgRNA 1 as control, upon 7 days of knockout induction (3 days in 200 ng/mL doxycycline followed by 4 days without doxycycline). (E) Confocal microscopy images of DQ BSA degradation in Lyset iKO and Gnptab iKO MEFs, upon 7 days of knockout induction (3 days in 300 ng/mL doxycycline followed by 4 days without doxycycline).

4.3.3 LYSET is a Golgi-resident protein

To further understand the role of LYSET and its importance for the trafficking of lysosomal enzymes, I defined its subcellular localisation. For that, I immunostained LYSET and the Golgi marker GM130 in MIA PaCa-2 bulk control and LYSET KO cells. I observed that LYSET completely co-localises with the Golgi marker, suggesting that LYSET resides in the Golgi (Figure 14A).

To understand if LYSET could affect the Golgi generally, I assessed the Golgi morphology and proteomic content of LYSET-depleted cells. To test Golgi morphology, I immunostained two Golgi-resident proteins GOLGA1 and GM130, expressed in the trans and cis-Golgi, respectively, in clonal LYSET KO of MIA PaCa-2 and HEK293T cells. The obtained confocal images did not show obvious differences in Golgi organisation (Figure 14B and C). Furthermore, the proteome analysis of MIA PaCa-2 LYSET-depleted and control cells did not show altered protein levels of Golgi-resident proteins (Figure 9A). Thus, LYSET is localised in the Golgi but is dispensable for Golgi morphology. This suggests that LYSET has no general effect on Golgi function, but rather a defined effect on the M6P pathway.

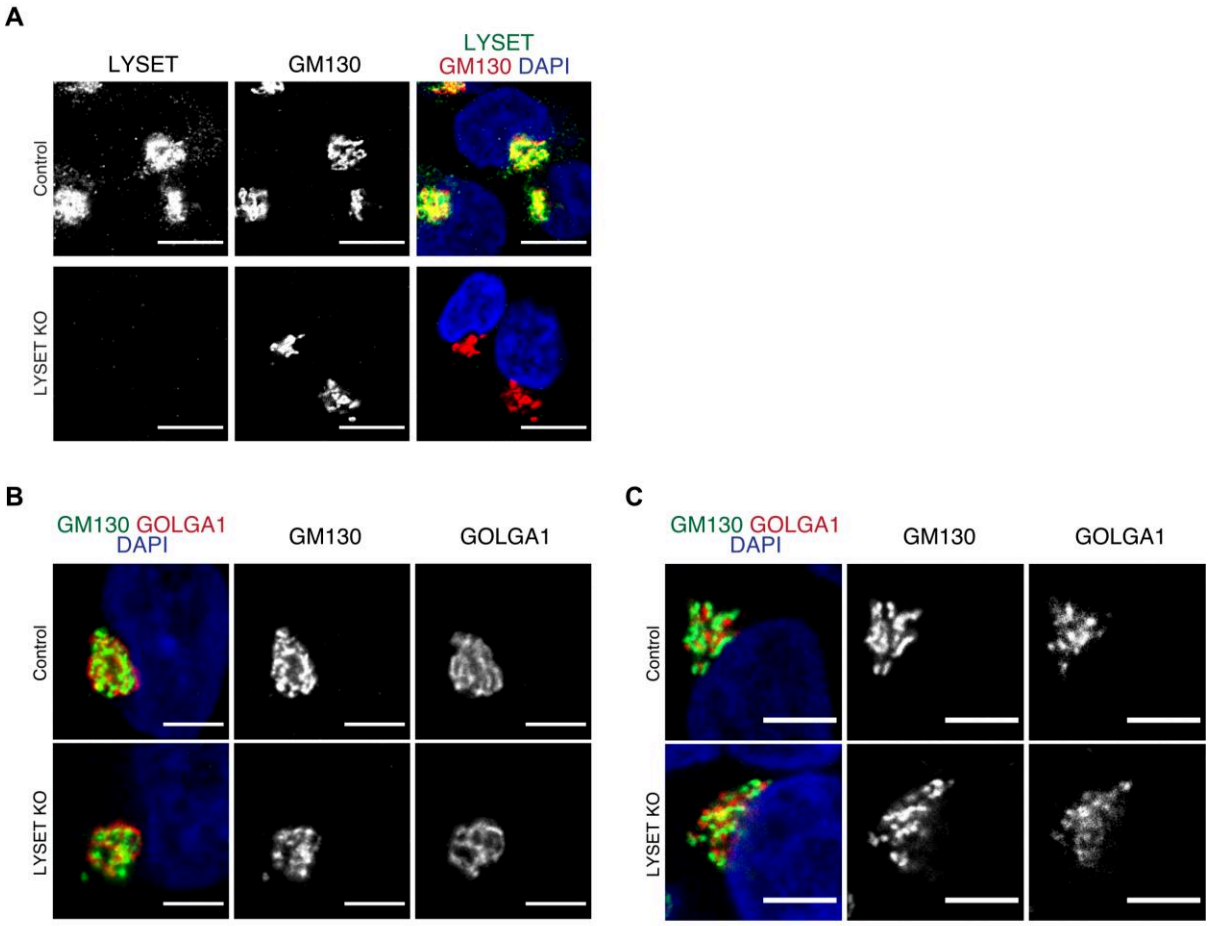

Figure 14 - LYSET is localised in the Golgi but it is dispensable for Golgi structure.
(A) Confocal microscopy images of MIA PaCa-2 cells immunostained with LYSET and GM130 antibodies. Scale bar = 10 µm. (B and C) Confocal microscopy images of MIA PaCa-2 (B) and HEK293T (C) clonal LYSET KO cells immunostained with GOLGA1 and GM130 antibodies for labelling of cis and trans-Golgi structure, respectively. Scale bar = 5 µm.

4.4 LYSET deficiency causes lysosomal storage disorder-like phenotypes at the cellular level

4.4.1 Lysosomal morphology of LYSET-depleted cells resembles GNPTAB depletion phenotypes

To characterise the pathophysiological relevance of LYSET for lysosomal disorders, I performed a comparison between LYSET and GNPTAB. GNPTAB loss-of-function mutations lead to a loss or reduction of the GlcNAcPT activity which results in a rare group of LSDs called mucolipidosis II and III, respectively, which lead to an accumulation of lysosomes with undigested cargo (Platt *et al.*, 2012). To test if LYSET depletion would result in similar cellular phenotypes, I stained LYSET- and GNPTAB-depleted MEFs, MIA PaCa-2, and HEK 293T cells with lysotracker, a dye that gets protonated and accumulates in acidic organelles. Lysotracker signal analysed by live imaging and flow cytometry was strongly increased in both gene knockouts (Figure 15). These data showed that LYSET depletion phenotypes resemble the lysosomal morphology characteristic of mucolipidosis II/III (Platt *et al.*, 2012, Khan and Tomatsu, 2020).

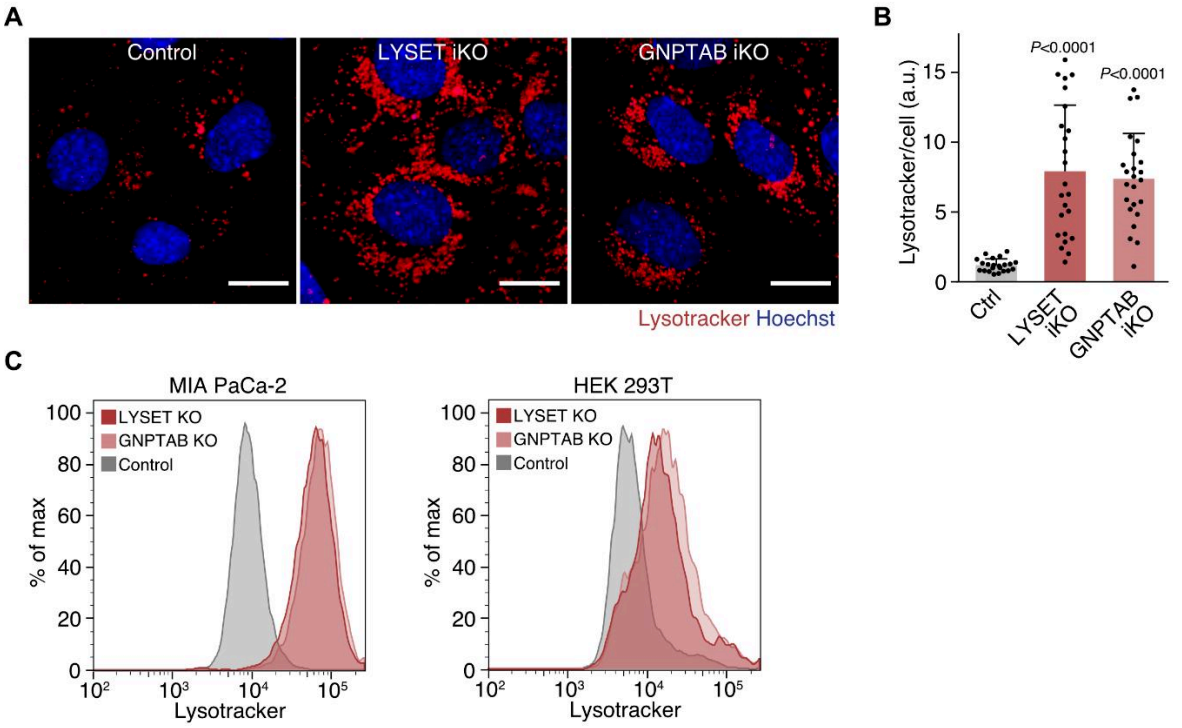

Figure 15 - LYSET and GNPTAB depletion leads to lysosomal changes.
(A) Confocal microscopy images of lysotracker accumulation in Lyset iKO and Gnptab iKO MEFs, upon 7 days of knockout induction (3 days in 300 ng/mL doxycycline followed by 4 days without doxycycline). Scale bar = 20 µm. (B) Quantification of confocal images represented in (A). Data are represented as means ± SD (N = 22-24 randomly chosen fields of view with a total of > 150 cells). P values were calculated by unpaired two-sided t-test with Welch correction. a.u., arbitrary units. (C) Flow cytometry analysis of lysotracker accumulation in MIA PaCa-2 clonal LYSET and GNPTAB KO cells and HEK 293T bulk LYSET and GNPTAB KO cells.

4.4.2 Expression of LYSET patient mutations leads to cellular phenotypes observed in lysosomal storage disorder-associated GNPTAB mutations

Two LYSET variants (R45W and Y72X) were identified in patients with familial skeletal dysplasia syndromes, with symptoms reminiscent of mucolipidosis (Ain *et al.*, 2021). To unravel the functional impact of the described LYSET variants, I and Marten Wittmann, a technician in our lab, engineered MIA PaCa-2 clonal LYSET KO and HEK 293T bulk LYSET KO cells to stably express the different loss-of-function mutations. To rescue the LYSET-depletion phenotype, I re-expressed the two isoforms of human LYSET in the MIA PaCa-2 LYSET KO clone. To this end, I cloned the two isoforms of LYSET into pBabe-PuroR and transduced those using retroviral particles. By immunoblotting, I observed that both isoforms fully rescued the depletion of mature cathepsin L and LC3-II accumulation (Figure 16A). As the short isoform (isoform 2) is the evolutionarily conserved isoform that is predominantly expressed in most cell types analysed, I and Marten Wittmann recloned it into plasmids with

a lower strength promoter (pRRL-pUbC-tagRFP-T-Hygro) and performed site-directed mutagenesis to obtain plasmids expressing LYSET^{wt}, LYSET^{R45W}, and LYSET^{Y72X} at levels comparable to endogenous. Of note, although I mutagenised the isoform 2 cDNA, the residue number identifying the mutations refers to the long isoform (isoform 1) and was kept for consistency with the original publication (Ain et al., 2021). I produced lentiviral particles from these plasmids and transduced them in the LYSET KO cells. Wild-type, LYSET KO, and LYSET^{wt}-, LYSET^{R45W}-, and LYSET^{Y72X}-expressing cells were prepared for immunoblotting of lysosomal enzymes and LC3 and characterisation of lysosomal morphology by flow cytometry and confocal microscopy. While wild-type LYSET fully rescued mature lysosomal enzyme levels and decreased LC3-II levels, LYSET patient mutations failed to rescue either phenotype (Figure 16B). Consistently, cells expressing LYSET^{R45W} or LYSET^{Y72X} displayed an accumulation of lysosomes, marked by the accumulation of lysotracker, to a similar extent as the LYSET knockout cells, while LYSET^{wt} led to a decrease in lysotracker signal (Figure 16C). Thus, the cellular phenotypes driven by the described LYSET patient mutations are comparable to the ones I observed in LYSET knockout cells.

To compare the phenotype of LYSET mutations to patient-derived GNPTAB mutations, Marten Wittmann cloned GNPTAB tagged with the affinity tag myc in its C-terminus (GNPTAB-myc) into pRRL-pUbC-HygroR. I produced lentiviral particles encoding this plasmid and transduced them in the GNPTAB knockout cells. Via site-directed mutagenesis, Robert Kalis produced pRRL-pUbC-HygroR plasmids encoding GNPTAB^{K4Q}- and GNPTAB^{S15Y}-myc, mutations described to generate unstable forms of the GlcNAc-1-Phosphotransferase (Van Meel *et al.*, 2014). By immunoblotting, I observed that both GNPTAB mutations are barely detectable. Consistently, GNPTAB mutations lead to the same cellular phenotypes as LYSET loss-of-function mutations: a decrease in mature lysosomal enzymes and an accumulation of LC -II (Figure 16D). Likewise, both proteins' knockout and respective patient-derived mutations revealed similar lysotracker staining phenotypes (Figure 16E). In summary, LYSET patient mutations resemble cellular phenotypes observed in LSD-associated GNPTAB mutations.

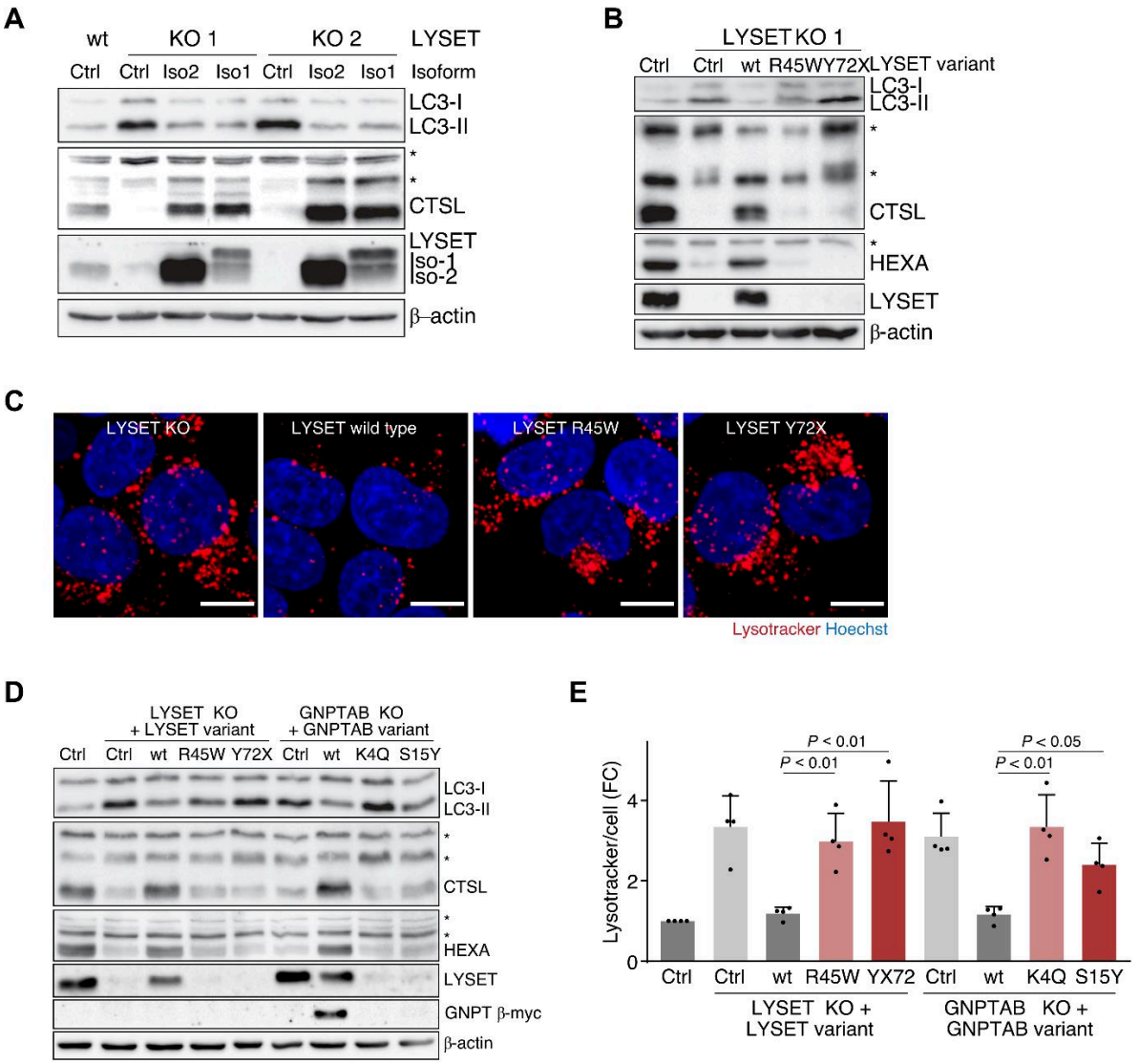

Figure 16 - Expression of LYSET patient mutations displays similar cellular phenotypes as expression of lysosomal storage disorders-associated GNPTAB mutations.

(A) Immunoblot analysis of LC3 and CTSL levels in MIA PaCa-2 clonal LYSET KO cells upon re-expression of human LYSET isoforms 1 or 2. The short isoform 2 is the predominant isoform in most cell types tested, evolutionarily conserved, and fully rescues lysosomal enzyme trafficking. * denotes immature enzymes. (B) Immunoblot analysis of LC3 and CTSL levels in MIA PaCa-2 clonal LYSET KO cells expressing human LYSET wild type (wt variant) or the two patient-derived mutations (R45W or Y72X variants). * denotes immature enzymes. (C) Confocal microscopy images of lysotracker accumulation in HEK293T bulk LYSET KO cells upon re-expression of human LYSET wt, R45W, or Y72X. Scale bar = 10 µm. (D) Immunoblot analysis of LC3 and luminal lysosomal enzymes (CTSL and HEXA) levels in HEK293T bulk LYSET and GNPTAB KO cells expressing human LYSET wild type (wt variant) or the two patient-derived mutations (R45W or Y72X variants). * denotes immature enzymes. Experiment performed by Marten Wittmann. (E) Flow cytometry quantification of lysotracker accumulation in lysosomes of e HEK293T bulk LYSET and GNPTAB KO cells expressing human LYSET wild type or the two patient-derived mutations (R45W or Y72X) or human GNPTAB-myc wild type or the pathogenic GNPTAB mutations (K4Q, S15Y). Data are represented as means ± SEM. N = 4 biologically independent experiments. P values were calculated by a two-sided unpaired t-test with Welch correction.

4.5 GlcNAc-1-phosphotransferase depends on LYSET

4.5.1 LYSET interacts with GlcNAc-1-phosphotransferase

To understand the molecular relationship between LYSET and GNPTAB, I examined their possible interaction. To this end, Marten Wittmann cloned GNPTAB C-terminally tagged with Flag (GNPTAB-Flag) into pLV-EF1a-IRES-BlastR and I lentivirally expressed it in MIA PaCa-2 cells. By immunofluorescent staining of Flag-tag and endogenous LYSET, I observed that both proteins co-localised in the Golgi (Figure 17A). Furthermore, I prepared MIA PaCa-2 control and LYSET knockout cells expressing GNPTAB-myc and I performed a proximity ligation assay (PLA) using antibodies against LYSET and myc. In control cells, where both LYSET and GNPTAB-myc were expressed, I observed a strong Golgi-like signal (Figure 17B). Contrarily, in cells not expressing either GNPTAB-myc or LYSET the PLA signal was barely detected (Figure 17C). To confirm the specificity of the PLA signal, I performed the PLA with LYSET and myc antibodies in combination with antibodies against the Golgi ubiquitously expressed proteins GM130 and GOLGA1, respectively. These stainings showed a much weaker signal (Figure 17D). Together, these assays suggested that LYSET is in close proximity to the GlcNAc-1-phosphotransferase complex in the Golgi.

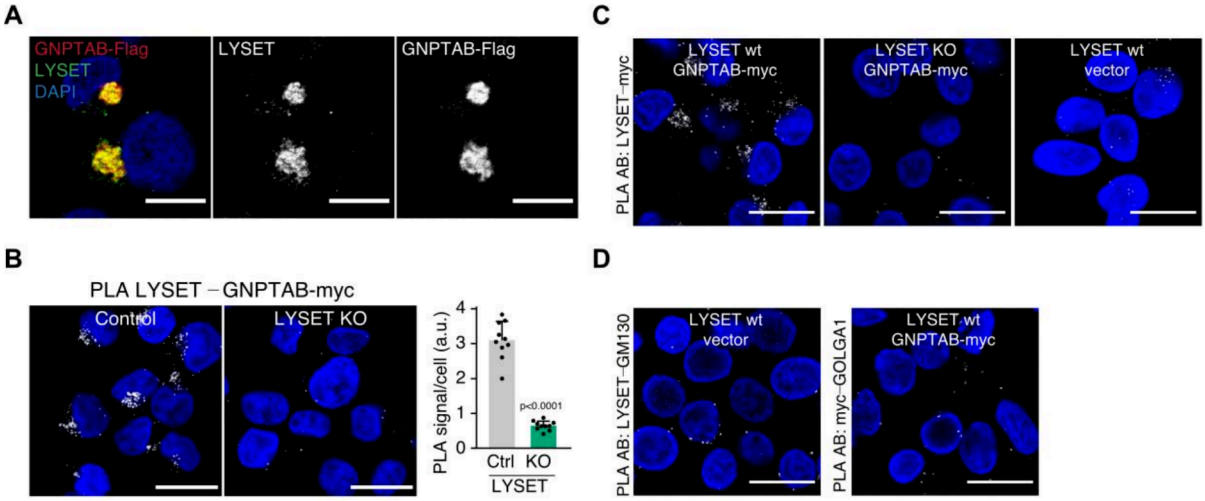

Figure 17 - LYSET co-localises with GNPTAB in the Golgi.
(A) Confocal microscopy images of MIA PaCa-2 cells expressing GNPTAB-Flag immunostained with Flag and LYSET antibodies. Scale bar = 10 µm. (B) Proximity ligation assay (PLA) between LYSET and myc in MIA PaCa-2 cells expressing GNPTAB-myc. Data are represented as means ± SD (N = 10 fields of view with ≥13 cells). P values were calculated by unpaired two-sided t-test with Welch correction. (C) PLA between LYSET and myc in the different indicated genetic manipulations of MIA PaCa-2 cells. (D) PLA between LYSET and the Golgi resident-protein GM130 (left) or between myc and the Golgi-resident protein GOLGA1 (right) in MIA PaCa-2 cells with the different indicated genotypes. Scale bar = 20 µm.

4.5.2 Loss of LYSET leads to a strong decrease in the mature GNPT α and β subunits

To assess if LYSET would have an impact on the GlcNAc-1-phosphotransferase complex proteins, I quantified the mRNA levels of the two genes encoding for the GlcNAc-1-phosphotransferase complex, *GNPTAB* and *GNPTG*, in MIA PaCa-2 control and LYSET-depleted cells using RT-qPCR. Data showed no decrease in the abundance of *GNPTAB* nor *GNPTG* mRNA in LYSET-depleted cells, suggesting that LYSET does not regulate the expression of these proteins at the transcription level (Figure 18A). Next, I examined the expression of GNPTAB-myc in LYSET-deficient cells. I drove the expression of GNPTAB-myc by lentiviral transduction of MIA PaCa-2 cells with or without endogenous deletion of LYSET. Upon selection of the transduced cells, I prepared organelle-enriched fractions by mechanically disrupting the cellular membrane with a dounce tissue grinder followed by two rounds of centrifugation to remove the nucleus content and pellet the membrane organelles, which I resuspended in lysis buffer for further immunoblotting analysis. Organelle-enriched fractions from control and LYSET knockout cells were immunoblotted for GOLGA1, used as loading control in organelle-enriched fractions immunoblots, and myc-tag for detection of the overexpressed GNPTAB-myc. As expected, I observed two myc bands in control cells, corresponding to the molecular weights of the GNPT α/β precursor and the cleaved epitope-tagged GNPT β subunit. GNPT α/β precursor levels were not changed while the mature GNPT β subunit was barely detected in LYSET-deficient cells (Figure 18B). To endogenously detect GNPTAB, I analysed HAP1 and SK-MEL-30 cells, two cell lines with high endogenous expression of GNPTAB. For this, Sven Groessl sequentially transduced and selected these cell lines with pLenti-Cas9-BlastR and Dual-hU6-sgRNA-mU6-sgRNA-EF1α-mCherry-P2A-PuroR harbouring Chr dsgRNA 1, LYSET dsgRNA 1 or GNPTAB dsgRNA 1. Next, I prepared organelle-enriched fractions of these cell lines and detected GNPT α subunit by immunoblotting, using an antibody developed to detect specifically the GNPT α. By first testing HAP1 cells, I could only detect one band using the antibody against GNPT α (Figure 18C), which possibly corresponded to non-resolved bands of GNPT α/β precursor and mature GNPT α. To better resolve the gel and separate the two bands, I treated the protein lysates with N-glycosidase F (PNGaseF), to remove N-linked glycosylation. When immunoblotting the deglycosylated samples, I could detect in control cells two bands, possibly corresponding to the GNPT α/β precursor and mature GNPT α (Figure 18D). In LYSET-deficient cells, the GNPT α band was barely detectable, confirming my observations using the GNPTAB-myc overexpression system (Figure 18B and D). These results were reproducible in SK-MEL-30 cells, where GNPT α band was lost in LYSET-deficient cells to the same extent as in GNPTAB-

deficient cells (Figure 18E). Thus, loss of LYSET leads to a strong decrease of the mature GNPT α and β subunits.

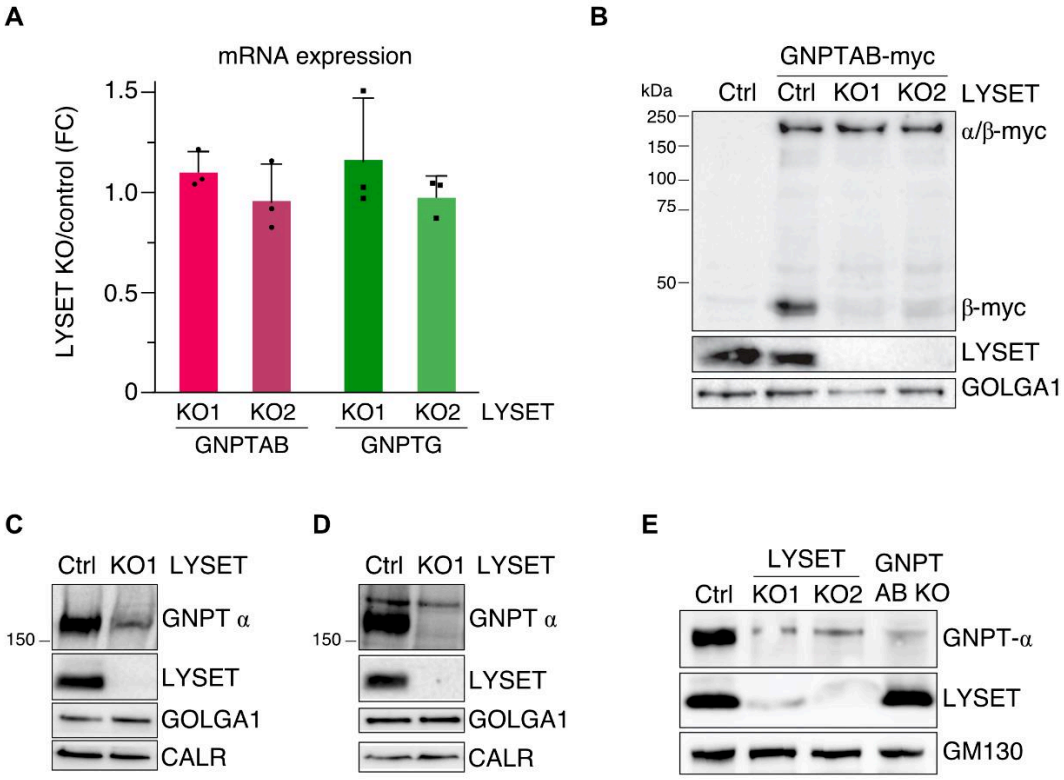

Figure 18 - Loss of LYSET leads to loss of the mature GNPT α and β subunits, but not to a decrease in GNPTAB mRNA or precursor protein levels.
(A) RT-qPCR analysis of GNPTAB and GNPTG mRNA levels in MIA PaCa-2 clonal LYSET KO cells. Data are represented as mean ± SD. *N* = 3. (B) Immunoblot analysis of overexpressed GNPTAB-myc levels in MIA PaCa-2 clones with endogenous deletion of LYSET. (C) Immunoblot analysis of endogenous GNPT α subunit levels in HAP1 bulk LYSET KO cells. (D) Immunoblot analysis of endogenous GNPT α subunit levels in lysates from HAP1 bulk LYSET KO cells upon deglycosylation. (E) Immunoblot analysis of endogenous GNPT α subunit levels in SK-MEL-30 bulk LYSET and GNPTAB KO cells cells. α/β-myc and β-myc denote the myc-tagged GNPTAB α/β precursor and β subunit, respectively.

4.5.3 LYSET is not required for the processing of GlcNAc-1-phosphotransferase

GNPT α and GNPT β are synthesised in the ER as a GNPT α/β precursor protein. There, the precursor protein is glycosylated and further trafficked to the Golgi. In the Golgi, GNPT α/β precursor is processed by S1P and the resulting mature GNPT α and GNPT β subunits are again modified. To clarify if the processing and cleavage of GNPT α/β into GNPT α and GNPT β are dependent on LYSET, I examined its glycosylation and S1P activity in LYSET-deficient cells. First, I prepared PNS lysates from HEK 293T control and LYSET-depleted cells transiently transfected with GNPTAB-myc, to enforce overexpression and

accumulation of GNPT β subunit. Then, I treated the PNS with endoglycosidase Hf (EndoHf) or PNGaseF, two enzymes used to monitor post-translation modifications in the Golgi apparatus. EndoHf removes mannose-rich oligosaccharide modifications in N-linked glycoproteins while PNGaseF removes all types of N-linked glycosylation. Upon treatments, I run the protein samples in an SDS gel electrophoresis followed by a transfer into nitrocellulose membranes and immunoblotting of myc-tag. Results show that LYSET-deficient cells are still capable of modifying high mannose- and complex-type glycans in GNPTAB (Figure 19A), suggesting a normal Golgi processing of GNPTAB.

Next, I tested S1P activity in MIA PaCa-2 clonal LYSET KO cells. To this end, I induced ER stress and determined the nuclear levels of cleaved ATF6. S1P cleaves ATF6 in response to ER stress and cleaved ATF6 is translocated to the nucleus (Katrin Marschner, 2011). I treated MIA PaCa-2 clonal control and LYSET KO cells with thapsigargin, a drug known to induce ER stress, and prepared cytoplasm and nucleus lysates. Immunoblotting showed that the absence of LYSET did not affect the cleavage of ATF6 in response to thapsigargin (Figure 19B). Thus, LYSET is not required for S1P activity and, hence, for the cleavage of GNPTAB.

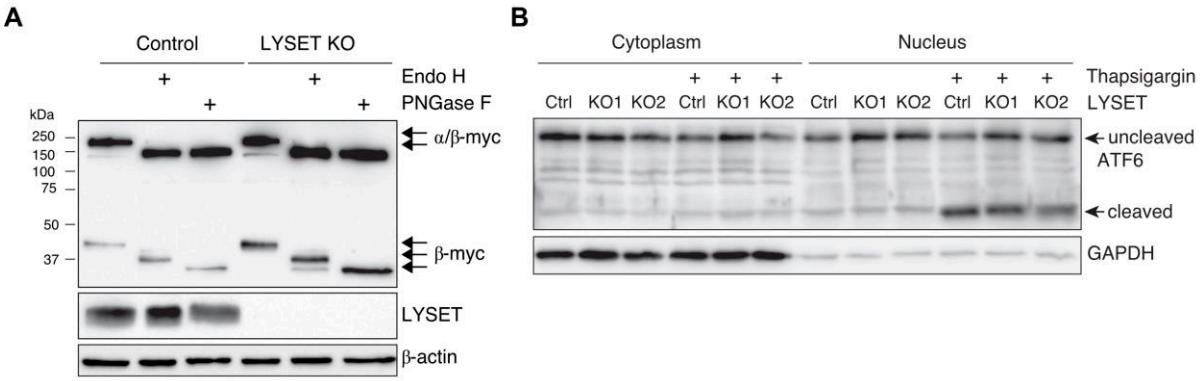

Figure 19 - Processing of GNPTAB is not affected by loss of LYSET.
(A) Immunoblot of GNPTAB-myc upon enforced transient overexpression in HEK293T bulk control or LYSET KO cells. High mannose- and complex-type N-linked glycans modifications were analysed by treatment with endoglycosidase Hf (Endo Hf) or N-glycosidase F (PNGase F). β subunit is partially Endo Hf-resistant, indicating the generation of complex-type N-linked glycans by Golgi-resident enzymes. (B) Immunoblot of ATF6 in MIA PaCa-2 clonal LYSET KO cytoplasmic and nuclear fractions, upon treatment with 1 μM thapsigargin for 5 h.

4.5.4 GlcNAc-1-phosphotransferase complex stability depends on LYSET

The above results suggested that LYSET is not involved in the processing of GNPTAB. Hence, I examined if LYSET is important for the stabilisation of the mature GNPT α and β subunits. To test stabilisation, I inhibited the two pathways known to degrade Golgi proteins (Schwabl and Teis, 2022): lysosomal proteolysis and proteasomal degradation. To inhibit lysosomal proteolysis, I incubated the cells with a cocktail of protease inhibitors or with bafilomycin A1. To block the proteasome, I treated cells with MG-132. As before, I prepared organelle-enriched fractions for immunoblotting. GNPT α was detected at the endogenous level in SK-MEL-30 cells while GNPT β was assessed by overexpression of GNPTAB-myc in MIA PaCa-2 cells. In LYSET-deficient cells, bafilomycin A1 treatment led to a stabilisation of both GNPT α and β subunits. When treated with protease inhibitors, LYSET-deficient cells likewise presented higher levels of GNPT α and β subunits (Figure 20A and B). In contrast, proteasome inhibition did not lead to the stabilisation of either GNPT α or β subunits (Figure 20C and D). In control cells, GNPT β-myc levels slightly increased in response to the inhibition of lysosomal proteases by bafilomycin A1 or protease inhibitors treatment (Figure 20E). By immunofluorescence, I observed that bafilomycin A1 treatment restored GNPT β-myc in the Golgi in LYSET-deficient cells (Figure 20F). This accumulation in the Golgi was due to a block in vesicular trafficking from the Golgi to lysosomes, upon treatment with bafilomycin A1. Bafilomycin A1 inhibits the v-ATPase complex, disturbing the pH gradient necessary for vesicular trafficking (Johnson *et al.*, 1993). Thus, these data suggested that GNPTAB is destabilised, removed from the Golgi, and degraded in the lysosome in the absence of LYSET.

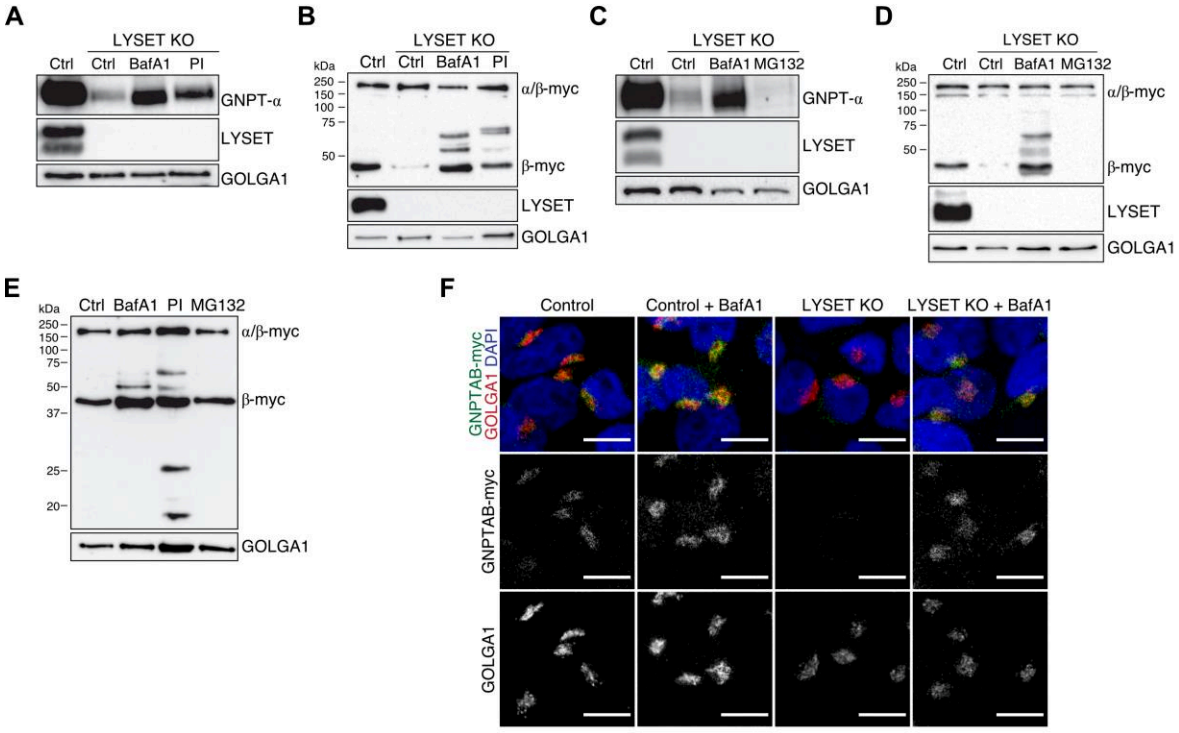

Figure 20 - Stabilisation of GNPTAB depends on LYSET.
(A and B) Immunoblot of GNPTAB-myc in MIA PaCa-2 (A) and GNPT α subunit in SK-MEL-30 (B) LYSET-deficient cells upon treatment with 100 nM bafilomycin A1 or lysosomal protease inhibitors for 16 hours. (C and D) Immunoblot of GNPTAB-myc in MIA PaCa-2 (C) and GNPT α subunit in SK-MEL-30 (D) LYSET-deficient cells upon treatment with 100 nM bafilomycin A1 or 10 µM MG132 for 16 hours. (E) Immunoblot of GNPTAB-myc in MIA PaCa-2 control cells upon treatment with 100 nM bafilomycin A1, lysosomal protease inhibitors, or 10 µM MG132 for 16 hours. (F) Confocal microscopy images of control and LYSET deficient PaTu 8988t cells expressing GNPTAB-Flag immunostained with myc and GOLGA1 upon treatment with 100 nM bafilomycin A1 for 16 h. Scale bar = 10 µm. α/β-myc and β-myc denote the myc-tagged GNPTAB α/β precursor and β subunit, respectively. GNPT-α denotes the α subunit band upon deglycosylation of the proteins in the lysates.

To assess how LYSET stabilises GNPTAB in the Golgi, David Haselbach analysed the predicted structure of GNPT *α* transmembrane domain 1 (TM1) using AlphaFold . Annotation of the amino acid residues present in the TM1 of human and fruit fly GNPTAB allowed the observation of an unusual hydrophilic and charged patch only present in the human protein. Due to their biophysical properties, the presence of this region creates an unstable helix less likely to be inserted in membranes (Figure 21A and B). Interestingly, fruit fly does not express LYSET and its GNPTAB homologue exhibits a regular hydrophobic helix. By analyzing the amino acid sequence of the TM1 of more organisms, Alexander Schleiffer observed that organisms with LYSET present an unfavourable TM1, while organisms without LYSET present a favourable TM1 (Figure 21A to C). To test the importance of this charged/hydrophilic region of GNPTAB TM1, Marten Wittmann cloned a GNPTAB-myc construct where the amino acids Q36 and E39 were mutated to leucine (GNPTAB^{Q36L,E39L}). I lentivirally expressed this construct in LYSET deficient, wild type, or overexpressing cells, in parallel with wild type GNPTAB

(GNPTAB^{wt}). By immunoblotting, I observed that, as expected, GNPTAB^{wt} was only detected in cells expressing LYSET, exhibiting increased levels when LYSET is overexpressed. In contrast, GNPTAB^{Q36L,E39L} was strongly detected, including in LYSET-depleted cells (Figure 21D). To test if GNPTAB^{Q36L,E39L} properly localised in the Golgi, I performed an immunofluorescence assay where I labeled both myc and the Golgi marker GOLGA1 in MIA PaCa-2 control or LYSET-depleted cells expressing either GNPTAB^{wt} or GNPTAB^{Q36L,E39L}. I observed that expression of the GNPTAB-stabilising mutations was sufficient to localise GNPTAB in the Golgi independently of LYSET, while GNPTAB^{wt} was only detected in LYSET-expressing cells (Figure 21E). To determine if the expression of a stable GNPTAB protein could alone lead to a functional lysosomal enzyme trafficking pathway, I assessed the lysosomal degradation capacity and lysotracker accumulation in LYSET-deficient cells expressing GNPTAB^{Q36L,E39L}. By flow cytometry, I observed that DQ BSA degradation in LYSET knockout cells expressing GNPTAB^{Q36L,E39L} was rescued to levels equivalent to control cells (Figure 21F). Accordingly, lysotracker accumulation observed in LYSET-depleted cells was partially rescued by GNPTAB^{wt} overexpression and fully rescued by GNPTAB^{Q36L,E39L} expression (Figure 21G). Expression of stable human GNPTAB rescues the phenotypes of LYSET deficiency. Thus, the expression of stable GNPTAB is sufficient to restore lysosomal function independently of LYSET, suggesting that LYSET is required for the stabilisation of GNPTAB.

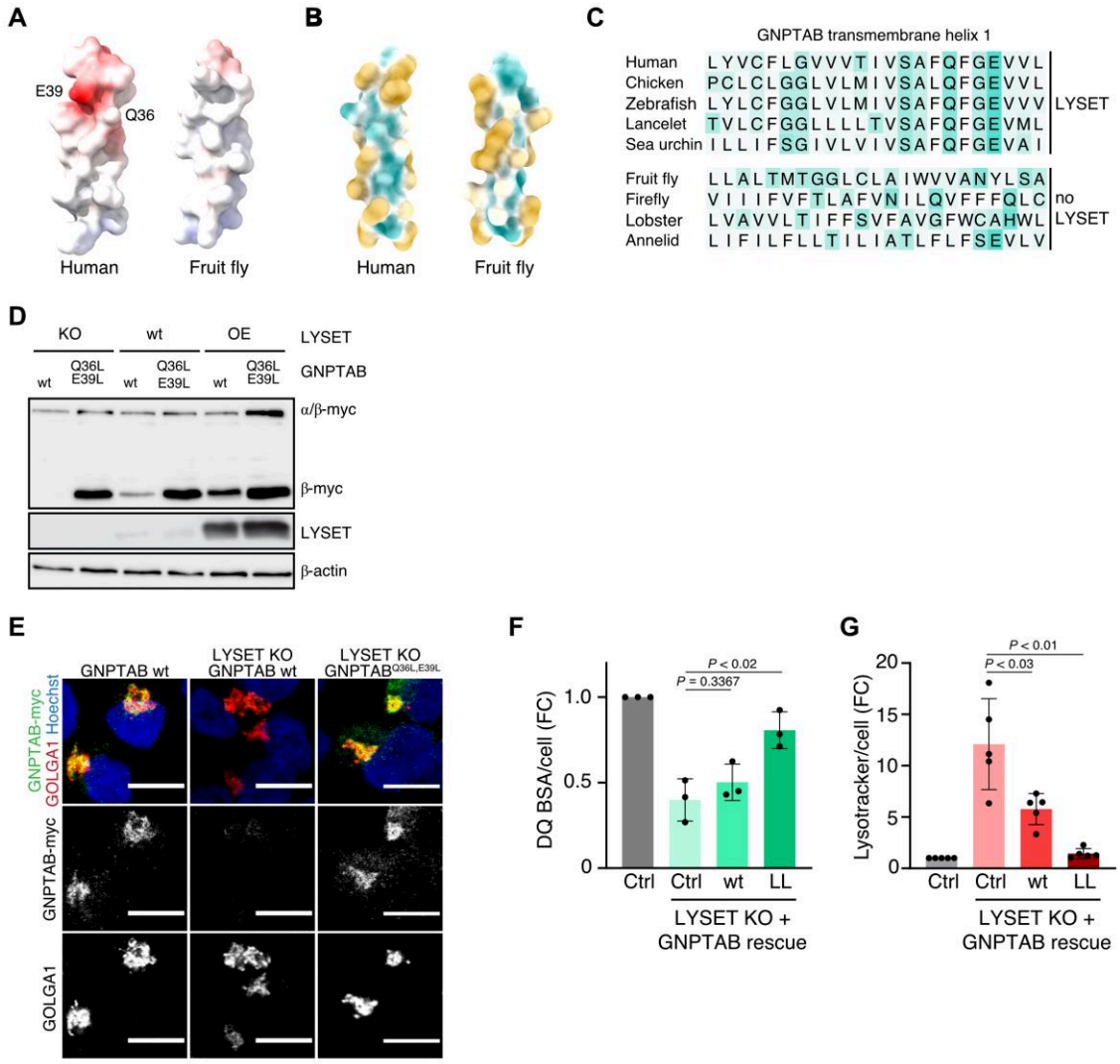

Figure 21 - LYSET arises evolutionarily with an unfavourable transmembrane domain of GNPTAB.
(A and B) AlphaFold prediction of transmembrane helix 1 of human and fruit fly GNPTAB. (A) Negative charge is indicated in red and positive charge in blue; (B) hydrophobic residues are indicated in ochre and hydrophilic residues in turquoise. (C) Evolutionary comparison of the GNPTAB transmembrane helix 1 residues in multiple organisms with or without LYSET homologues. Turquoise intensity designates the hydrophilicity of the residues. (D) Immunoblot of GNPTAB^{wt} and GNPTAB^{Q36L,E39L}-myc levels in MIA PaCa-2 cells with clonal LYSET KO (KO), wild type (wt) or overexpression (OE). α/β-myc and β-myc denote the myc-tagged GNPTAB α/β precursor and β subunit, respectively. (E) Confocal microscopy images of MIA PaCa-2 clonal control and LYSET KO cells expressing GNPTAB^{wt} or GNPTAB^{Q36L,E39L}-myc. GNPTAB was immunostained with myc antibody and the Golgi with GOLGA1 antibody. Scale bars = 10 mm. (F and G) Flow cytometry quantification of DQ BSA degradation and lysotracker signal in MIA PaCa-2 clonal LYSET KO cells expressing GNPTAB^{wt}(wt) or GNPTAB^{Q36L,E39L}(LL)-myc. Data are represented as means ± SEM. N = 3 biologically independent experiments in (F). N = 5 biologically independent experiments in (G).

5. Conclusion and discussion

In my PhD project, I performed genome-wide CRISPR screens in defined metabolic conditions that allowed the identification of genes essential for extracellular protein-dependent proliferation. The selection of screen hits led me to the discovery of the previously uncharacterised protein TMEM251, now renamed to LYSosomal Enzyme Trafficking factor (LYSET). Further characterisation showed that LYSET is required when cells feed on extracellular proteins *in vitro* and for tumour formation *in vivo*. Mechanistically, LYSET is a core component of the mannose-6-phosphate pathway, responsible for the sorting of lysosomal enzymes to the lysosome. Hence, in the absence of LYSET, lysosomal degradation of both endocytic and autophagic cargoes is impaired. By studying previously reported LYSET patient mutations, I uncovered a pathomechanism for a hereditary lysosomal storage disorder, resembling mucolipidosis-like phenotypes. Mucolipidosis disorders are caused by poor GlcNAc-1-phosphotransferase activity, an enzyme responsible for the tagging of lysosomal enzymes with mannose-6-phosphate and their sorting to the lysosome. Moreover, LYSET and GlcNAc-1-phosphotransferase reside together in the Golgi. Finally, my data suggests that LYSET stabilises GNPTAB in Golgi membranes, avoiding its premature degradation (Figure 22).

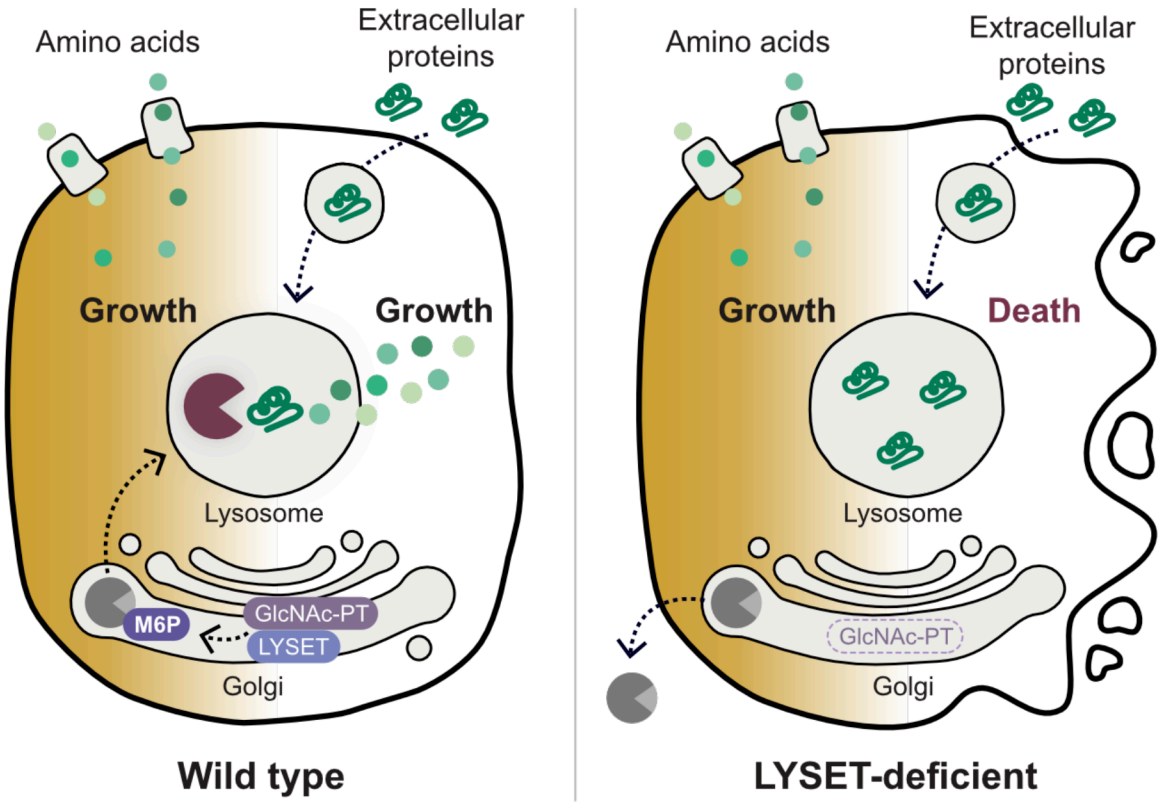

Figure 22 - Graphical summary of LYSET function in cells exposed to different nutrient environments. (left) In LYSET wild-type cells, the GNPT complex and LYSET interact in the Golgi allowing the proper function of the mannose-6-phosphate pathway. As a consequence, lysosomal enzyme precursors are sorted to the lysosome, where they are finally processed into their active state. LYSET wild-type cells have functional lysosomes. In conditions where the cells use either amino acids or extracellular protein, these cells can grow and proliferate. (right) In LYSET-deficient cells, the GNPT complex is destabilised, impairing the function of the mannose-6-phosphate pathway. As a consequence, lysosomal enzyme precursors are secreted to the extracellular medium instead of being sorted to the lysosome. LYSET-deficient cells exhibit non-functional lysosomes, where undigested cargo accumulates. In conditions where the cells use free amino acids, the lysosome is dispensable and cells can continuously grow and proliferate. When cells depend on extracellular protein, their impaired lysosomes do not degrade the internalised extracellular protein, which results in cell starvation and death.

5.1 CRISPR screens for albumin-dependent proliferation

Genetic loss-of-function screens are ideally suited to define genes and pathways that regulate cell survival and proliferation in different conditions. Over the last decade, genetic screens have been performed aiming at identifying essential genes and cancer vulnerabilities in the human genome (Sanjana *et al.*, 2014, Hart *et al.*, 2015, Michlits *et al.*, 2020). The vast majority of genetic screens in cancer cells were performed in conventional culture conditions, not taking into account the differences between the composition of the media and the physiological levels of different nutrients. Standard cell culture media does not mimic the biomass composition of human plasma. Cell culture media have an excess of glucose and free amino acids of around 3 to 5-fold and 5 to 15-fold, respectively, and a 10-fold decrease in proteins, when compared with human plasma (Ackermann and Tardito, 2019, Palm, 2019). Interestingly, the metabolic phenotypes identified *in vitro* can differ from the metabolism of cancers *in situ* (Muir *et al.*, 2018). In the cancer metabolism field, multiple attempts were made to approximate the *in vitro* conditions to the *in vivo* situation, by manipulating medium formulations (Muir *et al.*, 2018, Ackermann and Tardito, 2019, Rossiter *et al.*, 2021). Recently, Nofal *et al.* performed an albumin-dependent proliferation CRISPR screen. The authors identified genes involved in macropinocytosis, lysosomal positioning, lysosomal catabolism, and translation as required for extracellular protein-dependent growth. Additionally, Nofal *et al.* observed that GCN2 allows cells to adapt to the use of extracellular protein by promoting the expression of lysosomal hydrolases (Nofal *et al.*, 2022). In my PhD project, I combined the power of genetic screens with cell culture systems that model more physiologically relevant metabolic conditions (reduced free amino acid and increased extracellular protein concentration) (Pechincha *et al.*, 2022). For this, cells were grown in an amino acid-rich medium and/or leucine-poor media in the presence or absence of physiological levels of albumin. With my screening strategy, I could confirm that genes involved in endolysosomal trafficking, amino acid transporters, and amino acid sensors are essential for extracellular protein-dependent proliferation. Additionally, my CRISPR screens allowed the identification of the uncharacterised protein TMEM251/LYSET. Thus, the manipulation of *in vitro* cell culture systems, designed to better mimic the *in vivo* situation, has facilitated the identification of novel cellular responses and genes crucial for the sustained growth and adaptability of cancer cells.

5.2 The molecular function of LYSET

The sorting pathway for lysosomal enzymes to the lysosome was thought to be well-understood. However, I revealed that LYSET is a novel and indispensable component for the sorting of lysosomal enzymes to the lysosome. In the absence of LYSET, GlcNAc-1-phosphotransferase becomes destabilised due to a hydrophilic transmembrane domain that co-evolved with LYSET. Consequently, LYSET-deficient cells display a loss of M6P modification, missorting of lysosomal enzymes, impaired lysosomal protein turnover, and lysosomal storage disorder-like phenotypes (Pechincha *et al.*, 2022).

Interestingly, two additional independent studies employing genome-wide CRISPR screens identified LYSET as being important for reovirus infection of mammalian cells and lysosomal cargo turnover (Richards *et al.*, 2022, Zhang *et al.*, 2022). Richards, Jabs, and Qiao *et al.* revealed LYSET as essential for viral maturation and infection, a process occurring in the lysosome via cleavage of the virus by lysosomal enzymes, such as cathepsin L. At the cellular level, the authors observed similar missorting of lysosomal enzymes and GlcNAc-1-phosphotransferase decrease in LYSET-depleted cells. Mechanistically, the authors showed that in the absence of LYSET, M6P deposition on lysosomal enzymes was impaired and GlcNAc-1-phosphotransferase leaves the Golgi for lysosomal degradation (Richards *et al.*, 2022). In a third study, Zhang and Yang *et al.* described LYSET as essential for the degradation of a lysosomal membrane protein, degraded through lysosomal turnover. These authors also observed decreased lysosomal enzyme abundance, increased secretion of luminal enzymes, loss of M6P modification, and a decrease in GNPT β in LYSET-depleted cells (Zhang *et al.*, 2022). Additionally, Zhang and Yang *et al.* propose that LYSET is required for the specific cleavage and activation of GNPT α/β by S1P, although not affecting the cleavage of other S1P targets. Conversely, in my project, I observed that S1P is still able to cleave its targets in the absence of LYSET, including GNPT α/β (Pechincha *et al.*, 2022). Our and Richards, Jabs, and Qiao *et al.* data showed that mature GNPT α and β leave the Golgi and are degraded in the lysosome in the absence of LYSET. Together, the independent discovery of LYSET by multiple groups highlights the importance of challenging the existing screening methods by selecting the right readout to identify new gene functions. Additionally, the parallel report of LYSET phenotypes confirms my results and the importance of LYSET in diverse biological contexts.

The GlcNAc-phosphotransferase complex is a heterohexameric complex of three subunits (α2β2γ2) that assemble in the ER and are trafficked together to the trans-Golgi network (Encarnação *et al.*, 2011). Each GNPT α and β subunit has a transmembrane domain, being the complex composed of four transmembrane domains inserted in Golgi membranes. Additionally, LYSET is a small transmembrane protein composed of short N- and C-termini

and two transmembrane domains linked by a short intra-Golgi loop. David Haselbach's observation of a hydrophilic patch in the transmembrane domain 1 of GNPT α/β suggests that GNPT α/β by itself is unstable in Golgi membranes. To test the importance of this charged/hydrophilic region of GNPT α transmembrane, the conserved Q36 and E39 residues of GNPTAB were mutated to leucine to stabilise the protein. GNPTAB^{Q36L,E39L} was readily detected in the Golgi of both cells expressing or lacking LYSET and its expression was sufficient to rescue the LYSET knockout phenotypes. This raises the question of why the M6P pathway evolved in the direction where an additional protein is required for the formation of a stable GNPT complex. In the absence of LYSET, the GNPT complex is destabilised. When the two proteins are expressed, they are in close proximity in the Golgi, suggesting that LYSET can be part of the GNPT complex, functioning as a stabiliser element. However, the stoichiometry of the GNPT complex and LYSET remains to be elucidated. Additionally, whether GNPT α/β is not properly inserted in Golgi membranes or cannot be retained in the Golgi upon LYSET depletion remains to be understood.

GNPTAB instability was observed by the reduced levels of the mature proteins in the absence of LYSET. This suggested that the unstable mature GNPT α and GNPT β subunits were being removed from the Golgi and degraded. Golgi proteins can be degraded by either the proteasome or lysosomal proteases (Schwabl and Teis, 2022). In my PhD project, I examined if disturbing any of these degradation pathways would lead to an accumulation of GNPTAB in LYSET-deficient cells. Indeed, I observed an accumulation of GNPT α and β subunits in LYSET-depleted cells upon blockage of vesicular trafficking and inhibition of lysosomal proteases. Additionally, upon blockage of vesicular trafficking, I observed that GNPT β-myc was restored in the Golgi of LYSET-deficient cells. Similarly, Richards, Jabs, and Qiao *et al.* observed that the mature GNPT α is lost from the Golgi in LYSET-depleted cells and instead found in the lysosome (Richards *et al.*, 2022). Thus, these data suggest that GNPT α and β are not stable in the Golgi and get degraded in the lysosome, in the absence of LYSET. In accordance, patient-derived GNPTAB mutations lead to the expression of unstable forms of the GNPT complex which is likewise degraded in the lysosome (Van Meel *et al.*, 2014). Of note, GNPTAB KO cells do not have reduced LYSET expression, while the expression of the unstable GNPTAB mutants leads to the loss of LYSET. This may suggest that GNPTAB and LYSET are degraded together.

A key insight into the molecular function of LYSET was gathered from the atypical transmembrane domain of GNPTAB. This transmembrane domain contains numerous charged and hydrophilic amino acid residues that disfavour integration into membranes. Organisms without LYSET homologues show a more common transmembrane domain sequence, rich in hydrophobic residues, which is present in organisms from vertebrates to sea urchins (Pechincha *et al.*, 2022). GNPTAB catalytic function is similar to the one found in

bacterial sugar-phosphate transferases (Sperisen *et al.*, 2005, Muindi *et al.*, 2014). However, human GNPTAB is conserved amongst the phylum Chordata. Mammalian GNPTAB and homologues share functional domains which permit their role in the M6P pathway. Moreover, GNPTAB homologues were identified in arthropods and nematodes, such as *D. melanogaster* and *C. elegans* (Martin *et al.*, 2023). Interestingly, these organisms were not reported to use the M6P pathway for sorting of lysosomal enzymes and the function of their GNPTAB homologue remains unclear.

The mammalian M6P receptors (MPR300 and MPR46) and vertebrate homologue receptors have been extensively studied. These receptors are evolutionarily conserved, sharing similar structural and functional domains, from fish to mammals. Additionally, homologues of these receptors have been identified in invertebrates like echinoderms (starfish) and molluscs (unio) (Martin *et al.*, 2023). Notably, the Drosophila homologue does not recognise M6P residues but directly recognises lysosomal enzymes, rendering the sorting of lysosomal enzymes independently of mannose 6-phosphate modifications (Nadimpalli and Amancha, 2010, Bhamidimarri *et al.*, 2018). Interestingly, homologues of the M6P receptors were not found in *C. elegans* and *D. melanogaster*, unlike GNPTAB homologues. This implies that M6P receptors likely emerged later in the course of evolution, contributing to the functional development of the M6P pathway.

LYSET encodes for two isoforms in mammals, with 131 and 163 amino acid residues. The short isoform is very well conserved in vertebrates and homologues are found in several other metazoan organisms, where MPR and GNPTAB homologues were also identified (Martin *et al.*, 2023). Interestingly, LYSET coexists with the unstable GNPTAB homologues and MPR suggesting that LYSET became essential for the functionality of the GNPT complex during the evolutionary development of the M6P pathway.

A possible explanation for the existence of LYSET is that LYSET could function as a regulatory element of the M6P pathway. Post-translational modifications in GNPT γ were reported to be essential for the subcellular localisation and assembly of the GlcNAc-1-phosphotransferase complex in the ER. However, these modifications do not play a regulatory role (Encarnação *et al.*, 2011). Conversely, post-translational modification sites have also not been predicted in the structure of LYSET, suggesting that a possible regulation of the pathways does not depend on post-translational modifications. On the transcription level, TFEB is a known transcription regulator of lysosomal enzymes, but there was no evidence that TFEB regulates the expression of genes from the M6P pathway, except for *GNPTG* (Palmieri *et al.*, 2011). However, a recently developed tool, TFEBexplorer, predicts that both *GNPTAB* and *LYSET* have CLEAR sites in their promoters, suggesting that MiT/TFE-dependent transcription could regulate the complex expression (De Cegli *et al.*, 2022). The potential existence of TFEB binding sites within the promoters of *LYSET*, *GNPTAB*, and

GNPTG suggests the possibility of their co-regulation with lysosomal genes. However, I did not observe any evidence of a possible role of TFEB in regulating LYSET or other components of the GNPT complex (data not shown). Whether GNPT or LYSET levels are subjected to regulation in physiological or pathological contexts is a question that remains to be answered.

5.3 LYSET mutations cause a novel lysosomal storage disorder

My data show that LYSET deficiency results in similar cellular phenotypes as GNPTAB deficiency: accumulation of lysosomes depleted of catabolic enzymes, the inability to degrade endocytic and autophagic cargoes, and the accumulation of undigested lysosomal content. These phenotypes are a cellular signature of lysosomal storage disorders (Platt *et al.*, 2018). GNPTAB deficiency is the main cause of mucolipidosis II/III and multiple GNPTAB patient mutations have been identified as a cause for these autosomal recessive disorders (Tiede *et al.*, 2005, Van Meel *et al.*, 2014, Wang *et al.*, 2019). While I was developing my PhD project, Noor U. Ain *et al.* reported two cases of unrelated families with individuals presenting severe skeletal dysplasia syndromes, resembling mucolipidosis II/III-like lysosomal storage disorders. Using whole-exome sequencing they could identify two homozygous variants of TMEM251/LYSET (Ain *et al.*, 2021). By studying these two variants in our *in vitro* culture systems, I observed that these disease-associated loss-of-function mutations exhibit similar cellular phenotypes to the ones described for GNPTAB disease-associated mutations. Thus, LYSET deficiency can be the underlying cause of a novel lysosomal storage disorder.

Over the years, multiple mouse and zebrafish models have been developed to study mucolipidosis (Favret *et al.*, 2020, Zhang and Peterson, 2020). Richards, Jabs, and Qiao *et al.* generated *Lyset* knockout mice which exhibited high levels of lysosomal enzymes in the blood serum and isolated MEFs showed enlarged lysosomes with accumulated storage material. Interestingly, clinical dysplasia symptoms were not observed in the model (Richards *et al.*, 2022). Zhang *et al.* generated a zebrafish Lyset knockout model which showed severe development defects, heart edema, and skeletal dysplasia (Zhang *et al.*, 2022). The observed phenotypes in these animal models provide functional confirmation that LYSET deficiency leads to the manifestation of a novel lysosomal storage disorder.

5.4 The role of the mannose-6-phosphate pathway in cancer metabolism

The metabolic need for lysosomal nutrient generation manifests in solid tumours, where limited or dysfunctional blood vessels lead to regions lacking nutrients. In response to these conditions, cancer cells can exploit lysosomal protein catabolism to acquire amino acids (Palm *et al.*, 2015, Davidson *et al.*, 2017). Additionally, autophagy and macropinocytosis are stimulated by oncogenic signalling pathways (White, 2013). This increased lysosomal activity, often studied in pancreatic cancer, a poorly vascularised cancer type where lysosomal nutrient generation is upregulated, strengthens the metabolic adaptability and resilience of cancer cells. The use of macropinocytosis for tumour growth has been observed *in vivo* in multiple models, such as subcutaneous heterotopic xenograft pancreatic and orthotopic syngeneic breast cancer models. Inhibition of macropinocytosis using the pharmacological inhibitor EIPA, a Na+/H+ exchanger inhibitor, or using a genetic strategy that affects the actin capping protein regulator CARMIL1, showed reduced tumour growth and increased survival of mice (Commisso *et al.*, 2013, Jayashankar and Edinger, 2020). Autophagy exhibits dual effects on cancer, acting as both a promoter and a suppressor of tumourigenesis. Nevertheless, multiple cancer cells display elevated basal autophagic activity. Depletion of autophagy-related proteins, such as ATG5, substantially impacted tumour growth *in vivo* in a model of colorectal cancer (Lauzier *et al.*, 2019). Additionally, Ras-driven cancer cells depend on autophagy both *in vitro* and *in vivo* (Guo *et al.*, 2013, Guo *et al.*, 2013). Conversely, data from our lab showed that the genetic removal of ATG5 did not reduce the tumour growth of murine colorectal carcinoma cells when injected subcutaneously in mice. Thus, lysosomal catabolic activity, which includes both the recycling of intracellular macromolecules via autophagy and the generation of nutrients by retrieval of building blocks from extracellular macromolecules, is essential for tumour development in this model, while autophagy alone is insufficient. Additionally, my data showed that, in the tested pancreatic subcutaneous xenograft and orthotopic syngeneic models, LYSET knockout cells have an impaired capacity to form tumours when injected in mice (Pechincha *et al.*, 2022). Thus, LYSET and the M6P pathway have a pivotal role in the metabolic flexibility and robustness required by cancer cells to proliferate in harsh environments. Nevertheless, the importance of the M6P pathway for tumour growth in spontaneous models driven by oncogenic mutations has not been tested.

Several attempts have been made to target the lysosome in cancer, due to its role in cell metabolism and its importance in the response to chemotherapeutics. Lysosomes can accumulate cytotoxic drugs which can either reduce their effectiveness or lead to a breakage of lysosomal membranes. With increased membrane permeability and rupture, lysosomal

enzymes leak into the cytoplasm which results in lysosomal-induced apoptosis and cytotoxic effects (Trybus *et al.*, 2023). Targetting the lysosome has been attempted in preclinical and clinical settings via the use of antimalarial drugs (e.g. chloroquine and hydroxychloroquine). However, these compounds were reported to have low potency. Other than blocking lysosomal activity by neutralizing lysosomal pH, these drugs can bind to DNA and block signalling pathways in cancer cells, tumour vasculature, cancer-associated fibroblasts, and immune cells in the tumour microenvironment (Towers and Thorburn, 2017). Thus, alternative approaches and targets are required for the blockade of lysosomal catabolism.

Inhibiting LYSET and the lysosomal enzyme trafficking pathway could be a promising avenue to therapeutically target lysosomal catabolism. The possible side effects of targetting the M6P pathway in patients diagnosed with a solid tumour, perhaps poorly vascularised, remain unclear. On the one hand, the symptoms developed by patients with LSD are severe and lead to early mortality (Dogterom *et al.*, 2021). On the other hand, these disorders are genetic and affect primarily the development of these patients. The consequences of targetting the pathway transiently and in the adult phase could be diminished. Concomitantly, Richards, Jabs, and Qiao *et al. Lyset* knockout mice developed normally into the adult phase without signs of musculoskeletal dimorphism (Richards *et al.*, 2022). Moreover, my *in vitro* data shows that in nutrient-rich conditions LYSET-depleted cells proliferate normally. Together, these data suggest that a transient treatment targetting the lysosome via the M6P pathway could be advantageous for cancer therapy.

A striking cellular phenotype upon LYSET KO is the missorting and hypersecretion of lysosomal luminal enzymes, due to loss of M6P. Targetting this pathway, in the context of cancer therapy, would lead to increased enzyme hypersecretion, which can influence the tumour microenvironment. Cathepsin hypersecretion in tumours modulates the extracellular matrix and increases angiogenesis and immune cell invasion while contributing to EMT (Joyce *et al.*, 2004, Mitrović *et al.*, 2017, Vidak *et al.*, 2019). Our data, together with the literature, suggests that targetting the M6P pathway for cancer therapy might require a combined therapy targetting both the lysosome and the proteolytic activity in the microenvironment.

5.5 Open questions and future perspectives

My PhD project describes the function of LYSET as a core component of the M6P pathway, uncovers a pathomechanism for hereditary lysosomal storage disorders, and uncovers the impact of lysosomal catabolic activity in cancer metabolism. This project raises several questions which can be addressed in the future.

My data suggests that LYSET is part of the GNPT complex, stabilising GNPTAB in Golgi membranes. A detailed understanding of this interaction at the structural level remains to be addressed. Structural analysis of the complex, taking into account the existence of this new element, will allow a better comprehension of where and when LYSET interacts with GNPTAB and the stoichiometry of the complex. Moreover, the structure of GNPTAB is not completely resolved. Researchers report issues in purifying the whole mammalian GNPTAB for further cryo-electron microscopy analysis. An approach to facilitate this analysis could be the purification of human LYSET and GNPTAB and the analysis of the structure of the two proteins together, which form a more stable complex.

The regulation of lysosomal protein expression and lysosome biogenesis has been well-characterised and largely attributed to transcription regulation by TFEB. Conversely, a possible regulation of the M6P pathway is not yet understood. Although my recent data (not shown) suggest that TFEB does not have a role in regulating GNPT or LYSET levels, the discovery of a potential regulatory mechanism of the M6P pathway is of high interest.

The discovery of LYSET as a new core component of the M6P pathway, expands the understanding of lysosomal storage disorders and increases the opportunity for a better clinical diagnosis of patients with mucolipidosis-like diseases. Samples from patients with symptoms similar to mucolipidosis, but without mutations or alterations in the expression of GNPT complex proteins, can now be re-evaluated. The presence of LYSET mutations in these samples can lead to a more accurate diagnosis and a better understanding of the disease.

My data suggest that the M6P pathway is an effective target to suppress the lysosomal activity of cancer cells and hence the resilience acquired by cancer cells to proliferate depending on extracellular protein. Given the structure and function attributed to GNPT and LYSET, a possibility to target the M6P would be to block the activity of GNPTAB, the catalytic component of the complex, or to block the interaction between LYSET and GNPTAB.

The effect of targetting the lysosome of cancer cells in the tumour microenvironment remains to be assessed. To understand its possible impact, I propose to study the impact of hypersecretion of enzymes by the cancer cells in other tumour cell compartments. Additionally, it is of great interest to expand our knowledge on lysosomal catabolism in the cancer cell to the complex context of tumour biology. Based on this, a future direction can be to explore the contribution of each cell type in the tumour microenvironment to the lysosomal catabolism of tumours, including non-transformed cells, such as cancer-associated fibroblasts.

6. References

ACKERMANN T, TARDITO S. Cell Culture Medium Formulation and Its Implications in Cancer Metabolism. Trends in Cancer. 2019;5(6):329-332.

AIN NU, MUHAMMAD N, DIANATPOUR M, BARONCELLI M, IQBAL M, FARD MAF*, et al.* Biallelic TMEM251 variants in patients with severe skeletal dysplasia and extreme short stature. Human Mutation. 2021;42(1):89-101.

AKTER F, BONINI S, PONNAIYAN S, KOGLER-MOHRBACHER B, BLEIBAUM F, DAMME M*, et al.* Multi-Cell Line Analysis of Lysosomal Proteomes Reveals Unique Features and Novel Lysosomal Proteins. Mol Cell Proteomics. 2023;22(3):100509.

AKTER F, PONNAIYAN S, KÖGLER-MOHRBACHER B, BLEIBAUM F, DAMME M, RENARD BY*, et al.* Multi cell line analysis of lysosomal proteomes reveals unique features and novel lysosomal proteins. 2020.

AMYERE M, PAYRASTRE B, KRAUSE U, VAN DER SMISSEN P, VEITHEN A, COURTOY PJ. Constitutive Macropinocytosis in Oncogene-transformed Fibroblasts Depends on Sequential Permanent Activation of Phosphoinositide 3-Kinase and Phospholipase C. Molecular Biology of the Cell. 2000;11(10):3453-3467.

BAJAJ L, LOTFI P, PAL R, RONZA AD, SHARMA J, SARDIELLO M. Lysosome biogenesis in health and disease. Journal of Neurochemistry. 2019;148:573-589.

BALLABIO A, BONIFACINO JS. Lysosomes as dynamic regulators of cell and organismal homeostasis. In: Nature Reviews Molecular Cell Biology. Nature Research, 2020. p. 101-118.

BAO M, BOOTH JL, ELMENDORF BJ, CANFIELD WM. Bovine UDP-N-acetylglucosamine:Lysosomal-enzyme N-Acetylglucosamine-1-phosphotransferase I. Purification and subunit structure. J Biol Chem. 1996;271(49):31437-45.

BHAMIDIMARRI PM, KRISHNAPATI LS, GHASKADBI S, NADIMPALLI SK. Mannose 6-phosphate-dependent lysosomal enzyme targeting in hydra: a biochemical, immunological and structural elucidation. FEBS Letters. 2018;592(8):1366-1377.

BRAULKE T, BONIFACINO JS. Sorting of lysosomal proteins. Biochimica et Biophysica Acta - Molecular Cell Research. 2009;1793(4):605-614.

BRAULKE T, POHL S, STORCH S. Molecular analysis of the GlcNac-1-phosphotransferase. Journal of Inherited Metabolic Disease. 2008;31:253-257.

CARVALHO DR, SPECK-MARTINS CE, BRUM JM, FERREIRA CR, SOBREIRA NLM. Spondyloepimetaphyseal dysplasia with elevated plasma lysosomal enzymes caused by homozygous variant in MBTPS1. Am J Med Genet A. 2020;182(7):1796-1800.

CHEONG H, WU J, GONZALES LK, GUTTENTAG SH, THOMPSON CB, LINDSTEN T. Analysis of a lung defect in autophagy-deficient mouse strains. Autophagy. 2014;10(1):45-56.

COMMISSO C. Macropinocytosis: Functions and Mechanisms. Springer; 2022.

COMMISSO C, DAVIDSON SM, SOYDANER-AZELOGLU RG, PARKER SJ, KAMPHORST JJ, HACKETT S*, et al.* Macropinocytosis of protein is an amino acid supply route in Ras-transformed cells. Nature. 2013;497(7451):633-637.

COOPER GM. Endocytosis. In: The Cell: A Molecular Approach. Sunderland (MA): Sinauer Associates, 2000.

COX J, HEIN MY, LUBER CA, PARON I, NAGARAJ N, MANN M. Accurate proteome-wide label-free quantification by delayed normalization and maximal peptide ratio extraction, termed MaxLFQ. Mol Cell Proteomics. 2014;13(9):2513-26.

COX J, MATIC I, HILGER M, NAGARAJ N, SELBACH M, OLSEN JV*, et al.* A practical guide to the MaxQuant computational platform for SILAC-based quantitative proteomics. Nat Protoc. 2009;4(5):698-705.

DAFNA BAR-SAGI JRF. Induction of Membrane Ruffling and Fluid-Phase Pinocytosis in Quiescent Fibroblasts by ras Proteins. Science. 1986;233(4768):1061-1068.

DANYUKOVA T, SCHONECK K, POHL S. Site-1 and site-2 proteases: A team of two in regulated proteolysis. Biochim Biophys Acta Mol Cell Res. 2022;1869(1):119138.

DAVIDSON SM, JONAS O, KEIBLER MA, HOU HW, LUENGO A, MAYERS JR*, et al.* Direct evidence for cancer-cell-autonomous extracellular protein catabolism in pancreatic tumors. Nature Medicine. 2017;23(2):235-241.

DE ALMEIDA M, HINTERNDORFER M, BRUNNER H, GRISHKOVSKAYA I, SINGH K, SCHLEIFFER A*, et al.* AKIRIN2 controls the nuclear import of proteasomes in vertebrates. Nature. 2021;599(7885):491-496.

DE CEGLI R, CARRELLA D, SICILIANO D, GAMBARDELLA G, NAPOLITANO G, DI MALTA C*, et al.* TFEBexplorer: An integrated tool to study genes regulated by the stress-responsive Transcription Factor EB. Autophagy Reports. 2022;1(1):295-305.

DE PACE R, COUTINHO MF, KOCH-NOLTE F, HAAG F, PRATA MJ, ALVES S*, et al.* Mucolipidosis II-related mutations inhibit the exit from the endoplasmic reticulum and proteolytic cleavage of GlcNAc-1-phosphotransferase precursor protein (GNPTAB). Human Mutation. 2014;35(3):368-376.

DEBNATH J, GAMMOH N, RYAN KM. Autophagy and autophagy-related pathways in cancer. Nature Reviews Molecular Cell Biology. 2023;24:560-575.

DEGENHARDT K, MATHEW R, BEAUDOIN B, BRAY K, ANDERSON D, CHEN G*, et al.* Autophagy promotes tumor cell survival and restricts necrosis, inflammation, and tumorigenesis. Cancer Cell. 2006;10(1):51-64.

DOGTEROM EJ, WAGENMAKERS MAEM, WILKE M, DEMIRDAS S, MUSCHOL NM, POHL S*, et al.* Mucolipidosis type II and type III: a systematic review of 843 published cases. Genetics in Medicine. 2021;23:2047-2056.

DU S, WANG G, ZHANG Z, MA C, GAO N, XIAO J. Structural insights into how GlcNAc-1-phosphotransferase directs lysosomal protein transport. J Biol Chem. 2022;298(3):101702.

E. F. PETTERSEN, T. D. GODDARD, C. C. HUANG, E. C. MENG, G. S. COUCH, T. I. CROLL*, et al.* UCSF ChimeraX: Structure visualization for researchers, educators, and developers. Protein Sci. 2021(30,):70–82.

ENCARNAÇÃO M, KOLLMANN K, TRUSCH M, BRAULKE T, POHL S. Post-translational modifications of the γ-subunit affect intracellular trafficking and complex assembly of GlcNAc-1-phosphotransferase. Journal of Biological Chemistry. 2011;286(7):5311-5318.

FAVRET JM, WEINSTOCK NI, FELTRI ML, SHIN D. Pre-clinical Mouse Models of Neurodegenerative Lysosomal Storage Diseases. Frontiers in Molecular Biosciences. 2020;7:57.

FREEMAN SA, GRINSTEIN S, ORLOWSKI J. DETERMINANTS, MAINTENANCE, AND FUNCTION OF ORGANELLAR pH. Physiological Reviews. 2023;103:515-606.

GHOSH P, DAHMS NM, KORNFELD S. Mannose 6-phosphate receptors: New twists in the tale. Nature Reviews Molecular Cell Biology. 2003;4(3):202-212.

GÓMEZ-VIRGILIO L, SILVA-LUCERO MDC, FLORES-MORELOS DS, GALLARDO-NIETO J, LOPEZ-TOLEDO G, ABARCA-FERNANDEZ AM*, et al.* Autophagy: A Key Regulator of Homeostasis and Disease: An Overview of Molecular Mechanisms and Modulators. Cells. 2022;11(15):2262.

GORELIK A, ILLES K, BUI KH, NAGAR B. Structures of the mannose-6-phosphate pathway enzyme, GlcNAc-1-phosphotransferase. Proc Natl Acad Sci U S A. 2022;119(33):e2203518119.

GORELIK A, ILLES K, NAGAR B. Crystal Structure of the Mannose-6-Phosphate Uncovering Enzyme. Structure. 2020;28(4):426-436.e3.

GU F, CRUMP CM, THOMAS G. Trans-Golgi network sorting. Cell Mol Life Sci. 2001;58(8):1067-84.

GUO JY, KARSLI-UZUNBAS G, MATHEW R, AISNER SC, KAMPHORST JJ, STROHECKER AM*, et al.* Autophagy suppresses progression of K-ras-induced lung tumors to oncocytomas and maintains lipid homeostasis. Genes and Development. 2013;27(13):1447-1461.

GUO JY, XIA B, WHITE E. Autophagy-mediated tumor promotion. Cell. 2013;155(6):1216-9.

HART T, CHANDRASHEKHAR M, AREGGER M, STEINHART Z, BROWN KR, MACLEOD G*, et al.* High-Resolution CRISPR Screens Reveal Fitness Genes and Genotype-Specific Cancer Liabilities. Cell. 2015;163(6):1515-26.

HASANAGIC M, WAHEED A, EISSENBERG JC. Different Pathways to the Lysosome: Sorting out Alternatives. International Review of Cell and Molecular Biology. 2015;320:75-101.

HIESBERGER T, HÜ TTLER S, ROHLMANN A, SCHNEIDER W, SANDHOFF K, HERZ J. Cellular uptake of saposin (SAP) precursor and lysosomal delivery by the low density lipoprotein receptor-related protein (LRP). The EMBO Journal. 1998;17:4617-4625.

JADOTS M, CANFIELDQ WM, GREGORY W, KORNFELD S. Characterization of the Signal for Rapid Internalization of the Bovine Mannose 6-Phosphate/Insulin-like Growth Factor41 Receptor. THE JOURNAL OF BIOLOGICAL CHEMISTRY 1992;267:11069-11077.

JAN E. CARETTE, CARLA P. GUIMARAES, MALINI VARADARAJAN, ANNIE S. PARK IW, ALZBETA GODAROVA, MACIEJ KOTECKI, BRENT H. COCHRAN, ERIC SPOONER, HIDDE L. PLOEGH AND THIJN R. BRUMMELKAMP. Haploid Genetic Screens in Human Cells Identify Host Factors Used by Pathogens. Science. 2009;326(5957):1231 - 1235.

JAYASHANKAR V, EDINGER AL. Macropinocytosis confers resistance to therapies targeting cancer anabolism. Nature Communications. 2020;11(1):1121.

JOHNSON LS, DUNN KW, PYTOWSKI B, MCGRAW TE. Endosome Acidification and Receptor Trafficking: Bafilomycin A1 Slows Receptor Externalization by a Mechanism Involving the Receptor's Internalization Motif. Molecular Biology of the Cell. 1993;4:1251-1266.

JOYCE JA, BARUCH A, CHEHADE K, MEYER-MORSE N, GIRAUDO E, TSAI F-Y*, et al.* Cathepsin cysteine proteases are effectors of invasive growth and angiogenesis during multistage tumorigenesis. Cancer Cell. 2004;5(5):443-53.

K MELLSTRÖM, C H HELDIN, WESTERMARK B. Induction of circular membrane ruffling on human fibroblasts by platelet-derived growth factor. Experimental Cell Research. 1988;177:359-359.

KAMPHORST JJ, NOFAL M, COMMISSO C, HACKETT SR, LU W, GRABOCKA E*, et al.* Human pancreatic cancer tumors are nutrient poor and tumor cells actively scavenge extracellular protein. Cancer Research. 2015;75(3):544-553.

KATRIN MARSCHNER KK, MICHAELA SCHWEIZER, THOMAS BRAULKE AND SANDRA POHL. A Key Enzyme in the Biogenesis of Lysosomes Is a Protease That Regulates Cholesterol Metabolism. Science. 2011;333(6038):87 - 90.

KHAN SA, TOMATSU SC. Mucolipidoses Overview: Past, Present, and Future. Int J Mol Sci. 2020;21(18):6812.

KIM K, GADILA SKG. Cargo trafficking from the trans-Golgi network towards the endosome. Biol Cell. 2016;108(8):205-18.

KIM SM, NGUYEN TT, RAVI A, KUBINIOK P, FINICLE BT, JAYASHANKAR V*, et al.* PTEN deficiency and AMPK activation promote nutrient scavenging and anabolism in prostate cancer cells. Cancer Discovery. 2018;8(7):866-883.

KIMMELMAN AC, WHITE E. Autophagy and Tumor Metabolism. Cell Metabolism. 2017;25:1037-1043.

KLIONSKY DJ, PETRONI G, AMARAVADI RK, BAEHRECKE EH, BALLABIO A, BOYA P*, et al.* Autophagy in major human diseases. The EMBO Journal. 2021;40(19).

KONDO Y, FU J, WANG H, HOOVER C, MCDANIEL JM, STEET R*, et al.* Site-1 protease deficiency causes human skeletal dysplasia due to defective inter-organelle protein trafficking. JCI insight. 2018;3(14):e121596.

KORNFELD S, MELLMAN I. The biogenesis of lysosomes. Annu. Rev. Cell Bioi. 1989;5:483-525.

KRAJCOVIC M, KRISHNA S, AKKARI L, JOYCE JA, OVERHOLTZER M. MTOR regulates phagosome and entotic vacuole fission. Molecular Biology of the Cell. 2013;24(23):3736-3745.

LAUZIER A, NORMANDEAU-GUIMOND J, VAILLANCOURT-LAVIGUEUR V, BOIVIN V, CHARBONNEAU M, RIVARD N*, et al.* Colorectal cancer cells respond differentially to autophagy inhibition in vivo. Scientific Reports. 2019;9(1):11316.

LAWRENCE RE, ZONCU R. The lysosome as a cellular centre for signalling, metabolism and quality control. Nature Cell Biology. 2019;21:133-142.

LEBOVITZ CB, BORTNIK SB, GORSKI SM. Here, There Be Dragons: Charting Autophagy-Related Alterations in Human Tumors. Clinical Cancer Research. 2012;18(5):1214-1226.

LEROY JG, DEMARS RI. Mutant enzymatic and cytological phenotypes in cultured human fibroblasts. Science. 1967;157(3790):804-806.

LI H, LEE WS, FENG X, BAI L, JENNINGS BC, LIU L*, et al.* Structure of the human GlcNAc-1-phosphotransferase alphabeta subunits reveals regulatory mechanism for lysosomal enzyme glycan phosphorylation. Nat Struct Mol Biol. 2022;29(4):348-356.

LUM JJ, DEBERARDINIS RJ, THOMPSON CB. Autophagy in metazoans: cell survival in the land of plenty. Nat Rev Mol Cell Biol. 2005;6(6):439-48.

MARKMANN S, THELEN M, CORNILS K, SCHWEIZER M, BROCKE-AHMADINEJAD N, WILLNOW T*, et al.* Lrp1/LDL Receptor Play Critical Roles in Mannose 6-Phosphate-Independent Lysosomal Enzyme Targeting. Traffic. 2015;16(7):743-759.

MARTIN FJ, AMODE MR, ANEJA A, AUSTINE-ORIMOLOYE O, AZOV AG, BARNES I*, et al.* Ensembl 2023. Nucleic Acids Res. 2023;51(D1):D933-D941.

MARTÍNEZ-FÁBREGAS J, PRESCOTT A, VAN KASTEREN S, PEDRIOLI DL, MCLEAN I, MOLES A*, et al.* Lysosomal protease deficiency or substrate overload induces an oxidative-stress mediated STAT3-dependent pathway of lysosomal homeostasis. Nature Communications. 2018;9(1):5343.

MERCER J, HELENIUS A. Virus entry by macropinocytosis. Nat Cell Biol. 2009;11(5):510-20.

METTLEN M, CHEN P-H, SRINIVASAN S, DANUSER G, SCHMID SL. Regulation of Clathrin-Mediated Endocytosis. Annual Review of Biochemistry. 2018;87:871-896.

MICHLITS G, JUDE J, HINTERNDORFER M, DE ALMEIDA M, VAINORIUS G, HUBMANN M*, et al.* Multilayered VBC score predicts sgRNAs that efficiently generate loss-of-function alleles. Nature Methods. 2020;17(7):708-716.

MIRDITA M, SCHUTZE K, MORIWAKI Y, HEO L, OVCHINNIKOV S, STEINEGGER M. ColabFold: making protein folding accessible to all. Nat Methods. 2022;19(6):679-682.

MITROVIĆ A, PEČAR FONOVIĆ U, KOS J. Cysteine cathepsins B and X promote epithelial-mesenchymal transition of tumor cells. European Journal of Cell Biology. 2017;96(6):622-631.

MUINDI KM, MCCARTHY PC, WANG T, VIONNET J, BATTISTEL M, JANKOWSKA E*, et al.* Characterization of the meningococcal serogroup X capsule N-acetylglucosamine-1-phosphotransferase. Glycobiology. 2014;24(2):139-49.

MUIR A, DANAI LV, VANDER HEIDEN MG. Microenvironmental regulation of cancer cell metabolism: Implications for experimental design and translational studies. DMM Disease Models and Mechanisms. 2018;11(8).

MULLER-LOENNIES S, GALLICIOTTI G, KOLLMANN K, GLATZEL M, BRAULKE T. A novel single-chain antibody fragment for detection of mannose 6-phosphate-containing proteins: application in mucolipidosis type II patients and mice. Am J Pathol. 2010;177(1):240-7.

NADIMPALLI S, AMANCHA P. Evolution of Mannose 6-Phosphate Receptors (MPR300 and 46): Lysosomal Enzyme Sorting Proteins. Current Protein & Peptide Science. 2010;11(1):68-90.

NANCY M. DAHMS MKH. P-type lectins. Biochimica et Biophysica. 2002;1572:317 – 340.

NATALIE PORAT-SHLIOM, YOEL KLOOG, DONALDSON JG. A Unique Platform for H-Ras Signaling Involving Clathrin-independent Endocytosis. Mol Biol Cell. 2008;19(3):765–775.

NIELSEN R, COURTOY PJ, JACOBSEN C, DOM G, LIMA WR, JADOT M*, et al.* Endocytosis provides a major alternative pathway for lysosomal biogenesis in kidney proximal tubular cells. Proceedings of the National Academy of Sciences of the United States of America. 2007;104(13):5407-5412.

NOFAL M, WANG T, YANG L, JANKOWSKI CSR, HSIN-JUNG LI S, HAN S*, et al.* GCN2 adapts protein synthesis to scavenging-dependent growth. Cell Systems. 2022;13(2):158-172.e9.

NOFAL M, ZHANG K, HAN S, RABINOWITZ JD. mTOR Inhibition Restores Amino Acid Balance in Cells Dependent on Catabolism of Extracellular Protein. Molecular Cell. 2017;67(6):936-946.e5.

OLIVARES O, MAYERS JR, GOUIRAND V, TORRENCE ME, GICQUEL T, BORGE L*, et al.* Collagen-derived proline promotes pancreatic ductal adenocarcinoma cell survival under nutrient limited conditions. Nature Communications. 2017;8:16031.

PALM W. Metabolic functions of macropinocytosis. Philosophical Transactions of the Royal Society B: Biological Sciences. 2019;374.

PALM W, ARAKI J, KING B, DEMATTEO RG, THOMPSON CB. Critical role for PI3-kinase in regulating the use of proteins as an amino acid source. Proceedings of the National Academy of Sciences of the United States of America. 2017;114(41):E8628-E8636.

PALM W, PARK Y, WRIGHT K, PAVLOVA NN, TUVESON DA, THOMPSON CB. The Utilization of Extracellular Proteins as Nutrients Is Suppressed by mTORC1. Cell. 2015;162(2):259-270.

PALM W, THOMPSON CB. Nutrient acquisition strategies of mammalian cells. Nature. 2017;546:234-242.

PALMIERI M, IMPEY S, KANG H, DI RONZA A, PELZ C, SARDIELLO M*, et al.* Characterization of the CLEAR network reveals an integrated control of cellular clearance pathways. Human Molecular Genetics. 2011;20(19):3852-3866.

PECHINCHA C, GROESSL S, KALIS R, DE ALMEIDA M, ZANOTTI A, WITTMANN M*, et al.* Lysosomal enzyme trafficking factor LYSET enables nutritional usage of extracellular proteins. Science. 2022;378(6615):eabn5637.

PERERA RM, ZONCU R. The Lysosome as a Regulatory Hub. Annu Rev Cell Dev Biol. 2016;32:223-253.

PLATT FM, BOLAND B, VAN DER SPOEL AC. Lysosomal storage disorders: The cellular impact of lysosomal dysfunction. Journal of Cell Biology. 2012;199(5):723-734.

PLATT FM, D'AZZO A, DAVIDSON BL, NEUFELD EF, TIFFT CJ. Lysosomal storage diseases. Nature Reviews Disease Primers. 2018;4(1):27.

RATTO E, CHOWDHURY SR, SIEFERT NS, SCHNEIDER M, WITTMANN M, HELM D*, et al.* Direct control of lysosomal catabolic activity by mTORC1 through regulation of V-ATPase assembly. Nat Commun. 2022;13(1):4848.

RECZEK D, SCHWAKE M, SCHRÖDER J, HUGHES H, BLANZ J, JIN X*, et al.* LIMP-2 Is a Receptor for Lysosomal Mannose-6-Phosphate-Independent Targeting of β-Glucocerebrosidase. Cell. 2007;131(4):770-783.

RICHARDS CM, JABS S, QIAO W, VARANESE LD, SCHWEIZER M, MOSEN PR*, et al.* The human disease gene LYSET is essential for lysosomal
enzyme transport and viral infection. Science. 2022;378(6615).

RITCHIE ME, PHIPSON B, WU D, HU Y, LAW CW, SHI W*, et al.* Limma powers differential expression analyses for RNA-sequencing and microarray studies. Nucleic Acids Research. 2015;43(7):e47-e47.

ROSSITER NJ, HUGGLER KS, ADELMANN CH, KEYS HR, SOENS RW, SABATINI DM*, et al.* CRISPR screens in physiologic medium reveal conditionally essential genes in human cells. Cell Metab. 2021;33(6):1248-1263 e9.

S. TYANOVA, J. COX. Perseus: A Bioinformatics Platform for Integrative Analysis of Proteomics Data in Cancer Research. Methods Mol. Biol.; 2018.

SAFTIG P, KLUMPERMAN J. Lysosome biogenesis and lysosomal membrane proteins: Trafficking meets function. Nature Reviews Molecular Cell Biology. 2009;10:623-635.

SANJANA NE, SHALEM O, ZHANG F. Improved vectors and genome-wide libraries for CRISPR screening. Nature Methods. 2014;11:783-784.

SCHINDELIN J, ARGANDA-CARRERAS I, FRISE E, KAYNIG V, LONGAIR M, PIETZSCH T*, et al.* Fiji: An open-source platform for biological-image analysis. Nature Methods. 2012;9:676-682.

SCHWABL S, TEIS D. Protein quality control at the Golgi. Curr Opin Cell Biol. 2022;75:102074.

SCHWEITZER GG, GAN C, BUCELLI RC, WEGNER D, SCHMIDT RE, SHINAWI M*, et al.* A mutation in Site-1 Protease is associated with a complex phenotype that includes episodic hyperCKemia and focal myoedema. Mol Genet Genomic Med. 2019;7(7):e00733.

SHEVCHENKO A, TOMAS H, HAVLIS J, OLSEN JV, MANN M. In-gel digestion for mass spectrometric characterization of proteins and proteomes. Nat Protoc. 2006;1(6):2856-60.

SKORDA A, LAURIDSEN AR, WU C, HUANG J, MRACKOVA M, WINTHER NI*, et al.* Activation of invasion by oncogenic reprogramming of cholesterol metabolism via increased NPC1 expression and macropinocytosis. Oncogene. 2023;42(33):2495-2506.

SPERISEN P, SCHMID CD, BUCHER P, ZILIAN O. Stealth proteins: in silico identification of a novel protein family rendering bacterial pathogens invisible to host immune defense. PLoS Comput Biol. 2005;1(6):e63.

STAUDT C, PUISSANT E, BOONEN M. Subcellular Trafficking of Mammalian Lysosomal Proteins: An Extended View. Int J Mol Sci. 2016;18(1).

STEHLE G, SINN H, WUNDER A, SCHRENK HH, CHARLES J, STEWART M*, et al.* Plasma protein (albumin) catabolism by the tumor itself-implications for tumor metabolism and the genesis of cachexia. Critical Reviews in Oncology/Hematology. 1997;26:77-100.

STEPHANE LEFRANCOIS JZ, A JACOB HASSAN, MARYSSA CANUEL, CARLOS R MORALES. The lysosomal trafficking of sphingolipid activator proteins (SAPs) is mediated by sortilin. The EMBO Journal. 2003;22(24):6430-7.

STOLZ A, ERNST A, DIKIC I. Cargo recognition and trafficking in selective autophagy. Nature Cell Biology. 2014;16:495-501.

SWANSON JA. Shaping cups into phagosomes and macropinosomes. Nature Reviews Molecular Cell Biology. 2008;9:639-649.

TASDEMIR E, MAIURI MC, GALLUZZI L, VITALE I, DJAVAHERI-MERGNY M, D'AMELIO M*, et al.* Regulation of autophagy by cytoplasmic p53. Nature Cell Biology. 2008;10(6):676-687.

THOMAS BRAULKE, JAN E CARETTE, PALM W. Lysosomal enzyme trafficking: from molecular mechanisms to human diseases. Trends Cell Biology. 2023;S0962-8924(23):00128-9.

TIEDE S, STORCH S, LÜBKE T, HENRISSAT B, BARGAL R, RAAS-ROTHSCHILD A*, et al.* Mucolipidosis II is caused by mutations in GNPTA encoding the α/β GlcNAc-1-phosphotransferase. Nature Medicine. 2005;11(10):1109-1112.

TOKHTAEVA E, MARENINOVA OA, GUKOVSKAYA AS, VAGIN O. Analysis of N- and O-glycosylation of lysosomal glycoproteins. Methods in Molecular Biology. 2017;1594:35-42.

TOWERS CG, THORBURN A. Targeting the Lysosome for Cancer Therapy. Cancer Discov. 2017;7(11):1218-1220.

TRYBUS W, TRYBUS E, KROL T. Lysosomes as a Target of Anticancer Therapy. Int J Mol Sci. 2023;24(3).

TYANOVA S, TEMU T, COX J. The MaxQuant computational platform for mass spectrometry-based shotgun proteomics. Nature Protocols. 2016;11(12):2301-2319.

VAN MEEL E, LEE WS, LIU L, QIAN Y, DORAY B, KORNFELD S. Multiple domains of GlcNAc-1-phosphotransferase mediate recognition of lysosomal enzymes. Journal of Biological Chemistry. 2016;291(15):8295-8307.

VAN MEEL E, QIAN Y, KORNFELD SA. Mislocalization of phosphotransferase as a cause of mucolipidosis III αβ. Proceedings of the National Academy of Sciences of the United States of America. 2014;111(9):3532-3537.

VELHO RV, DE PACE R, KLÜNDER S, SPERB-LUDWIG F, LOURENÇO CM, SCHWARTZ IVD*, et al.* Analyses of disease-related GNPTAB mutations define a novel GlcNAc-1-

phosphotransferase interaction domain and an alternative site-1 protease cleavage site. Human Molecular Genetics. 2015;24(12):3497-3505.

VIDAK E, JAVORŠEK U, VIZOVIŠEK M, TURK B. Cysteine cathepsins and their extracellular roles: Shaping the microenvironment. Cells. 2019;8(3):264.

W. HUBER, A. VON HEYDEBRECK, H. SÜLTMANN, A. POUSTKA, VINGRON M. Variance stabilization applied to microarray data calibration and to the quantification of differential expression Bioinformatics. 2002;18:S96–S104.

WAHEED A, POHLMANG R, HASILIK A, VON FIGURA K, LEROY JG. Deficiency of UDP-N-acetylglucosamine:lysosomal enzyme N-acetylglucosamine-1-phosphotransferase in organs of I-cell patients. Biochem Biophys Res Commun. 1982;105(3):1052-8.

WANG Y, YE J, QIU WJ, HAN LS, GAO XL, LIANG LL*, et al.* Identification of predominant GNPTAB gene mutations in Eastern Chinese patients with mucolipidosis II/III and a prenatal diagnosis of mucolipidosis II. Acta Pharmacologica Sinica. 2019;40(2):279-287.

WATERS AM, DER CJ. KRAS: The Critical Driver and Therapeutic Target for Pancreatic Cancer. Cold Spring Harb Perspect Med. 2018;8(9):a031435.

WEI LI, HAN XU, TENGFEI XIAO, LE CONG, MICHAEL I LOVE, FENG ZHANG*, et al.* MAGeCK enables robust identification of essential genes from genome-scale CRISPR/Cas9 knockout screens. Genome Biology. 2014;15(12):554.

WEST MA, BRETSCHER MS, WATTS C. Distinct endocytotic pathways in epidermal growth factor-stimulated human carcinoma A431 cells. Journal of Cell Biology. 1989;109(6 I):2731-2739.

WHITE E. Exploiting the bad eating habits of Ras-driven cancers. Genes and Development. 2013;27:2065-2071.

YADATI T, HOUBEN T, BITORINA A, SHIRI-SVERDLOV R. The Ins and Outs of Cathepsins: Physiological Function and Role in Disease Management. Cells. 2020;9.

YAMAMOTO K, VENIDA A, PERERA RM, KIMMELMAN AC. Selective autophagy of MHC-I promotes immune evasion of pancreatic cancer. Autophagy. 2020;16(8):1524-1525.

YANG C, WANG X. Lysosome biogenesis: Regulation and functions. Journal of Cell Biology. 2021;220.

ZHANG T, PETERSON RT. Modeling Lysosomal Storage Diseases in the Zebrafish. Frontiers in Molecular Biosciences. 2020;7.

ZHANG W, LI X, WANG S, CHEN Y, LIU H. Regulation of TFEB activity and its potential as a therapeutic target against kidney diseases. Cell Death Discovery. 2020;6.

ZHANG W, YANG X, LI Y, YU L, ZHANG B, ZHANG J*, et al.* GCAF(TMEM251) regulates lysosome biogenesis by activating the mannose-6-phosphate pathway. Nat Commun. 2022;13(1):5351.